POLITECNICO DI MILANO

Scuola di Ingegneria Industriale e dell'Informazione

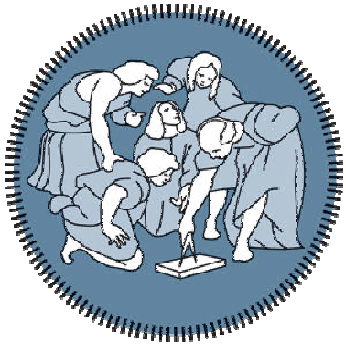

Dipartimento di Chimica, Materiali e Ingegneria Chimica "Giulio Natta"

Corso di Laurea Magistrale in Ingegneria Chimica

MEMBRANE SEPARATIONS IN BIOREFINERY

Development of a general predictive model

Relatore: Prof. Flavio MANENTI

Relatore: Prof. Attilio CITTERIO

Correlatore: Ing. Alessandro ROSENGART

Tesi di laurea di:

Mattia VIZZI Matr. 832748

Anno Accademico 2015-2016

Contents

Ringraziamenti

Rivolgo il primo ringraziamento ai miei relatori e a tutti coloro che hanno partecipato a questo lavoro di tesi per l'opportunità e il supporto fornitomi. Un ringraziamento particolare va all'Ing. Alessandro Rosengart, che mi ha accompagnato durante tutto il lavoro di ricerca e di stesura, dimostrandosi più di un correlatore, ma guida e amico.

Vorrei ringraziare i compagni di viaggio con cui ho condiviso il mio percorso al Politecnico, dagli amici di Jean Claude ai Cinque Tronky, al magistrale gruppo dei Ua: per i bei momenti passati insieme, le risate e i sorrisi. E perché ognuno, a suo modo, ha contribuito a fare di me ciò che sono oggi. Ringrazio chi mi è stato vicino in questi anni milanesi, sopportandomi ogni giorno tra lamentele e discorsi senza fine, e chi mi ha sempre incoraggiato e sostenuto, nonostante la distanza.

Infine la gratitudine maggiore va alla mia famiglia, che mi ha dato tutti gli strumenti per percorrere questo cammino fino alla fine, che ha sempre creduto in me, sostenendomi e aiutandomi a superare gli ostacoli e le difficoltà della vita, e a cui devo tutto.

Abstract

Microfiltration and ultrafiltration are wide used separation techniques in chemical industry, and in particular, in bioprocesses are indicated for biomass removal (full cell harvesting) and fermentation broth clarification. The presence of a predictive model able to describe the phenomenon of membrane fouling and to provide an economic estimation of total cost could be useful in every design stage, from preliminary analysis to feasibility study, and also to final plant employment.

Nevertheless, the complex mechanism of membrane fouling and the different involved phenomena hinder the development of a general predictive model. For these reasons, micro- and ultrafiltration have always been treated in a fully empirical way and each proposed model presents a strong dependency on the experimental conditions in which it was developed. During preliminary design stages for conceptual design, however, it is not always possible to proceed with the usual empirical approach where quick and less detailed evaluations are required.

To overcome the limited applicability of fully empirical solutions and develop a simple and most general possible model, the filtration process is described using the Darcy equation with additive resistances. Each resistive contribution is studied and analysed, to calculate trans-membrane flux reduction curve, whose average value is considered as the main parameter for economic evaluations and as input variable of the cost function. The usual empirical parameters, in absence of experimental calibration, are treated as *fuzzy* variables in their respective existence intervals, since the model will be based on microorganism characteristics taken from literature, hence affected by experimental uncertainty and in some cases, different experimental conditions. Possibility theory is then applied to study the uncertainty propagation on final output variables, introduced by the empirical parameters, in terms of both flux reduction curve and total costs. The developed algorithm,

implemented and tested on different computing platforms, is subsequently used to estimate the range of variability of the upper cost of filtration for a biorefinery case study (lactic acid production plant).

In the end, the model output could be seen as the economic risk linked to the limited experimental knowledge, that is the measure of how the lack of practical test (so the low accuracy of empirical values) impacts on the total equipment cost. The wider availability of experimental data and the comparison with industrial cases could considerably improve the model in its technical aspects, resulting in a narrower cost interval.

Keywords: *Biorefining, Membranes, Microfiltration, Ultrafiltration, Conceptual design, Possibility theory, Uncertainty propagation, Economic assessment.*

Sommario

Microfiltrazione e ultrafiltrazione sono tecniche di separazione ampiamente diffuse nell'industria chimica e particolarmente utilizzate nei bioprocessi per la rimozione di biomasse e la chiarificazione di brodi di fermentazione. L'esistenza di un modello predittivo in grado di descrivere il fenomeno di sporcamento della membrana e di fornire valutazioni economiche sui costi totali dell'operazione è fondamentale in ogni fase di progettazione, dalle analisi preliminari allo studio di fattibilità, all'esercizio finale dell'impianto.

Tuttavia, la complessità del meccanismo di sporcamento della membrana e la diversità (spesso anche di scala) dei fenomeni coinvolti ostacolano lo sviluppo di un modello predittivo generale. Per questi motivi micro- e ultrafiltrazione sono finora state affrontate su basi pienamente empiriche e qualsiasi modello proposto presenta una forte dipendenza dalle condizioni sperimentali nelle quali è stato sviluppato. Nelle fasi di progettazione, però, non è sempre possibile procedere con il solito approccio empirico e valutazioni rapide e dettagliate sono richieste già nei primi stadi.

Per superare la limitata applicabilità delle soluzioni completamente empiriche e sviluppare un modello semplice e il più generale possibile, si propone una descrizione del processo di filtrazione basata sul modello dell'equazione di Darcy con resistenze in serie. Ogni contributo resistivo è studiato e analizzato e il comportamento complessivo dell'apparecchiatura è descritto dalla curva di riduzione del flusso trans-membrana, il cui valore medio è impiegato come parametro principale per le stime economiche e come variabile d'ingresso della funzione di costo. In assenza di valutazioni sperimentali, i parametri empirici sono considerati come variabili *fuzzy* all'interno del rispettivo campo di esistenza (o verosimiglianza), dato che il modello caratterizza i microorganismi utilizzando i

valori disponibili in letteratura, quindi affetti da incertezza epistemica e spesso ottenuti in diverse condizioni sperimentali. La teoria della possibilità è poi utilizzata per studiare la propagazione dell'incertezza sulle variabili finali di output, introdotta dai parametri empirici, sia in termini di curva di riduzione di flusso che, infine, in termini economici. L'algoritmo elaborato, implementato e testato su diverse piattaforme di calcolo, è successivamente impiegato per valutare l'intervallo di variabilità dei costi massimi per un caso di studio di bioraffineria (impianto di produzione di acido lattico).

In ultima analisi, l'indicazione finale fornita dal modello si può intendere come il rischio economico dovuto alla limitata conoscenza sperimentale, ovvero quanto la mancanza di un set di esperimenti (e quindi di accuratezza dei valori empirici) impatti sul costo totale dell'apparecchiatura. La maggiore disponibilità di dati sperimentali, così come il confronto con realtà industriali, comporta un notevole miglioramento al modello nei suoi aspetti prettamente tecnici, che si traduce nella riduzione dell'ampiezza dell'intervallo di costo.

Parole chiave: *Bioraffineria, Membrane, Microfiltrazione, Ultrafiltrazione, Progettazione concettuale, Teoria della possibilità, Propagazione dell'incertezza, Analisi economica.*

Chapter 1

Introduction and theoretical background

This chapter provides background information on membrane separations, specially on crossflow ultrafiltration. This is followed by a brief review on the literature with a focus on models and theories used for predicting permeate flux. Subsequently, the semi-empirical approach is introduced, with a short description of statistical and numerical tools adopted to treat the uncertainty propagation from parameters to model output.

1.1 Membrane filtration and bioprocesses

Separation, recovery and purification of a product from a complex mixture are basic operations in chemical engineering, but the overall downstream processing represents a critical aspect for a production plant, in terms of both product quality and economic feasibility. The development of a competitive recovery stage is usually the bottleneck of the whole process, especially in bio-based industry, and its overcoming could enable new industrial route for chemical productions.

Efficient separation steps are required in each chemical process: to obtain high-grade products for food and drug industries, to produce pure water, to recover costly compounds and to remove hazardous components from effluent streams. For

these tasks, many well established separation techniques are employed, such as distillation, extraction, adsorption, crystallization. Recently, beside these conventional methods, membrane processes are gaining more popularity, and in some applications they directly compete. The simpler operability and scalability, the lower environmental impact and the higher energy efficiency make membrane separations more attractive than traditional techniques. The various industrial applications require membranes with different features (structure, function, driving force and operating conditions), therefore different membrane processes have been developed.

Table 1.1: Classification of membrane separation processes.

Name of process	Driving force	Separation size range
Microfiltration	Pressure gradient	10 - 0.1 μm
Ultrafiltration	Pressure gradient	< 0.1 μm - 5 nm
Reverse osmosis	Pressure gradient	< 5 nm
Dialysis	Concentration gradient	< 5 nm
Electrodialysis	Electric field gradient	< 5 nm

The different membrane processes with their respective features are summarized in Tab. 1.1 and Fig. 1.1.

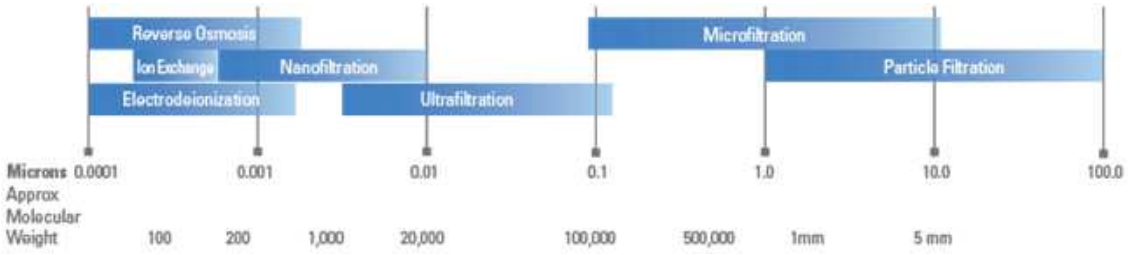

Figure 1.1: Different membrane separation processes.

Membrane filtration does not involve phase change or hazardous chemical agents that have to be discharged, also no heat is generated.

Separation by porous media minimizes both physical damage and denaturation of products, that could occur using distillation or generic heat-driven processes. This aspect makes membrane filtration one of the most common separation techniques in bio-based productions, where microorganisms and biological substrates or products are very sensitive to temperature effects, for example in pharmaceutical or food industry. Among membrane processes, microfiltration and ultrafiltration are the most widely used techniques in chemical and particularly biochemical plants [1] , where they are effectively employed for fermentation broth clarification, microorganisms harvesting and separation of bioproducts, because of their high throughput, high recovery and cost effectiveness [2]. However, part of chemical industry still considers membrane systems a feasible alternative to conventional separation techniques only from a theoretical point of view, as in the field of wastewater treatment, seawater desalination and part of food & beverage industry, where membrane filtrations have been rarely applied. Beer clarification is a representative case: although membrane separation has been encouraged by governments, at the moment it has only 10% of the market volume [3]. In order to make membrane filtration a reliable industrial technology, a deeper understanding of fouling mechanism is required, as well as extensive application know-how and long-term experience. On the contrary, as in the case of ultrapure water production and food products separation, ultrafiltration offers clear benefits and no reasonable alternatives are available. Ultrafiltration has been applied widely in food processing industry for the last 20 years and it becomes an essential part in food technology as a tool for separation and concentration: it ensures higher quality, preserving the nutrition of fresh food with lower risk of contamination; simplifies the process flow and eliminates the use of polluting materials (e.g. diatomaceous earth) that could lead to health and environmental problems. The dairy industry has been one of the pioneers in the development of ultrafiltration equipments based on the experience gained from its application in the production of cheese (whey and milk processing). Ultrafiltration is recognized as a standard tool also in beverage industry, where it is employed in the concentration process for fruit juice production, as well as in the recovery of bioactive components [4].

Ultrafiltration plays a major role in the biotechnology industry, where new systems have been developed over the last years to meet the increasing requirements

in terms of product purity: membranes are designed to provide high retention of proteins, enzymes and other macromolecules with biological activity [5].

Biorefinery represents an emerging field of application for membrane separations. From the very first hopes on a *green revolution* in industry, nowadays biorefineries have become a reality.

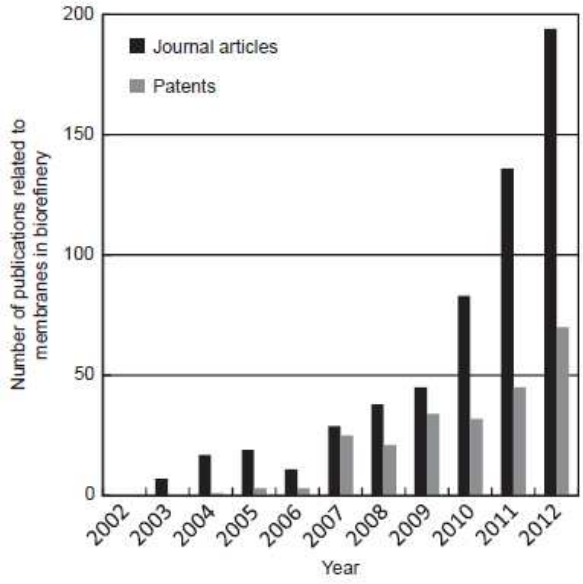

Figure 1.2: Publications of journal articles and patents related to membranes in biorefinery over the last decade [6].

Biomass removal and fermentation broth clarification are important unit operations also in this field, but differently than in pharma and food industry, in this case the economical constraints and the scalability are of primary importance. In addition, bioprocesses propose other challenges, due to the intrinsic complexity of product streams, that make separation harder: the concentration of fermentation products in the aqueous broth is very low and a lot of by-products with similar physicochemical properties are present. Several feasibility studies have been carried out for different chemical productions and different bacterial strains: e.g. ultrafiltration has proven to be a suitable technology in both lactic acid [7] and succinic acid [8] productions, and it could open new routes for downstream processing as well as for the development of more convenient plants [9].

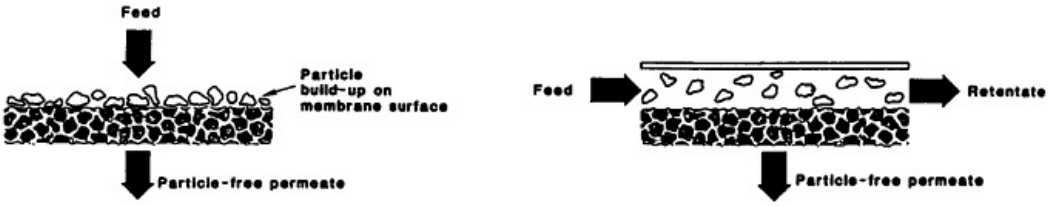

Figure 1.3: Schematic representation of dead-end (left) and crossflow (right) ultrafiltration.

Filtration operation could be run in two different ways depending on the direction of the fluid velocity, normal or tangential, with respect to the plane of the membrane. In normal flow filtration (also defined *dead-end* or deposition mode) an influent (feed) and an effluent (permeate) stream are present. The fluid passes through the membrane under pressure and it drags solutes with it to the membrane surface, where they accumulate and cause the formation of a *cake* layer, which increases the filter hydraulic resistance. Typically, retained solids are removed from filtration systems by backwashing. However, in some cases, particles are re-suspended using a periodic *backpulse* or a short interval of inverse flow, avoiding the complete removal of solids from the system. Dead-end ultrafiltration is used for the industrial clarification or sterilisation of liquids, but is only suitable for feeds containing very low concentrations of particles, as otherwise the membrane becomes too rapidly clogged.

In crossflow filtration (or suspension) mode, the presence of the tangential stream facilitates backflow of particles and prevents pore plugging, thus reduces fouling: the cake layer is washed away continuously during the filtration process and it results in a longer operational time. For this reason, crossflow ultrafiltration is employed at manufacturing scale, in spite of the intrinsic complexity due to the tangential flow.

1.2 Crossflow ultrafiltration: state of the art

In this process the feed suspension is pumped parallel to the plane of the membrane at a velocity in the range of 1-8 m/s and with a pressure difference of 1-5

bar [10], with the permeate flow in the perpendicular direction. The liquid permeation through the membrane leads to a more concentrated feed at the exit of the module. The key aspect of this configuration is the limited build-up of the cake layer on the membrane surface: the shear provided by the tangential flow reduces the accumulation of rejected particles, thus the lifespan of the filter unit is increased and a higher overall liquid removal rate is achieved.

Unlike dead-end mode, crossflow ultrafiltration can be used as a continuous process and is recommended for feeds with high concentrations of small particles. In addition, the retentate remains as a solution and may be recovered directly or easily recirculated, allowing thorough processing of large volumes of liquids. All these features make crossflow ultrafiltration a suitable technology for each level, from research at lab-scale to product development and manufacturing processes. Typically it is used in chemical and biochemical plants for cell harvesting, cell (or lysate) clarification, product fractionation and concentration. Several solutions have been studied for each application in terms of membrane materials, filter configuration and system layout and a wide range of combinations can be found in process industry.

1.2.1 Materials and structures of synthetic membranes

Membranes used for pressure-driven systems are thin porous solids that perform separation by retaining and passing solutes according to their sizes and molecular scales. Ultrafiltration membranes are characterized by pores with an effective size from 0.001 μm to 0.1 μm and are capable to retain solutes such as macromolecules, nanoparticles, colloids and cells from suspensions while passing smaller fractions. The retention properties are expressed as molecular weight cut-off (MWCO), defined as the approximate molecular weight of a dilute globular solute (typical protein) which is 90% retained by the membrane. This value gives only a rough indication of the membrane rejection potential due to the differences in molecular shape: a molecule’s shape can affect directly its retention by a membrane. Values of MWCO typically lie in the range 2-1000 kDa with values of the order of 10 kDa being most common.

In addition to retention capability, other key membrane properties include solvent permeability, chemical compatibility, mechanical strength, consistency and cost. All these features are strongly affected by the materials of which the membrane is made. Initially most membranes were cellulosic and these are now being replaced by polysulfone, polycarbonate, polyamide and other advanced polymers. Each of these materials has different properties with respect to the surface charge, degree of hydrophobicity, pH and oxidant tolerance, strength and flexibility, but polymers in general have improved both chemical stability and microbial attack resistance. Most of the time polymeric membranes are modified by blending bulk polymers with hydrophobic materials to provide better antifouling properties. Nevertheless, these surface modifications may negatively impact membrane characteristics such as pore size distributions as well as degrade the mechanical, chemical and thermal stability.

Recently new ultrafiltration membranes based on inorganic oxide materials have been developed: zirconia (ZrO_2), alumina (α-Al_2O_3 and γ-Al_2O_3) and titania (TiO_2) are the most used.

Table 1.2: Properties of membrane materials.

Material	Advantages	Disadvantages
Polyethersulfone (PES)	Resistance to temperature, pH, Cl_2; easy fabrication	Hydrophobic
Regenerated cellulose	Hydrophilic; low fouling	Sensitive to temperature, pH, Cl_2, microbial attack, mechanical creep
Polyvinyldiene fluoride (PVDF)	Resistance to temperature, Cl_2; easy fabrication	Hydrophobic; coating sensitive to high pH
Inorganic	Resistance to temperature, pH, Cl_2, high pressure, solvents; long life	Cost; brittleness; high crossflow rates

Inorganic oxide-based membranes are produced by two main techniques:

a) deposition of colloidal metal oxide on to a supporting material (such as carbon);
b) as purely ceramic materials by high temperature sintering of spray-dried oxide microspheres.

Ceramic membranes present several advantages over polymeric membranes especially in industrial applications that operate at extreme conditions and require aggressive chemical cleaning at high pH and/or temperatures. Increased chemical resistance allows for higher concentration and longer exposure times to cleaning agents and thus, more efficient foulant removal without compromising the integrity of the membrane, that leads to increase its lifespan (ca. 10 years vs. 3-6 of polymeric membranes). Their high mechanical strength also allows for high backwash pressure. In spite of these benefits, their high production costs have generally limited their use in industrial processes. However, the cost over the last decade has significantly decreased due to the technological advance in membrane materials and manufacturing processes and is expected to continue to decrease [11].

Synthetic membranes show a large variety in their physical structure, but the most used in pressure-driven separations belong to the classes of porous and asymmetric structures. Porous membranes consist of a solid matrix with pores having a diameter from 1 nm to 10 μm and the separation of the various components is based on the sieving mechanism. They can be made from several materials such as graphite, ceramics, metals, metal oxides and polymers and preparation techniques include simple pressing and sintering of polymer or ceramic powders, irradiation and leaching of templates, phase-inversion, polymer precipitation and sol-gel conversion systems. In asymmetric membranes structural and transport properties vary over the cross-section. These membranes consist of a 0.1-1 μm thick *skin* layer on a highly porous 100-200 μm thick substructure: the skin represents the selective barrier, while the thicker structure serves only as a support and has little effect on separation performances. Two different techniques are used to prepare asymmetric membranes: phase-inversion process, which leads to an integral structure; two-step process that produces a composite structure where a thin layer is deposited on a porous substructure [12].

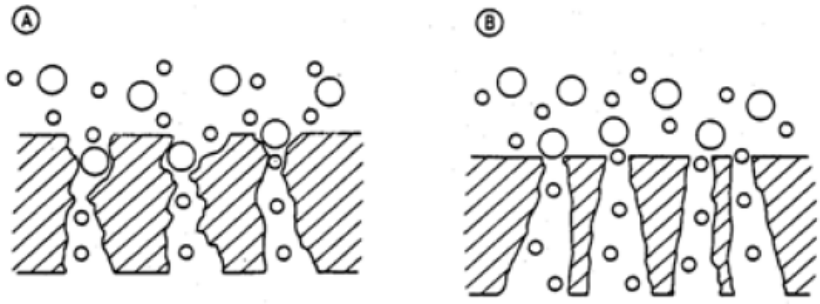

Figure 1.4: Filtration mechanism of depth (A) and surface (B) filters.

Asymmetric membranes act as *surface filters*: all the rejected particles remain on the surface and are removed by the shear due to the tangential feed. On the contrary in *depth filters* large particles are able to penetrate inside the structure increasing the membrane fouling, thus reducing the permeate flux.

1.2.2 Membrane modules

In industrial applications membranes are not used as they are, but are installed in proper devices, known as modules. Membrane modules must meet certain requirements with regard to packing density, fouling control, energy consumption and production costs, thus module selection is a critical aspect in the design of a membrane separation process. The modules used in large-scale applications are quite different and there is no module type that is suitable for all the various processes. The different modules which are commercially available are designed and optimized for a certain application in which they provide the best solution. In process industry four basic module types are used: tubular, hollow-fiber, spiral-wound and cassettes.

Tubular membrane modules

The tubular membrane module consists of several membrane tubes placed into porous pipes. The pressurized feed stream flows in parallel through the tubular bundle and the permeate of the individual tubes is collected on the outer side of the

porous support pipe. Usually, 10-30 tubular membranes are installed in the larger tube. Tubular membrane modules are employed in applications where the benefit due to fouling control overcomes their high costs. They are generally applied where feed with high solids contents and viscosity must be treated and other modules present problems for membrane fouling and plugging. This is the case of certain processes in the food and pharmaceuticals industry as well as in the treatment of certain industrial effluents.

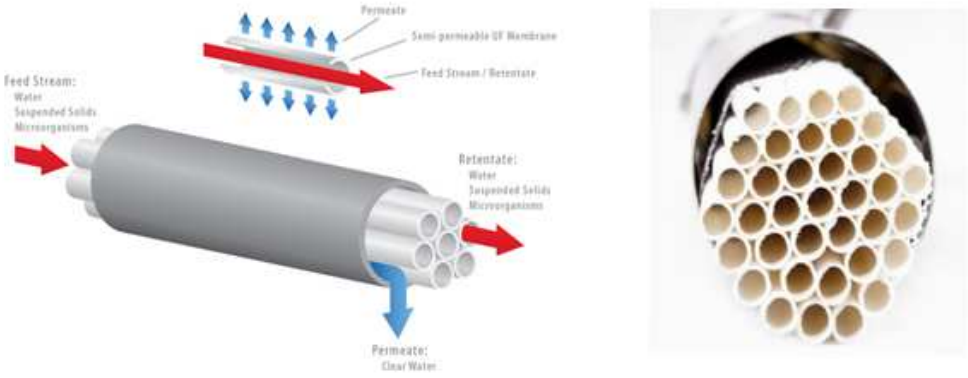

Figure 1.5: Tubular membrane module configuration (left) and cross-sectional view (right).

Hollow-fiber membrane modules

Hollow-fiber modules are tubular devices containing fiber bundles. There is a lumen side (flowing along the inside of the fibers) and a shell side, outside the fiber bundle. For most crossflow filtration operations, feed flows through the lumen side while the permeate is collected from the shell side (*inside-out* mode). The small-diameter lumen promotes better back transport from the membrane surface, thus increases fluxes by reducing the solute concentration. Other variants of hollow-fiber modules feed the process stream on the shell side of the module with permeate exiting in the fiber bundle (*outside-in* mode). In this case the selective layer is on the outside of the fibers and fouling control is more difficult. However, there is a larger external surface area and the fibers are more resistant to high external pressures than internal pressures: in this configuration, modules can be operated at pressures in excess of 100 bar.

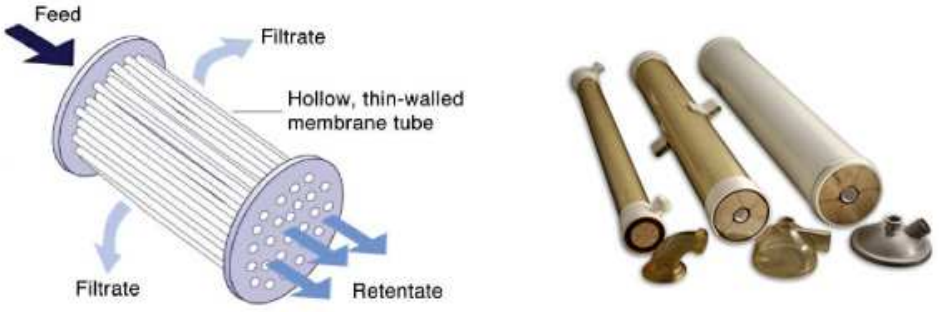

Figure 1.6: Hollow fiber flow pattern (left) and modules (right).

Hollow-fiber membrane modules have the highest packing density of all module types commercially available on the market and their production is very cost effective. Their main disadvantage is the difficult control of membrane fouling: an extensive pre-treatment is required when they operated with liquid solutions because the modules do not tolerate any particles, macromolecules or other materials that can easily precipitate at the membrane surface.

Spiral-wound modules

Spiral modules are tubular devices containing flat sheet membrane in a *jelly roll* type configuration: the feed channel spacer, the membrane and the porous membrane support form an envelope which is rolled around a perforated central collection tube and inserted into an outer tubular pressure shell. The feed solution passes in axial direction through the feed spacer along the module length and then exits out the retentate end of the module. The permeate flows radially through the membrane under a trans-membrane pressure driving force and is collected in the perforated tube in the center of the roll.

Large-scale production of spiral modules is quite cost effective and module costs per membrane area are quite low. However, these modules are sensitive to fouling and the feed channels can easily be blocked: pre-treatment are required in order to remove particles or fibers from feed solutions.

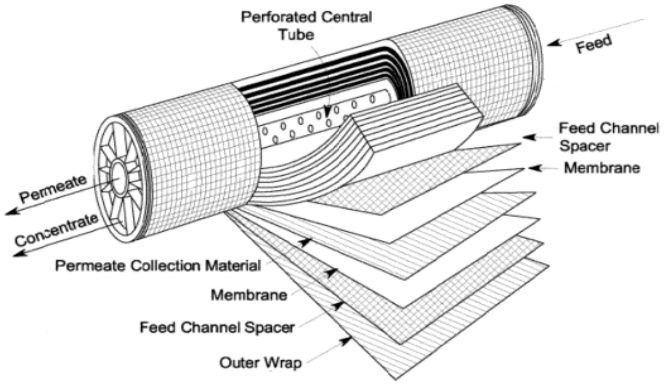

Figure 1.7: .Schematic of a spiral-wound module.

Cassettes

In cassette modules, several flat sheets of membrane are held apart from each other and from the rectangular housing by support screens. To make them, membranes are layered with a porous permeate channel spacer in between to create a *membrane sandwich*. The membrane and permeate spacers have pre-cut holes that act as feed, permeate and retentate flow channels. The feed passes into the spaces between two sheets and permeate is collected from the opposite side of the sheets. Cassettes are widely used in small-scale applications such as the production of some pharmaceuticals active ingredients, bioproducts or fine chemicals. These units are quite expensive and the exchange of the membranes is labour-intensive.

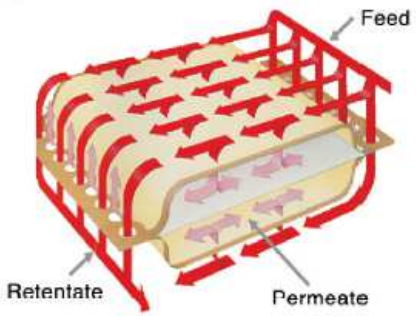

Figure 1.8: Cassette flow pattern.

1.2.3 Process configurations

Four basic process configurations are used in commercial applications of crossflow ultrafiltration: single-pass, batch, fed-batch and diafiltration, as shown schematically in Fig. 1.9.

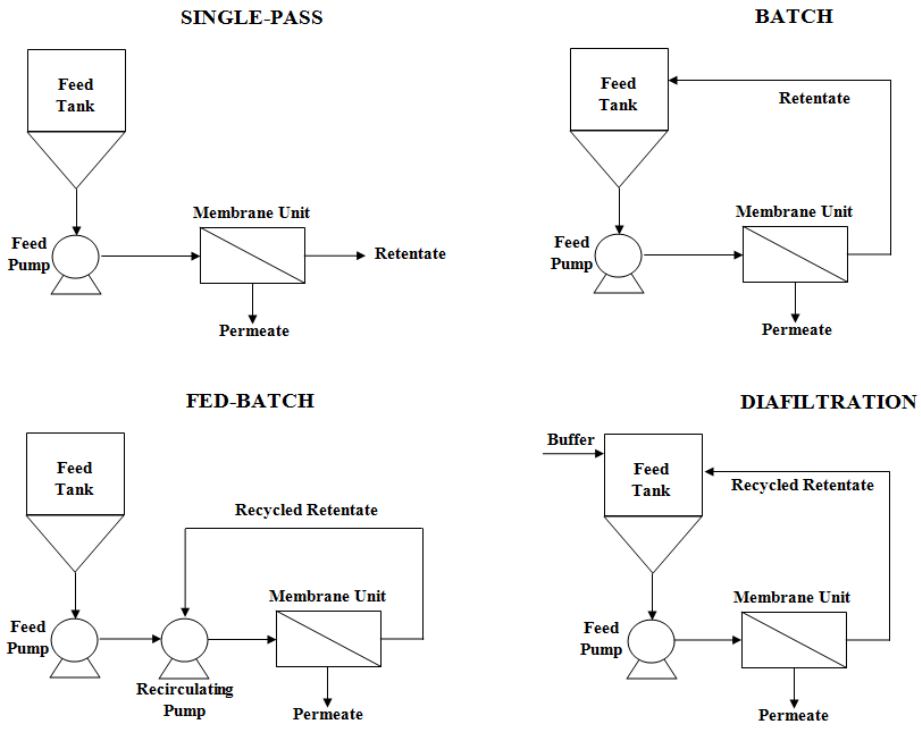

Figure 1.9: Comparison of single pass, batch, fed-batch and diafiltration configurations for crossflow ultrafiltration.

The single-pass operation is the simplest process configuration: the feed is pumped through the membrane unit and the retentate is collected or fed to a subsequent processing step. The difficulties in obtaining the desired permeate flow rate in a single pass are indicated as the main limitation for industrial applications of these systems. However, single-pass ultrafiltration processes have been developed for a number of water purification systems, such as for the removal of trace particulates and microorganisms in both pharmaceutical and electronic industries. In these applications, the filtration is usually performed in dead-end mode: all the feed is forced through the membrane into the permeate and no outlet retentate is obtained.

Batch filtration process is the most common configuration for small-scale applications. The entire quantity to be processed is stored in a tank and a feed from it is pumped through an ultrafiltration membrane, while the retentate is sent back to the tank. The conversion (defined as fraction of the feed solution passing through the membrane as permeate) is typically very low: this means that a retentate recirculation through the module in multiple passes is required to achieve the desired level of conversion. As the permeate flow is withdrawn from the system, the tank volume drops and the fluid contained in the tank becomes more concentrated. The process is completed when the concentration inside the retentate tank reaches the target specification or a critical value that makes the fluid motion no more convenient because of high pumping costs. Batch operation has the advantage of requiring the minimum membrane area, but the largest tank. Pumping costs are high because the circulating loop pressure is lost continuously.

Fed-batch configuration is used in most large-scale commercial processes and almost all continuous industrial membrane separations. The retentate is returned to a smaller retentate tank instead of returning to a feed tank containing the entire batch volume. The retentate tank level remains constant during operations: feed is also pumped into the retentate tank at the same rate as permeate is withdrawn from the system. This configuration allows longer operational time due to the slower increase of concentrations inside the retentate tank. The process is stopped if the viscosity of the recirculating solution is too high due to the increasing concentration.

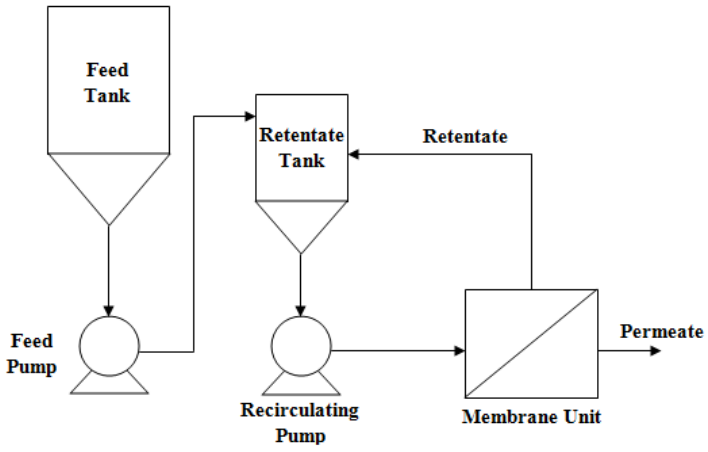

Figure 1.10: Detail of fed-batch configuration.

In diafiltration configuration, new buffer (or clean solvent) is added to the retentate tank at the same flow rate as the permeate leaving the system. Unretained solutes are flushing through the system more efficiently and the balancing of flows keeps the volume constant during the process. Diafiltration is used mainly to produce high-purity products and to fractionate high-value compounds as well as to wash out permeable contaminants from a solution or exchange buffers.

All these configurations are employed in large-scale industrial applications of ultrafiltration. There is no a suitable system for all the various processes and each operation has its pros and cons: batch concentration requires the smallest membrane area; fed-batch uses a smaller retentate tank, but requires more pump passes; single-pass is a compact system and enables continuous operation; diafiltration is necessary in the case of buffer exchange. In short, each configuration has advantages in some applications and its implementation should be considered on a case-by-case basis.

The performance of each configuration can be determined using material balances on the total mass and the phase of interest with the proper initial conditions, thus obtaining a system of non-linear differential equations. The integration and the numeric solution allow the characterization of the system for both simulation and design problems, but several assumptions are required before writing material balances. These assumptions and the corresponding balances are discussed in more detail in Chapter 2.

1.2.4 General membrane behaviour: phenomena of fouling

The performance of membrane equipment is quantitatively measured in terms of permeate flux that is withdrawn from the system. As the feed solution flows through the module, large particles and solutes are rejected by the membrane and their accumulation near and on the membrane surface hinders the free flow of permeate, that declines over operating time. The permeate flux is thus governed by the resistances due to the membrane and the accumulated layers. The build-up of these layers, which is commonly referred to as membrane fouling, depends on various diffusive and convective mechanisms of particle transport and on phenomena of different origins taking place at the membrane interface. Also, it

involves operating conditions, fluid composition, particle size and membrane geometry, among other variables [13-15].

The research activity of the late ‘80s and first half of the ‘90s managed to highlight the main aspects of fouling mechanism, but failed in providing a general paradigm valid for any type of microorganism [16-19]. The complexity of biological solutions, the weakness of the theoretical models and the non-linear interactions between different causes have been pointed as the major obstacles for a good modelling [20]. At present, it is not possible to provide a system of equations that allows the prediction from first principles of the membrane permeation rate for a given real separation. For this reason, phenomenological descriptions are used.

The general membrane equation is an attempt to state the factors which may be important in determining the permeate flux, that can be written as:

$$\text{flux} = \frac{\text{driving force}}{\text{viscosity} \cdot \text{total resistance}} \tag{1.1}$$

which in the case of pressure-driven processes such as ultrafiltration becomes the Darcy’s law

$$J = \frac{\Delta P_{TM} - \Pi_{\text{TM}}}{\mu \cdot R_{tot}} \tag{1.2}$$

J is the permeate flux, expressed as volumetric rate per unit area, ΔP_{TM} is the applied transmembrane pressure, Π_{TM} is the transmembrane osmotic pressure (in ultrafiltration process is usually considered negligible compared to the applied ΔP_{TM} since the molecule being rejected have a large molecular weight), μ is the dynamic viscosity and R_{tot} is the total resistance to the flux. This term takes into account not only the physical resistance by the membrane, but also the hindrance due to the different layers deposited on the membrane surface.

There are different type of fouling and not only cake deposition: it could be characterized by whether it can be removed (reversible or irreversible), by the material causing it (particles, colloids) and by the mechanism of formation (pore adsorption, cake layer, concentration polarization). All these factors induce additional resistances on the feed side to the transport across the membrane that increase the permeate flux decline.

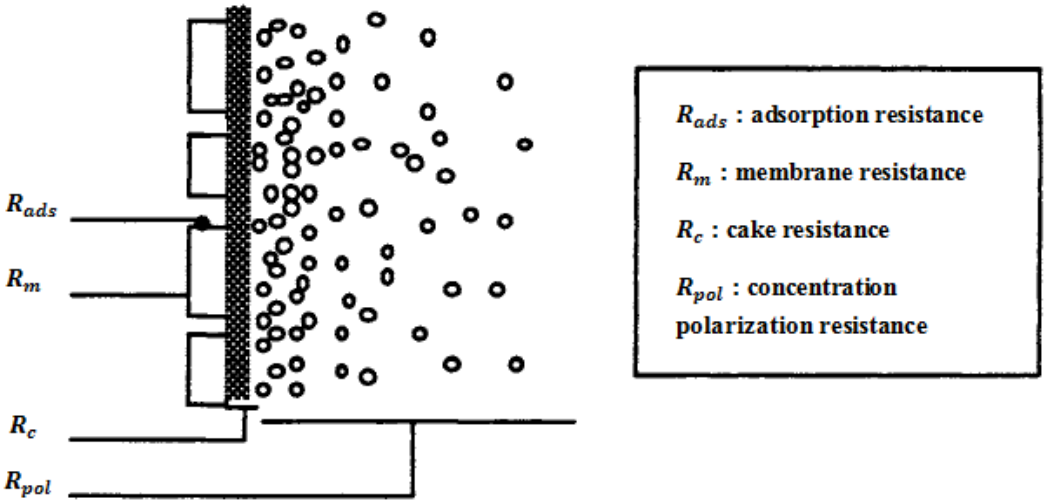

Figure 1.11: Various types of resistance.

The various resistances depicted in Figure 1.11 contribute to a different extent to the total resistance, that is given by the sum of each resistive contribution (resistance-in-series model):

$$R_{tot} = R_m + R_{ads} + R_c + R_{pol} \qquad (1.3)$$

where R_m is the membrane resistance, R_{ads} is the adsorption resistance caused by the adsorption of small particles inside the membrane pores, R_c is the cake resistance due to the formation of the cake layer on the membrane surface and R_{pol} is the concentration polarization resistance caused by the colloidal particles suspended in the feed solution. A deeper analysis of the resistance-in-series model with all the resistive contributions is present in the next chapter.

The typical behaviour of the permeate flux of an ultrafiltration unit is shown in Fig 1.12: starting from the *free water flow*, the permeation rate (or permeate flux) declines over operational time as filtration proceeds, due to the increasing fouling effects.

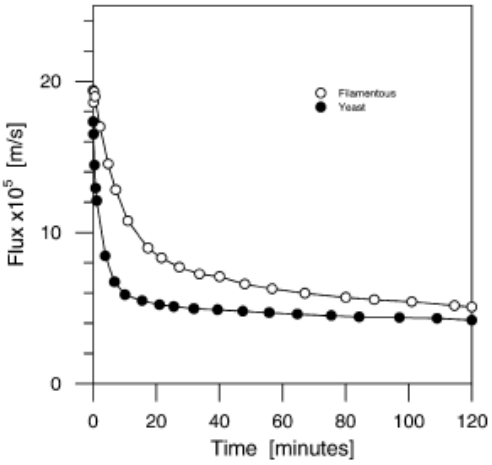

Figure 1.12: Flux behaviour as a function of time [21].

Flux decline has a negative effect on the economics of a membrane operation and, for this reason, countermeasures must be taken to help reduce the flux reduction over an economically acceptable period of operating time.

Incorporating a backwash step into the operation cycle of the ultrafiltration system can drastically reduce the membrane fouling. The backwash process is designed to remove the surface cake that develops during the filtration cycle. Several variations of backwashing exist and they all involve reverse flow of permeate or air for 30 seconds to 3 minutes that dislodges the contaminants at the membrane surface and washes accumulated particles out. The frequency of backwash is not only dependent upon the quality of the feed, but can be affected by the imposed operating flux; nevertheless, it usually ranges between 30 and 120 minutes for most low-pressure systems. Foulant removal through effective and optimized backwash steps could reduce the operating costs.

Chemical cleaning also controls membrane fouling and is performed once the backwash cycle is not able to remove the clogged or absorbed material on the membrane. Although cleaning intervals may vary on a system-by-system basis (from a few days to several months), gradual accumulation of fouling agents makes chemical treatment necessary. However, extending intervals between chemical cleanings means lower cost of operation. There are various chemicals that can be used for membrane cleaning and each one is targeted to remove a specific form of fouling; for this reason, it is often necessary to use a combination of different chemicals to address multiple types of fouling. Some widely used chemicals are

acids (strong, as H_3PO_4, or weak, as citric acid), alkali (NaOH), detergents, enzymes, complexing agents (EDTA) and disinfectants (H_2O_2, NaOCl) [22].
Any foulant that is removed by either the backwash or chemical cleaning process is known as reversible fouling. Over time, membrane processes also experience some degree of irreversible fouling which cannot be removed through these solutions. Irreversible fouling occurs in all membrane systems and eventually requires membrane replacement [23].

Figure 1.12 also points out the dependence of the permeate flux reduction on the shape of microorganisms: two different curves have been obtained for two different types of bacteria, filamentous and spherical (yeast). The problem of representing microorganism suspensions in industrial crossflow filters has been extensively studied, but the results are strongly dependent on the experimental conditions and little reproducibility has been achieved, even for the same bacterial strains. The available models have been developed for specific case-studies and their applicability even for similar situations is reasonable, but not experimentally validated. The complexity of biological substrates is only one of the various obstacles that do not allow the development of a general predictive model as well as a set of equations valid for all the possible configurations. In the following point the main challenges for any attempt of modelling membrane fouling:

- Eq. 1.3 underlines the overlap of several multi-scale phenomena, different from each other but tightly correlated, that complicates the fluid dynamics of the system and the understanding of fouling mechanisms;
- a wide range of membranes and system layouts with various features is commercially available and employed in process industry, thus governing equations and balances must be written on a case-by-case basis;
- filtration is a dynamic operation, and the absence of a real steady-state condition makes system simulation harder.

Over the years, all these complexities have led to fully empirical models and strongly experience-based methods to scale-up filtration units, but this approach is no more possible when assessing the economic feasibility of a new process.

1.3 Literature review: previous models

Although ultrafiltration has been applied for a century, no general approaches are available to design membrane separation units. Membrane design has been always treated in a very empirical way and only in late 1980s methodical attempts to describe this operation were discussed. At first, researchers were interested in understanding the membrane behaviour in presence of foulant agents in order to underline the main aspects of fouling mechanisms [16-19]. Their failure in providing a general predictive model, due to the evasiveness of the fouling phenomena, has moved research efforts towards new purposes. Two main directions have been proposed: the first involves adaptive models to represent empirical data (Pore Blocking models are some of the most popular); the second is based on highly detailed computational fluid dynamic (CFD) simulations of cross-flow filters, or on the use of artificial neural networks (ANNs). A brief description of the proposed models is reported hereafter.

1.3.1 Pore Blocking models

A widely used approach for characterizing membrane fouling is based on four different kinds of filtration modes known as complete blocking model, standard blocking model, intermediate blocking model and cake formation, shown schematically in Figure 1.13.

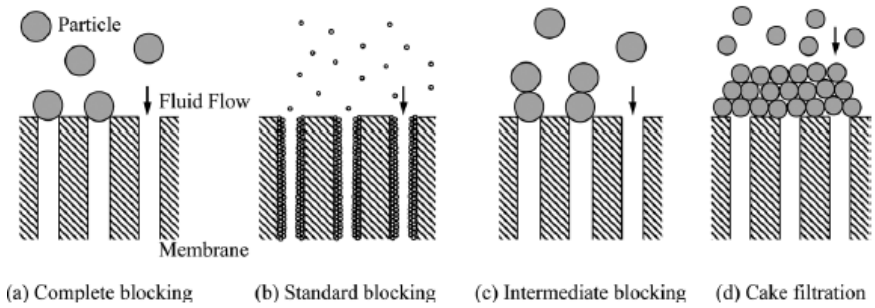

Figure 1.13: Schematic illustration of mechanisms of four filtration models.

A series of simple laws referred to as *blocking filtration laws* were proposed in order to understand the physical phenomena of pore blocking.

With the complete blocking law (Figure 1.13a) it is assumed that each particle reaching an open pore seals the pore opening completely, thus it is applied to systems involving only particles of size larger than the pores of the membrane.

In standard blocking (Figure 1.13b), particle deposit on the pore walls involves the decrease of pore volume with eventual plugging of the pores.

In intermediate blocking (Figure 1.13c), particles arriving on the membrane have a specific probability of blocking a pore. In other words, each particle does not necessarily occlude a pore and the probability of landing on particles already on the membrane surface is accounted for. This law was not derived mechanistically and has previously been considered totally empirical. Later, stochastic approaches such as pure birth model and birth-death model have been proposed to motivate it.

In cake filtration (Figure 1.13d), the cake layer formed onto the membrane surface grows as filtration proceeds and it increases the resistance to permeate flow, thus increasing the flux decline.

The equations for the four fouling mechanisms have been described in several studies where the membranes were operated under constant flux or pressure as well as applying dead-end or crossflow filtration [24-26]. In general, the flux decline behaviours can be seen as a two-step process: the initial fouling due to pore blocking is followed by the long-term cake layer build-up. The characteristic form for blocking filtration laws can be solved when a single fouling mechanism is present or dominates flux dynamics. However, in real practice different fouling phenomena may occur simultaneously and concurrent combined models are required to describe these complex systems. The use of combined fouling mechanisms usually improves the fitting of experimental data indicating that more than one mechanism is involved in the real fouling process. In addition, the combined models usually confirm the single fouling mechanism indentified as dominant by using single basic models [27].

Pore blocking models based on blocking filtration laws are easy to implement and convenient in order to identify the operative fouling mechanism from experimental data. However, they use several adaptive parameters [28], providing results highly context dependent [3]. All the filtration laws stem from a common differential equation by adjusting the values of some constants, thus partially losing

their physical meaning. Applying these models usually means relying on a number of fixed assumptions, that make models process specific and only valid within a limited operating range [29]. The main assumption is that the membrane is considered as a parallel collection of cylindrical tubes, whose radius determining the pore size. This picture of a membrane is often far from reality for polymeric or ceramic membranes, characterized by highly interconnected pore space. In the end, the empirical data required to estimate the adaptive parameters lead to not generalizable models.

1.3.2 CFD simulations

The use of computational fluid dynamic (CFD) simulations allows a deep and detailed insight of ultrafiltration systems and provides a model capable of predicting fouling phenomena in crossflow operations. This approach involves the resolution of the Navier-Stokes equations and the convection-diffusion equations to describe respectively the hydrodynamics and the solute distribution, coupled through the velocity and the viscosity [30]. The numeric results of CFD simulations are highly precise and in good agreement with the experimental data. However, this method is complicated and time demanding as well as computationally intensive and applicable only to simplified systems.

1.3.3 Artificial Neural Networks models

Neural networks are statistical tools capable of modeling highly complex and non-linear systems without requiring any explicit formulation of the physical relationship of the problem. The principle of the artificial neural networks (ANNs) model is based on a highly interconnected system of simple processing elements (neurons) able to learn complex interrelationship between dependent and independent variables, considering available theoretical or empirical knowledge about the process. This *black-box* approach is very useful to characterize complex problems with several factors and parameters affecting the different involved

phenomena. Indeed, ANNs have been recently employed in a number of studies to model the flux dynamics of crossflow filtration processes, including ultrafiltration [31-33]. Excellent agreement between prediction and experimental data has been obtained implementing ANNs models and they seem to be very effective in simulating complex membrane fouling processes [29]. However, ANNs models require big databases of experimental data that limit their applicability to different systems. In addition, as black-box models, they are characterized by a lack of physical meaning, thus are not able to explain the multiscale fouling phenomena occurring onto the membrane surface.

1.3.4 Additive resistance models

In order to develop a general model able to predict membrane performances in real industrial filtrations, neither fully adaptive models nor complex CFD simulations are suitable, due to their poor flexibility. Similarly, the limited applicability of fully empirical design, as well as scale-up methods based on proprietary know-how, makes them useless during feasibility assessment stages. Conceptual design relies commonly on heuristics and *rules of thumb* to evaluate the economic and environmental performances of filtration units [34], thus any model based on physical interpretation of phenomena, though involving different parameters, could be useful to provide a reasonable description of crossflow operations. This approach rehabilitates all the old resistance-in-series models based on Darcy's law, characterized by a certain degree of approximation but rather flexible, that are able to predict the performances of complex and little investigated systems. In order to reach this purpose, parameters estimation from experimental data is required. As it is often complex (and costly) to measure directly some of these values even from dedicated experimental set-up, the use of bounded domains that collect all the empirical values available in literature is preferable and could lead to conservative estimations. This lack of experimental assessments could be seen as an incomplete knowledge, defined *epistemic uncertainty*: it derives from the application of a semi-empirical model whose experimental parameters have been only roughly estimated or extended for analogy from similar systems. The presence of these uncertainties and their propagation from model parameters to the model

output requires special tools and statistical concepts, that are discussed in the following paragraph.

1.4 Uncertainty propagation and Possibility Theory

Empirical science has always been dealing with the concepts of error and uncertainty. The attempt to describe natural phenomena in mathematical terms leads to unavoidable model approximation; hence, several statistical tools have been developed over the last centuries, characterized by different conceptual or operational interpretations, but all based on the concept of *probability*, whose axiomatic definition was given only in 1933 by Kolmogorov [35]. The "classical" interpretation of probability dates back to de Laplace (1812) and it applies only in situations involving a finite number of outcomes which are equally likely to occur. For this reason, it is not applicable in most real-life situations beyond gambling and sampling. The "frequentist" interpretation of probability, which defines it as the ratio between the number of observed events and the number of experiments for an infinite number of experiments, is commonly adopted in practical applications, where nor the real value, neither the set of possible events are known a priori. Since the number of experiments cannot be infinite for real operations, measures provide an estimate of the probability of a certain event, which is closer to the expected value for a high number of experiments. Obviously, the conditions of independence and repeatability of the experiments must hold (the probability exists and is the same for all the observations). Statistical analysis is carried out to estimate the frequentist probability of situations characterized by a high number of observations, that can thus be modelled using common probability distributions. However, all those cases for which a large amount of experiments is infeasible cannot be described using the frequentist approach. In order to manage such problems, a new interpretation was introduced: "subjective" probability is based on the principle that the value of probability given to a certain event is conditioned to the current knowledge of the system [36, 37]. If the knowledge changes, also the value of probability might change: Bayes' theorem is the formal tool developed to tackle rigorously these

problems. When only a poor knowledge is available, the concept of "imprecise probability" gets involved, firstly introduced by Boole in 1854. Imprecision becomes the representation of the lack of knowledge and it is managed defining upper and lower probability limits.

A similar theoretical background can be found in the so called "Possibility Theory", developed by Zadeh to treat the uncertainty deriving from a limited number of available measures (epistemic uncertainty) and any partial belief on the likelihood of an event, as the experience of a professional [38, 39]. Possibility theory is a strong tool widely adopted in the treatment of uncertainties for practical decision-making situations from engineering and medicine to environmental impacts and natural disasters, security and financial risk management. These statistical concepts and the ones reported hereafter can be consulted in the more detailed review of Aven *et al.* [40] and the manual "Fuzzy logic with Engineering Applications" [41]. In particular, numerical methods based on the possibility theory will be applied to study the uncertainty propagation in the context of the present work.

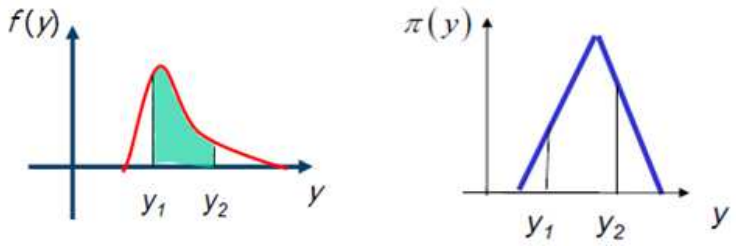

Figure 1.14: From probability distribution (left) to possibility distribution (right).

Although ultrafiltration has been extensively studied over last decades, a deep literature analysis demonstrates that standardized data and experimental knowledge on cross-flow filters are not detailed enough to describe uncertain parameters using probability distributions. For this reason, possibility theory becomes a central concept. The possibility distribution of the event y belonging to a set S, in symbol $\pi(y)$, is defined as follows: the statement $\pi(y) = 0$ means that the outcome of y is impossible, while $\pi(y) = 1$ means that the event y is likely, or in other words unsurprising, possible. The degree of knowledge expressed by $\pi(y) = 1$ is far lower than $P(y) = 1$, i.e. certain event, 100% of probability.

Unlike probability theory, which is a single-valued measure, possibility theory relies on a pair of dual set functions called Possibility and Necessity measures, that are required to interpret a possibility function π.
The Possibility of an event E, $\Pi(E)$, is defined as:

$$\Pi(E) = \sup_{y \in E} \pi(y) \tag{1.4}$$

and the associated Necessity measure, $N(E)$, is defined as:

$$\mathrm{N}(E) = 1 - \Pi(\bar{E}) = \inf_{y \notin E} (1 - \pi(y)) \tag{1.5}$$

where $\bar{E}$ is the complement of E. The following properties are satisfied:

$$\Pi(\varnothing) = 0 \tag{1.6}$$

$$\Pi(S) = 1 \tag{1.7}$$

$$\Pi(E \cup Z) = \max\{\Pi(E), \Pi(Z)\} \tag{1.8}$$

for disjointed subsets E and Z of S, where $\varnothing$ is the empty set. The properties of the Necessity measure can be hence derived, for example:

$$\mathrm{N}(E \cap Z) = \min\{\mathrm{N}(E), \mathrm{N}(Z)\} \tag{1.9}$$

Other properties could be obtained combining (1.5) with Possibility properties.

Considering a family of probability distributions $P(\pi)$ such that for all events E the following relation is satisfied:

$$\mathrm{N}(E) \leq P(E) \leq \Pi(E) \tag{1.10}$$

then:

$$\mathrm{N}(E) = \inf_{P(\pi)} P(E) \quad \text{and} \quad \Pi(E) = \sup_{P(\pi)} P(E) \tag{1.11}$$

In this way, Possibility and Necessity can be interpreted as upper and lower limits, respectively, of the probability of the same event. Any form of statistical distribution could describe the probability of the event within these limits, however, due to the

mentioned lack of knowledge, the possibility distribution does not provide further information.

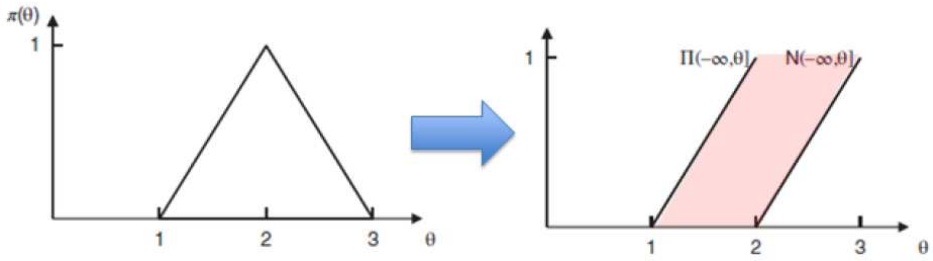

Figure 1.15: Triangular possibility distribution (left) and bounds for the probability measures (right).

Each possibility distribution generates the bounds for the probability measures (Figure 1.15 right). Considering an uncertain parameter that can take values in the range $[a\ b]$ and a most likely value c, this information seems to lead naturally to a representation by a triangular possibility distribution, as illustrated in Figure 1.15 (left). Another shape for possibility distribution is the rectangular, which means that the real value is comprised between $[a\ b]$, but in the interval all values are equally possible. However, the choice of a triangular distribution instead of any other possibility distribution with the same parameters presents a clear advantage: the family of probability distributions $P(\pi)$ induced by a triangular possibility distribution π with range $[a\ b]$ and core c contains all possible probability distributions with support $[a\ b]$ and mode c.

Once uncertainty has been represented, it must be propagated through the model, from uncertain parameters to model output. Possibility distributions are useful not only to describe epistemic uncertainty, but they can also be successfully applied to study its propagation when applied in modelling problems. Following the approach of Aven *et al.*, the idea of uncertainty propagation is illustrated by introducing a generic model $f(x)$ which receives as input a vector $x = (x_1, x_2, \dots, x_N)$ of N uncertain quantities and provides as output the quantity of interest F, that is:

$$F = f(x) \tag{1.12}$$

The output value F is affected by uncertainty because the N input variables are uncertain. The uncertainty analysis of F requires an assessment of the uncertainties about x and their propagation through the model f. The input uncertainty can be probabilistic, possibilistic or a combination of both; in this work only possibilistic uncertainty propagation will be mentioned, this means that the uncertainty of all model input quantities is represented by possibility distributions. Uncertainty propagation in a purely possibilistic problem is performed applying the *extension principle of fuzzy set theory*. If the input to the model is a vector of real-valued quantities $x_1, \dots, x_N$ described by possibility distributions $\pi_1(x_1), \dots, \pi_N(x_N)$ and F is a single real quantity, the principle extends the function f to a function that maps from and to the class of $\pi_i(x_i)$, that is the possibility distribution for F, as reported in the following equation:

$$\pi_F(F) = \sup_{x, f(x)=F} \min\{\pi_1(x_1), \dots, \pi_N(x_N)\} \tag{1.13}$$

In particular, the use of the minimum operator to combine the possibility distributions is justified by the fact that the joint possibility distributions of the N input quantities is defined by the minimum of the possibility distributions:

$$\min\{\pi_1(x_1), \dots, \pi_N(x_N)\} = \pi_{x_1,\dots,x_N}(x_1, \dots, x_N) \tag{1.14}$$

An alternative formulation of the extension principle is based on the representation of the output possibility distribution in the form of a nested set of intervals:

$$\mathrm{A}_\alpha = \left[\underline{F_\alpha}, \overline{F_\alpha}\right] = F\colon\ \pi_F(F) \geq \alpha \tag{1.15}$$

Which are usually referred to as α-cuts. Indicating as $x_{1\alpha}, \dots, x_{N\alpha}$ the N_α α-cuts of the input quantities $x_1, \dots, x_N$, the extension principle, for a given value of α in [0 1], becomes:

$$\underline{F_\alpha} = \inf\ (f(x_1, \dots, x_N), \quad x_1 \in x_{1\alpha}, \dots, x_N \in x_{N\alpha}) \tag{1.16}$$

$$\overline{F_\alpha} = \sup\ (f(x_1, \dots, x_N), \quad x_1 \in x_{1\alpha}, \dots, x_N \in x_{N\alpha}) \tag{1.17}$$

Figure 1.16 shows the application of the extension principle for a quadratic model in the form $C = f(R) = R^2$ [40]. The epistemic uncertainty related to R is described

by a triangular possibility distribution (left); the second plot represents the resulting possibility distribution of the output C.

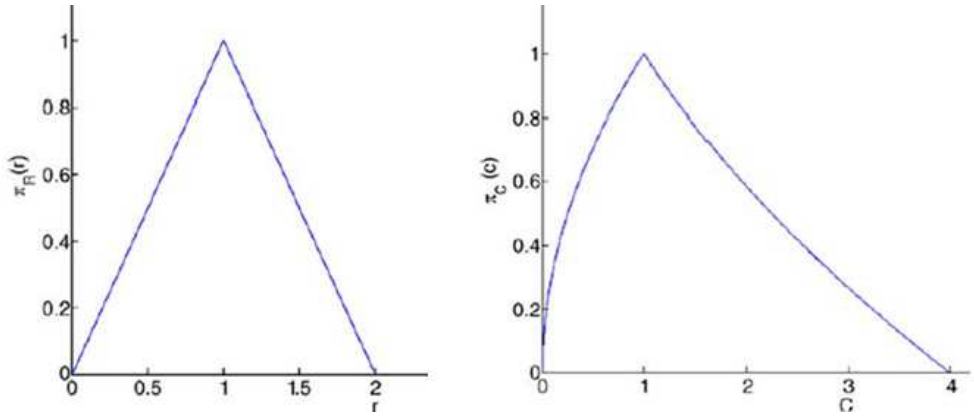

Figure 1.16: Input (left) and output (right) possibility distributions for a quadratic model using the extension principle.

Detailed information on the numerical method of the α-cuts to apply the fuzzy set extension principle is available in [42, 43].

1.4.1 Numerical modelling

The second formulation of the extension principle of fuzzy set theory, based on the α-cuts method, has been implemented in the resolutive algorithm to describe the uncertainty propagation in ultrafiltration operations. Given a value for the α-cut, the intervals of variability of the uncertain input vector are determined and the minimum (and the maximum) for the output quantity is calculated. From a numerical point of view, the problem thus becomes a minimization operation, referred to as *MinMax problem*. The core of the system is the fouling model, that involves the resistance-in-series model, based on Darcy's law, and the material balances of the selected configuration, hence transforming in a stiff system of differential-algebraic equations (DAEs). Since the minimization requires several solutions of this complex and stiff system, which results in an implicit and irregular function to be minimized, with risk of finding local minima, very robust and effective algorithm must be adopted. In the context of this work, two different

computational tools have been used to analyze the uncertainty propagation for industrial ultrafiltration operations.

As a first attempt, a MATLAB® built-in genetic algorithm was used, since the *fmin* function was not up to the task. This method solves both constrained and unconstrained optimization problems using a *natural selection process* that imitates biological evolution. It is very indicated to solve MinMax problems and to find the global minima even for highly non-linear systems. The algorithm repeatedly modifies a population of individual solution. At each step, it randomly selects individuals from the current population and uses them to generate, using random number generators, a population of points (unlike classical algorithms that generate a single point at each iteration, using deterministic computation). The best point in the population approaches an optimal solution. However, genetic algorithm is computationally intensive and time demanding, thus poorly efficient, because it requires the domain acquisition at each step.

In order to reduce the computational time required by the genetic algorithm, a new tool has been adopted to solve the MinMax problem. This second approach is based on a C++ programming using the *BzzMath* library, developed by Prof. Guido Buzzi-Ferraris at Politecnico di Milano [44]. A robust optimization algorithm has been implemented: *BzzMinimizationRobust*. This class is based on the hybrid Optnov-Simplex method, in which the robustness of the Simplex method is improved by the Optnov method, and is able to find global minima by exploiting the full domain, without stopping at local minima. The Optnov method iteratively selects a new starting point that is used by the Simplex method with a limited number of iterations. The clear advantage of using a C++ programming instead of MATLAB® genetic algorithm was the lower computational time, while any particular improvement in the solution quality occurred.

The main output of the simulation is the uncertainty profile of the average flux, i.e. its possibility distribution and the corresponding limit cumulative density functions. The average flux is then correlated to the cost function, providing the same type of plots.

Chapter 2

Additive resistance model development

In this chapter the general predictive model for flux prediction, based on Darcy's law, is developed. All the additive resistance contributions are analyzed individually, highlighting the empirical parameters that are required. The epistemic uncertainty related to these parameters is represented using possibility distributions. Batch and fed-batch configurations are considered as main industrial layouts and described in terms of material balances. The resolutive system, involving fouling model and material balances, is then characterized from a numerical point of view.

2.1 Statement of problem and pursued scope

The major challenge associated to membrane separation processes, which often limits their application, involves understanding and predicting the fouling behaviour and the corresponding permeate flux decline. Foulant agents and fouling mechanisms have not been understood in detail, although they considerably affect the performances of filtration units: fouling can decrease membrane efficiency, increase operating cost and decrease the lifetime of the membrane. Several foulant studies have been carried out using different approaches and operating conditions, from bench-scale experiments to full-scale plants, in order to investigate membrane

fouling and describe the fouling behaviour through a proper model. However, the evasiveness of the fouling phenomena hinders the development of a general predictive model. The main obstacle for a reasonable understanding is represented by the several multiscale (and often highly interconnected) mass transport phenomena that occur straddling the membrane. These processes involve the materials rejected by the membrane as the filtration proceeds, whose accumulation leads to the build-up of secondary layers near and on the membrane surface. The permeate flux, considered as the main parameter to quantitatively evaluate the performances of a filtration unit, declines over operating time due to the increasing resistances offered to permeation by these growing layers. Hence, a general predictive model that aims to describe flux reduction cannot omit the various diffusive and convective mechanisms of particle transport that, at different scales, affect the overall performance of membrane processes.

Several modelling approaches have been adopted to overcome the difficulties in providing a general paradigm for membrane fouling. The nature of a model, considered as a simplified representation of a real system, could be defined by the type of relation existing amongst its internal components, the input and the output variables. In particular, the degree of knowledge about the system (regarding the internal structure or the physical phenomena involved) allows the distinction of three different approaches to model development.

The most desirable type of modelling does only rely on the accurate physical description of the involved phenomena, starting directly from first principles without making assumptions. This is the so-called *white box* approach, where the system is represented as a “glass container”, whose inner components are known together with its inputs, outputs and the relationship between them. Applied to crossflow filtration, the white box approach could provide a flexible model, that could be easily extended to several applications. Also, it requires the distinction of the different involved fouling mechanisms as well as a deep understanding of their causes. The complexities recognized by Foley *et al*. [20] remain the largest challenges for membrane fouling description, and still this level of detail has not yet been achieved.

Conversely, with a *black box* approach, the system is viewed only in terms of its inputs and outputs, without any knowledge of its internal structure. This method is justified by the fact that the external behaviour is the only relevant aspect for practical purposes, especially in highly interconnected devices. The system is

described through the analysis of the response that makes to a given stimulus, both stored in observation tables and used as historic data. Black box modeling is a trial-and-error method based on parameters estimations, which are repeatedly refined by comparing real results and model outputs. This approach could be very useful in complex systems as it allows to skip the tricky physical description that characterizes their internal working. However, as previously discussed (Section 1.3.3), the absence of physical assessments and the necessity of big databases of historic data, especially in poor standardized systems as filtration units, have been considered as the main limitations for black box model applications.

An intermediate approach is represented by the *grey box* model, that combines a rigorous theoretical structure (peculiar of white box approach) with empirical parameters (as in black box). Grey box modelling is also known as semi-physical modelling, because of the partial knowledge of the internal structure: the main characteristics of what is going on inside the system are not entirely known, hence experimental data are required to complete the model. This method allows the development of a model with a sound physical interpretation, but with few and constrained parameters. Thus, the model is committed to experimental boundaries, due to the presence of empirical values. But the use of statistical tools able to describe the uncertainty, introduced by the parameters, and to observe its propagation from inputs to outputs, could provide a more general and flexible model.

The approach proposed in this work tries to predict the permeate flow reduction of a filtration unit using a selected number of fouling mechanisms, together with recent developed statistical models to deal with the experimental lack of knowledge. The resolutive system contains the fouling model, described by additive resistance contributions based on Darcy's law, and the material balances of the selected configuration. Once the flux reduction profile is known, it is possible to calculate the average permeate flux, the main output of the simulation. It is then correlated to a developed cost function in order to estimate the total cost of a filtration unit. The implementation of possibility theory to describe both uncertainty and its propagation through the model provides a new tool for decision-making processes to evaluate the utility of more detailed experimental campaign. The achievement of a cost value helps to understand the effects of epistemic uncertainty propagation, from highly specific parameters to the economic performances of a full-scale process. Indeed, the

uncertainty propagation analysis results in a more conservative cost estimation, expressed as the range of variability of the upper cost of filtration. In this way, the model also provides an indication of the economic risk due to the limited experimental knowledge. Results and their interpretations are widely discussed in Chapter 5.

2.2 Development of the fouling model

In ultrafiltration membranes, the permeate flux reduction is determined mainly by three aspects: the type of filtration equipment, the operation mode and the fouling properties of the solution that will be processed. Thus, it is necessary to define the bounds of applicability of the model studied in this work. As discussed in Chapter 1, different combinations of materials and modules are commercially available for industrial filtrations, and their selection affects the fouling behaviour of the equipment, thus its performance and the overall economics of the process. The variability of the filter geometries proposed for the single case of crossflow filtration is remarkable, with alternatives such as flat sheet, spiral wound, tubular and hollow fiber modules (Section 1.2.2). Also, several technological solutions have been applied to improve filter performance (e.g. vibrating modules, pulsed operation, etc.), resulting in an even wider range of equipment shapes [45]. In order to avoid excessive complications, the membrane implemented in this model is arranged in a simple multi-channel tubular layout, highly suitable for fouling systems as bacterial suspensions. A ceramic membrane is chosen, more expensive than polymeric ones, but resistant to chemical cleaning and durable, characterized by 0.1-0.2 μm of pore size. This configuration is the most popular for high throughput applications with fouling systems as typically found in bioprocesses.

As the main scope of this work is to provide a simple and flexible tool to predict the permeate flux reduction during industrial clarifications of fermentation broths, a model based on Darcy's law with additive resistance contributions is developed. Combining Eqs. 1.2 and 1.3 and highlighting the time-dependency of the different quantities, a general expression of the fouling model is obtained:

$$J(t) = \frac{\Delta P_{TM}}{\mu \cdot \left(R_m + R_{ads}(t) + R_{pol}(t) + R_c(t)\right)} \qquad (2.1)$$

The equation does not contain the osmotic pressure as the pore diameter is larger than 100 nm, a threshold for which the contribution of osmotic pressure on particles in negligible [16]. The permeate flux J decreases over operating time due to the increasing resistance to permeation offered by the different contributions. Their mechanisms are reported hereafter.

2.2.1 Membrane resistance

Membrane resistance R_m is the hydraulic resistance of the membrane itself. It is calculated when only clean solvent (water) is filtered, and is the resistance to flux due to the water permeation across a porous medium. It is a function of the size and number of pores, but also of their disposition (equally distributed or clustered) and the materials of the support. Analytical equations to predict R_m are available, if the physical properties of the membrane are known [16], but often membrane resistance is implicitly reported as a producer specification in the measured "free water flow" indication, provided in the technical datasheet of commercial membranes. This resistance has an intrinsic value that is assumed constant during each filtration cycle. However, a new membrane has a lower resistance than a used and regenerated one, due to irreversible fouling and aging [46]: considering an industrial plant, it is advisable to consider a free water flow reduced of the 20% or, in other words, a corresponding R_m increased of the 25% [47].

2.2.2 Adsorption resistance

Adsorption resistance R_{ads} is caused by the adsorption fouling, that occurs when smaller particles enter the membrane pores and undergo to physical adsorption on the internal channel walls, similarly to the standard blocking model. The deposition of these particles reduces the channel diameter, thus enhancing flow resistance. Membrane materials, surface treatments and broth compositions can

influence the rate of fouling, thus experimental data are necessary to provide the right value for this phenomenon. A typical approach to measure the adsorption resistance contemplates that the membrane is put in contact with the broth for 24 hours, then the surface is rinsed with fresh water and the permeate flux at a given pressure is measured [48]. Experimental evidence states that R_{ads} is time dependent and tends towards a constant "steady-state" value, corresponding to the maximum when there is no more surface available for adsorption. It is important to notice that adsorption fouling does not clog entirely the membrane, unlike standard blocking model that does not allow a steady-state resistance, but fouling continues until the flux is stopped [3, 28].

Table 2.1: Overview of the adsorption resistance values.

Reference	Membrane material	Fouling system	R_{ads}/R_m
[28]	Ceramic membrane 0.2 μm	*L. delbrueckii* fermentation broth	6.02-8.25
[49]	Ceramic membrane 0.04 μm	*E. coli* fermentation broth	0.2
[48]	Polysulfone membrane MWCO 40-100 kDa	Bovine serum albumin solutions	2
[46]	Ceramic membrane 0.2 μm	Red wine with addition of tannins	0.11
[50]	Polysulfone membrane MWCO 30 kDa	Passion fruit juice	4.61-4.86
[51]	Ceramic membrane 0.04 μm	Lactoglobulin aqueous solutions	1.46
[52]	Polysulfone membrane MWCO 10 kDa	Bovine serum albumin solutions	0.25
[53]	Polyamide membrane	β-lactoglobulin tryptic hydrolysate	0.6
[54, 55]	Various systems	Various systems	9 max

Different works on fermentation broth clarifications [7, 49] demonstrated that the steady state value is not sensitive to transmembrane pressure, neither to crossflow velocity. Although the qualitative behaviour of adsorption fouling has been recognised in all the studies, the complexity of the phenomenon and its dependency on the nature of the solutes, the thermodynamics of the system and the materials of the membrane produced very different experimental values, as shown in Tab. 2.1. Experimental data, specific for the case of study, are required to correctly estimate R_{ads}, due to its wide variability

Also, the dynamics to reach the steady-state condition are not univocally expressed. Following the approach of Carrère *et al.*, adsorption resistance is expressed as:

$$R_{ads}(t) = R_{ads}^{SS}\left(1 - e^{-\beta t}\right) \qquad (2.2)$$

where β is a time constant in the order of 10^{-4} s^{-1} [7], R_{ads}^{SS} is the steady-state value of the adsorption resistance, considered, in a first conservative guess, as 9 times the membrane resistance, the highest known contribution [55].

2.2.3 Concentration polarization resistance

Resistance due to concentration polarization effect, R_{pol}, is caused by the colloidal particles suspended in the fermentation broth, and their accumulation near the membrane surface that causes the local concentration to increase. This phenomenon is described by the *gel layer theory*, which says that in proximity of the membrane, on the retentate side, the rejected materials form a high concentration, high viscosity layer, which contrasts the solvent flux [56, 57]. The nature of this gel layer is little understood and its modelling requires an intimate knowledge of the involved colloidal particles, as well as the mass transfer phenomena that affect them. However, two main trends have been observed in micro-, ultra- and nanofiltration, which describe the layer build-up from the beginning of the operation to a pseudo steady-state value of polarization resistance:

1) The smallest rejected particles, carried by the permeating flux, accumulate at the membrane surface, but are re-suspended by the *Brownian back diffusion*. Since the rate of deposition is equal to the back transport rate, the gel layer

thickness reaches a steady-state value. Brownian diffusivity is a complex phenomenon depending on the thermodynamics of the system and its fluid-dynamics, and it can be calculated only for simple mixtures, having a limited number of solutes and well characterized mono-dispersed colloids [58]. For these reasons, no data are available to evaluate the Brownian effect in industrial fermentation broths;

2) Bigger particles also accumulate in an analogous way, and they are swiped away by the tangential flux, which causes the so-called *shear-induced diffusion* [16, 59]. Despite the different back-transport mechanism, the thickness of the gel layer reaches a pseudo steady-state value here too. It is possible to predict the diffusion coefficient from the shear rate of the tangential flow, using the correlations between mass and momentum transport, which are available in literature for a number of different shaped conducts.

The complicated estimation of the concentration polarization resistance derives from the fact that in any industrial filtration there is a population of colloidal particles (cell debris, organelles, or generic macromolecules) with a distribution of sizes and shapes, affected by either Brownian or shear-induced diffusion. Once again the complexity and the difficult reproducibility of industrial fermentation broths seem to be the main obstacles, and their description requires many adaptive parameters. Nevertheless, the problem could be simplified considering proper assumptions.
First, the rejected particles must be larger than 100 nm (pore size of the selected membrane); the smaller ones can permeate and pass the membrane. Moreover, the particles responsible for the polarization layer should be smaller than the bacteria (1 μm), otherwise they will be lifted away by the high shear rate resulting from the turbulent flow operation (crossflow velocity higher than 2 m/s). This second assumption is further supported by the evidence of the shear-induced particles segregation, that causes only smaller particles to deposit on the membrane [60]. The deposition of larger particles will be treated with the cake model, discussed in the next paragraph.

The two trends mentioned above refer to particles with particular sizes: Brownian motion affects particles smaller than 100 nm, while particles larger than 500 nm are described using the shear-induced mechanism. Particles having sizes in

the range 100-500 nm are the most complex to model, because they are too heavy for Brownian diffusion and too small to sense the shear lift, hence no predictive equations are available. Cho *et al.*, conscious of the complexity in calculating diffusivities in these conditions, managed to measure them directly [61], as reported in Fig. 2.1.

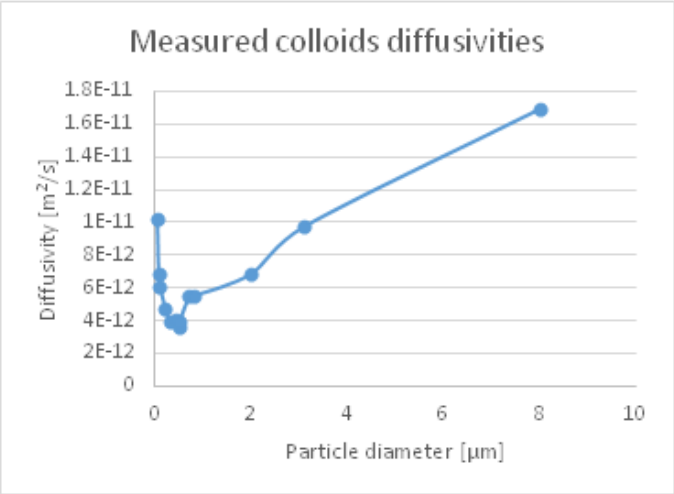

Figure 2.1: Measured values for the diffusivity of colloids from [61].

It is possible to notice that the minimum value of diffusivity characterizes particles with size of 500 nm, in correspondence with the transition of the mechanism dominating the particles mobility. Hence, colloids in this range are the major responsible for the bigger part of the gel layer build-up. Cho *et al.* measured these values for synthetic spheroidal particles, but neither Brownian nor shear-induced diffusion models, often applied to real biological products, can actually represent the true nature of a bio-derived colloid. Consequently, these experimental values are suitable as starting points for unknown fermentation broths. The true limit of this kind of predictive approach, shared with the other theories for concentration polarization effect, is that only spheroidal colloids are represented: in order to describe filamentous or sheet-like particles, as ribonucleic acids or some proteins, only adaptive regression models are suitable, but these exceed the scopes of this work.

The material balance on the gel boundary layer yields the following equation:

$$\frac{dm_x^{gel}}{A\,dt} = J_{pol} c_x^{bulk} - k_{mat}\left(c_x^{gel} - c_x^{bulk}\right) \tag{2.3}$$

where m_x^{gel} is the mass of the colloids in the boundary layer, c_x^{bulk} and c_x^{gel} are the colloids concentration in the bulk phase and gel phase respectively, J_{pol} is the permeating flux and k_{mat} is the mass transfer constant. The polarization layer is increased by the new particles carried by the permeating flux, while the combined effect of Brownian and shear-induced diffusion determine the colloids re-suspension, represented by the overall mass transfer coefficient. At steady-state, applying the Darcy equation for flux and approximating $c_x^{gel} \gg c_x^{bulk}$, the equation becomes:

$$J_{pol}^{SS} \approx k_{mat} \frac{c_x^{gel}}{c_x^{bulk}} = k_{mat} \frac{\Phi_x^{gel}}{\Phi_x^{bulk}} = \frac{\Delta P_{TM}}{\mu \cdot R_{pol}^{SS}} \tag{2.4}$$

where R_{pol}^{SS} is the steady-state resistance due to concentration polarization effect and the concentration ratio is expressed with the particle volume fraction (solidosity) $\Phi_x^{gel}/\Phi_x^{bulk}$ [62]. The variables in the equation are function of the axial coordinate. To simplify the model, the following assumptions are made: bulk composition does not change along the membrane channel, since the permeate flow rate is far lower (<1%) than the bulk flow rate [63]; the flux is fully developed. The overall mass transfer coefficient k_{mat} can be calculated using the correlations for fully developed flux, derived from Chilton Colburn analogies in different geometries and for rough ducts [64]. These semi-empirical correlations provide axial averaged mass transfer coefficients, which could actually simplify the real dynamics of a permeating membrane. In addition, most of the available literature correlations were originally calculated for non-permeating ducts, and extending them to the case of membranes can lead to relevant approximations. However, the simplification of this approach are less noticeable with high turbulence, since the flow profile is not disturbed by permeation with Reynolds number greater than $2 \cdot 10^4$ [16]. The correlation used in this work is the following:

$$Sh = 0.00929(e/d)^{0.15} Re\, Sc^{0.5}\left(1.11 + 0.44 Sc^{-1/3} - 0.7 Sc^{-1/6}\right) \tag{2.5}$$

it was developed with the surface renewal model and for high Schmidt number, where e is the absolute roughness (empirically determined) and d is the pipe diameter. The adimensional groups are defined as:

$$Re = \frac{\rho \cdot v \cdot d}{\mu}; \qquad Sc = \frac{\mu}{\rho \cdot D_x}; \qquad Sh = \frac{k_{mat} \cdot L}{D_x} \tag{2.6}$$

where ρ and μ are, respectively, the density and the dynamic viscosity of the fluid, v is the crossflow velocity, d and L are the internal diameter and the length of the membrane module, D_x is the measured colloids diffusivity.

It should be noted that the transmembrane pressure does not affect directly the flux. This is peculiar of the polarization phenomenon that produces a loose gel layer which shrinks in case of higher pressure, resulting more compact, which compensates with higher resistance the enhanced permeate flux [57]. Wall particle solidosity, or gel concentration, is then a pressure-dependent value, but also depends on the nature of the gel. As it is complex to measure directly the dynamic gel concentration on the membrane, the use of the limit values of gel solidosity could lead to preferable conservative estimations. For example, if the colloidal particles were mono-dispersed and spherical, the gel fraction would have the maximum analytical value of 0.64 [65]; however, due to experimental evidence, it is preferable to consider an interval comprised between 0.58 and 0.75 [57, 63]. The colloid volume fractions for industrial fermentation broths are typically included between 0.1% and 0.3% [3, 58, 66], and from these values is possible to calculate the range of variation of the solidosity ratio, that spans from 193 to 750. This interval determines the shape of the possibility distribution for the solidosity ratio, considered as the first empirical parameter of the model. Since no most likely values have been obtained from literature, a rectangular possibility distribution is built, shown in Fig. 2.2.

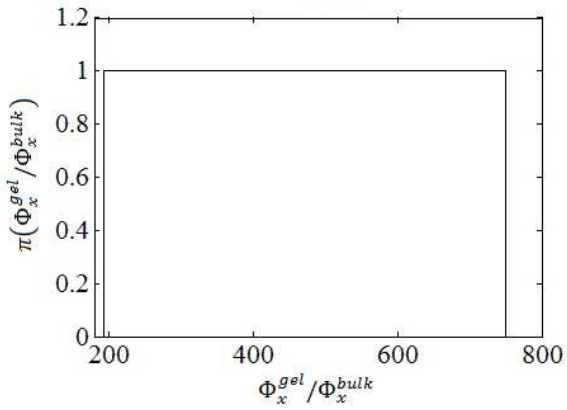

Figure 2.2: Solidosity ratio possibility distribution.

In the context of this work addressing unknown mixtures, the model should consider the whole interval, resulting in an epistemic distribution of values, whose uncertainty will propagate to the final aggregated value of the average permeate flux.

The transient formation of the gel layer is modelled considering the same dynamics of the adsorption resistance:

$$R_{pol}(t) = R_{pol}^{SS}\left(1 - e^{-\beta t}\right) \tag{2.7}$$

The solidosity ratio is used to calculate the steady-state flux first, and then the steady-state value of the concentration polarization resistance, according to Eq. 2.4.

2.2.4 Cake resistance

As filtration proceeds, the rejected particles build up a compressible cake layer on the membrane surface, that hampers the flux permeation. This contribution is referred to as cake resistance. In dead-end filters, it is the main responsible of the permeate flow reduction, outstanding rapidly the other resistances, and the cake layer grows continuously until the filtration operation is stopped. Crossflow filters were developed with the intention of reducing the build-up of this layer, exploiting the tangential feed stream in order to increase the operating time. Indeed, caking becomes relevant for crossflow configuration only in case of high suspension

concentration or laminar flow condition [16], but the usual industrial operations, with high tangential velocities and enhanced shear stress, reduce this occurrence.

The value for cake resistance is determined by the following equation:

$$R_c = \alpha \cdot \frac{m_{cells}}{A} \tag{2.8}$$

where α is the specific cake resistance and m_{cells} is the mass of deposited particles. The filtration area A is assumed to be constant:

$$A = 2\pi L(d - \delta) \approx 2\pi dL \tag{2.9}$$

where δ, cake layer thickness, is negligible in the operating conditions considered in this work, d and L are the internal diameter and the length of the tubular membrane module. Carman-Kozeny equation, which defines specific cake resistance for uncompressible spheres of the same size, can describe the flux resistance across packed particles:

$$\alpha = \frac{180 \cdot (1 - \varepsilon)}{\rho_s d_p \varepsilon^3} \tag{2.10}$$

where ε is the cake porosity, ρ_s and d_p are respectively the density and the diameter of the solid particles. However, microorganisms are compressible and except for few cases, their shape is far from spherical. This introduces several complications in the mathematical representation of their behaviour. Mota *et al.* proposed a modified version of the Carman-Kozeny equation [67]:

$$\alpha = \frac{36 \cdot K_0 T^2 \cdot (1 - \varepsilon)}{\rho_s d_p \varepsilon^3} \tag{2.11}$$

where K_0 is a shape coefficient depending on a cross-section capillary pore shape. T is the tortuosity, which can be expressed as a function of the cake porosity:

$$T = \varepsilon^{-\theta} \tag{2.12}$$

Both the coefficient θ, higher for species more sensitive to compression, and K_0 are function of packing density and particle shape, and it is impossible to estimate them

a priori without experimental data. It could be easier to use the empirical definition of specific cake resistance [68-70]:

$$\alpha = \alpha_K \cdot \Delta P_{TM}{}^{n} \tag{2.13}$$

that relates the experimental specific cake resistance constant α_K, measured at constant pressure in dead-end or crossflow configuration, to the resistance at other pressure according to n, the compressibility index. As the macroscopic properties of bacterial cakes depend on many variables (partially summarized in Tab. 2.2), there is not a unique value for neither α_K nor n, even for the same strain of bacteria.

Table 2.2: List of the main process variables affecting cake fouling.

Reference	Variable	Driving phenomena
[21]	Cell shape	Microorganism (spheroidal, rod-like, flat)
[71]	Cell compressibility	pH, ionic strength
[21, 72]	Cell size distribution	Microorganism (mono-dispersed, skew distribution)
[73]	Cell age	Process conditions
[74]	Presence of extracellular colloids	Microorganism strain / fermentation conditions
[71]	Membrane roughness/hydrophilicity	Membrane selection / surface treatments
[75]	Cell concentration	Operation (pre-treatment)

The main contributions to the study of α_K and n for industrially relevant bacteria are reported in Tab. 2.3. The compressibility index is lower for spheroidal microorganisms as yeasts, denoting a better packing, whereas resistance for rod-shaped bacteria is more sensitive to pressure because, in dead-end filters, a higher pressure results in particles rearrangement. This rearrangement is less significant in

crossflow filters, which means lower n, because of the shear-induced particles orientation, which causes a closer packing.

Table 2.3: Filtration properties of selected microorganisms.

Ref.	Microorganism	Shape	Size		α_K	n	Flow
			Diameter [μm]	Length [μm]	[m/kg/Pa^n]		
[21]	*K. martianus*	Rod / filamentous	5	-	2.88E+09	0.5	DE
[7]	*L. delbrueckii*	Rod	1	8	1.20E+09	0.63	CF
[69]	*L. delbrueckii*	Rod	0.5	3 to 6	2.02E+07	1	DE
[69]	*E. coli*	Rod	0.5	2 to 3	2.73E+10	0.51	DE
[68]	*S. cerevisiae*	Spheroidal	5.35	-	1.01E+09	0.7	DE
[2]	*B. subtilis*	Rod	-	-	3.53E+08	0.8	DE

DE: dead-end filter measurement
CF: crossflow filter measurement

While the specific cake resistance measured at fixed pressure, α_K, is a measured experimental value, the compressibility index is considered as the second uncertain parameter of the model, in particular affected by epistemic uncertainty, which has to be studied. From the data of Tab. 2.3, the epistemic distributions of the compressibility index for spheroidal and rod-shaped bacteria are derived, shown in Fig. 2.3. The use of triangular distributions is justified by the presence of the “most likely” values, obtained from experimental tests. The specific cake resistance α, determined by both the measured value of the specific cake resistance constant and the range of variation of the compressibility index, is thus used to calculate the overall resistance due to the cake layer build-up.

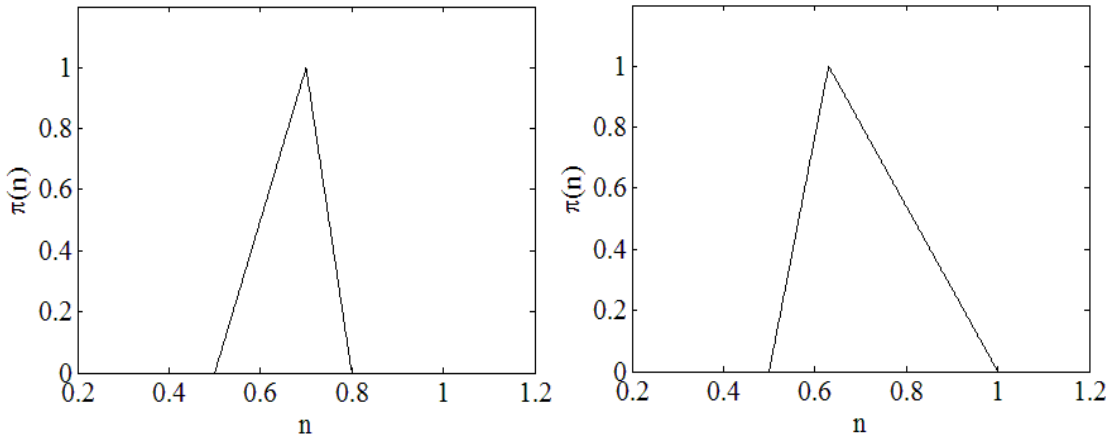

Figure 2.3: Possibility distribution of the compressibility index for spheroidal (left) and rod-shaped (right) microorganisms.

Before doing so, it is necessary to quantify the mass of particles deposited on the membrane surface, taking into consideration the different transport phenomena that occur. First, particles arrive to the membrane from the bulk phase, due to permeation; then, a back-transport mechanism is present, which moves the deposited particles from the cake layer to the bulk. As the phenomenon of caking concerns the bigger particles in higher concentrations, in this case the microorganisms, Brownian diffusion is negligible and the back diffusion is determined by the shear stress. Hence, cake layer build-up is described by the following material balance:

$$\frac{dm_{cells}^{c}}{A\,dt} = J c_{cells}^{bulk} - k_{mat}\left(c_{cells}^{c} - c_{cells}^{bulk}\right) \qquad (2.14)$$

where m_{cells}^{c} is the mass of the cake layer, J is the permeate flux, c_{cells}^{bulk} and c_{cells}^{c} are the concentration of bacteria in the bulk phase and on the cake, respectively, and k_{mat} is the overall mass transport coefficient, calculated with the same adimensional correlation for turbulent flux used for the concentration polarization resistance. In this case, the shear-induced diffusion coefficient is calculated applying the empirical equation proposed by Cho *et al.*:

$$D_{cells} = D' \cdot \dot{\gamma} \cdot (d_{cells})^2 \qquad (2.15)$$

where D' is the dimensionless diffusion coefficient, $\dot{\gamma}$ is the shear rate and d_{cells} is the particle diameter. The dimensionless coefficient depends on particle size under the limitation of diluted solution, and a list of tabulated values for different sizes is available [61].

The physical meaning of the predicted values is maintained introducing the following constrain:

$$\frac{dm_{cells}^{c}}{A\,dt} = J c_{cells}^{bulk} - k_{mat}\left(c_{cells}^{c} - c_{cells}^{bulk}\right) \geq 0 \qquad (2.16)$$

that simply guarantees that caking is an irreversible process, unless the filtration is stopped and the filter is regenerated. In fact, differently from the case of concentration polarization resistance, considering a "pseudo-steady-state" condition would give an unrealistic prediction of the fouling behaviour.

The bulk concentration of cells grows steadily, affecting the transport phenomena and consequently the permeate flux: because c_{cells}^{bulk} is far higher than the colloidal concentration, its variation causes appreciable changes. When it reaches a specific value that enhances the cake layer build-up (with a quick drop of permeate), filtration membranes must be cleaned.

The cells concentration on the cake, c_{cells}^{c}, is defined as:

$$c_{cells}^{c} = \rho_{cells}(1 - \varepsilon) \qquad (2.17)$$

where ρ_{cells} is the microorganisms wet-based density and ε is the cake porosity. Modern experimental techniques allow a precise measurement for bacterial density: for example, for yeast cell is around 1.10 g/mL [76], while for E. coli is 1.16 g/mL [77]. Cake porosity ε, instead, is a derived variable which cannot be measured directly, but is rather deduced from Carman-Kozeny relation (Eq. 2.10): the calculated value is thus affected by unavoidable experimental errors, but also by the fact that the Carman-Kozeny model was originally developed only for spheroidal and uncompressible particles [67]. Cake porosity is the third empirical parameter used in the developed model, described by its corresponding possibility distribution, shown in Fig. 2.4.

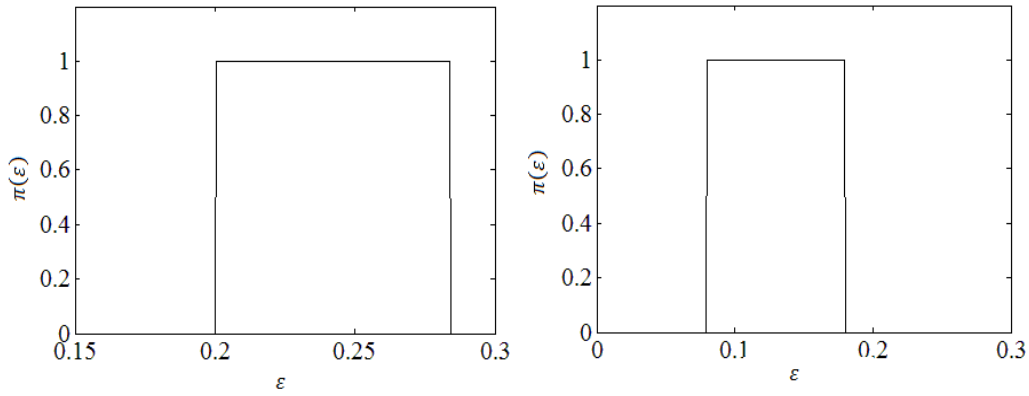

Figure 2.4: Possibility distribution of the cake porosity for spheroidal (left) and rod-shaped (right) microorganisms.

Geometrical considerations on the packing of particles allow setting a lower value to the epistemic distribution, while the little amount of data in literature [67] sets the upper.

2.2.5 Summary: fouling equations

Highlighting the main equations, widely discussed in the previous paragraphs, the final fouling system is the following:

$$\begin{cases} J(t) = \dfrac{\Delta P_{TM}}{\mu \cdot \left[R_m + \left(R_{ads}^{SS} + R_{pol}^{SS}\right) \cdot (1 - e^{-\beta t}) + \alpha_K \cdot {\Delta P_{TM}}^n \cdot \dfrac{m_{cells}}{A}\right]} \\ \dfrac{d(m_{cells}^c/A)}{dt} = J c_{cells}^{bulk} - k_{mat}\left(c_{cells}^c - c_{cells}^{bulk}\right) \end{cases} \tag{2.18}$$

The cells concentration of the bulk phase is determined using the proper material balances on the filtration equipment, thus different configurations lead to different resolutive systems. All the other quantities are calculated using the equations reported in the specific section. As mentioned before, the model requires three empirical parameters ($\Phi_x^{gel}/\Phi_x^{bulk}$, n, ε), whose epistemic distributions have already been described according to possibility theory.

2.3 Overall material balances

The material balances for the filtration units have been written according to the typical balance definition “Accumulation = Input – Output”, which considers the inlet streams as positive and the streams leaving the system as negative. Before writing mathematically the balances, the definition of the boundaries of the system is required, in order to define properly the involved mass flows. The governing equations, expressing the conservation laws, are added to the fouling system (Eq. 2.18), that is hence able to describe the real behaviour of the filtration equipment, in terms of permeate flux. In the context of this work, batch and fed-batch configurations have been studied, because of their relevance in industrial scale applications and commercial processes.

2.3.1 Batch configuration

The most common bioprocessing layout, particularly for small-scale applications, is batch configuration, shown in Fig. 2.5.

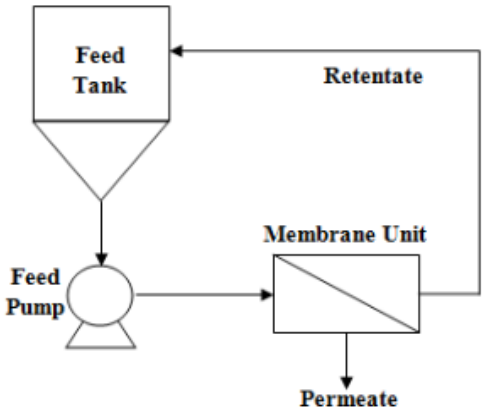

Figure 2.5: Batch configuration.

As complete cells retention is assumed, the material balance on the microorganisms in the bulk phase is the following:

$$\frac{d\left(c_{cells}^{bulk} \cdot V\right)}{dt} = 0 \tag{2.19}$$

The volume inside the filtration circuit will not be constant, due to the permeation, thus the material balance on the volume is:

$$\frac{dV}{dt} = -J(t) \cdot A \tag{2.20}$$

Using the differentiation product rule, Eq. 2.19 becomes:

$$V\frac{dc_{cells}^{bulk}}{dt} = -c_{cells}^{bulk}\frac{dV}{dt} \tag{2.21}$$

which correlates the loss of volume due to the permeate flux with the increasing concentration of the solution contained in the tank. The performance of a batch filtration unit is thus described combining Eq. 2.18 with 2.20 and 2.21:

$$\begin{cases} J(t) = \dfrac{\Delta P_{TM}}{\mu \cdot \left[R_m + \left(R_{ads}^{SS} + R_{pol}^{SS}\right) \cdot (1 - e^{-\beta t}) + \alpha_K \cdot {\Delta P_{TM}}^n \cdot \dfrac{m_{cells}}{A}\right]} \\ \dfrac{d(m_{cells}^c/A)}{dt} = Jc_{cells}^{bulk} - k_{mat}\left(c_{cells}^c - c_{cells}^{bulk}\right) \\ V\dfrac{dc_{cells}^{bulk}}{dt} = -c_{cells}^{bulk}\dfrac{dV}{dt} \\ \dfrac{dV}{dt} = -J(t) \cdot A \end{cases} \tag{2.22}$$

The solution of the system provides the permeate flux reduction curve.

2.3.2 Fed-batch configuration

For large-scale commercial processes or continuous applications, clear advantages offered by fed-batch configuration make it the most common industrial layout. As already mentioned (and shown in Fig. 1.9), two tanks of different sizes are employed to perform the separation, and the material balance on the microorganisms (in the retentate tank) is the following:

$$\frac{d\left(c_{cells}^{bulk} \cdot V\right)}{dt} = c_{cells}^{0} \cdot J(t) \cdot A \tag{2.23}$$

where c_{cells}^{0} is the constant cells concentration in the feed tank. This equation considers as inlet stream the feed that is pumped into the retentate tank at the same rate as permeate is withdrawn from the system. Because of this continuous addition of fresh solution, the volume in the circuit is kept constant:

$$\frac{dV}{dt} = 0 \tag{2.24}$$

The final system to be solved is:

$$\begin{cases} J(t) = \dfrac{\Delta P_{TM}}{\mu \cdot \left[R_m + \left(R_{ads}^{SS} + R_{pol}^{SS}\right) \cdot (1 - e^{-\beta t}) + \alpha_K \cdot {\Delta P_{TM}}^{n} \cdot \dfrac{m_{cells}}{A}\right]} \\ \dfrac{d(m_{cells}^{c}/A)}{dt} = J c_{cells}^{bulk} - k_{mat}\left(c_{cells}^{c} - c_{cells}^{bulk}\right) \\ \dfrac{dc_{cells}^{bulk}}{dt} = \dfrac{c_{cells}^{0}}{V} \cdot J(t) \cdot A \\ \dfrac{dV}{dt} = 0 \end{cases} \tag{2.25}$$

The main results provided by the system are the profiles of both permeate flux reduction and cells concentration inside the retentate tank, which should be kept under observation to optimize the filtration performances.

2.4 Numeric problem characterization

The resolutive systems written for batch (Eq. 2.22) and fed-batch configuration (Eq. 2.25) are composed of both algebraic and differential equations: the material balances on cells concentration, cake mass and overall volume are in differential form, while the Darcy-based expression for permeate flux is an algebraic equation. Mathematically, systems having this composition are referred to DAEs system and required particular tools in order to be solved, especially considering their stiffness and the presence of implicit functions: the interactions of several

multi-scale phenomena involving different time-scales provide a numerically complicated problem, that requires robust resolutive algorithms.

Usually, DAEs systems are solved combining ODE solver (as MATLAB® *ode15s*) with the mass matrix, whose diagonal values are equal to 1 for differential equations and 0 for algebraic ones. One of the major problems in the solution of DAEs is the necessity of consistent initial conditions, which means that initial conditions cannot be arbitrarily set and they must fulfill all the present constraints. The set of initial conditions adopted in this work will be discussed in Chapter 5, as well as the stopping criteria for the integration time.

Once the system is solved and the flux reduction profile is known, the average permeate flux is calculated, considering also the time for membrane cleaning, which reduces further the throughput. From this value, the number of required units for a target productivity is then obtained. A cost function based on literature data, discussed in Chapter 4, is implemented to evaluate the filtration expenses. However, uncertainty must be taken into consideration. Its propagation from the empirical parameters to the model output provides the possibility distribution (and the two corresponding limit cumulative density functions) of the average flux, that is then correlated to the cost of filtration via the cost function, in order to obtain an economic assessment and a more powerful “worst condition design” approach.

The implemented algorithm is summarized in Fig. 2.6.

The α-cuts method provides a MinMax problem, that is first solved using MATLAB® genetic algorithm. For each value of α, the DAEs system is solved twice in order to obtain both the minimum and maximum value of the objective function in the bounded domain. The iterative process builds up the possibility distribution of the average permeate flux, subsequently correlated to the cost function. The same approach has been applied using the *BzzMinimizationRobust* in C++ programming, obtaining identical results, but with a shorter computation time.

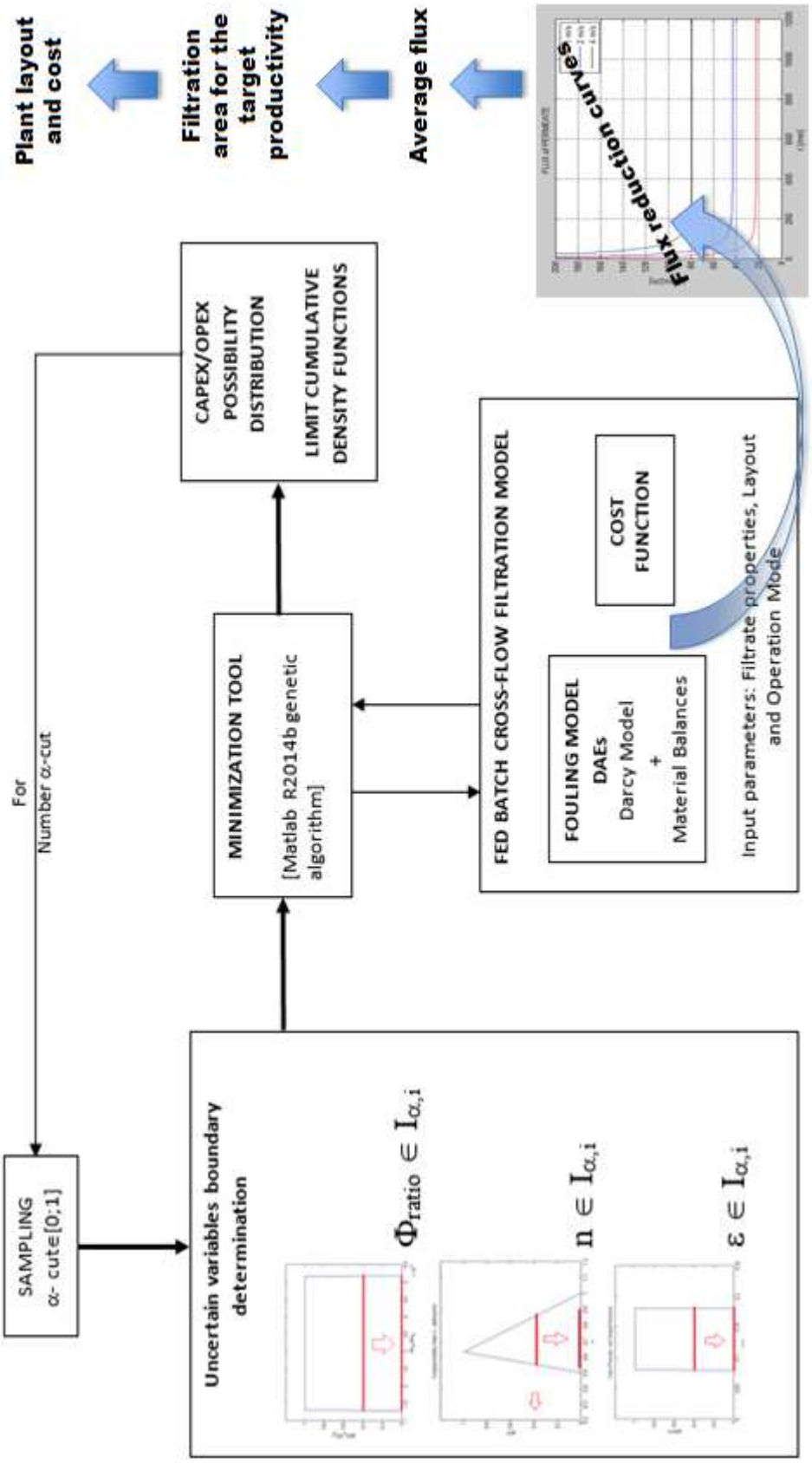

Figure 2.6: Algorithm scheme.

Chapter 3

Model validation

An industrial crossflow filtration unit is simulated using the proposed model, developed in the previous chapter, together with the data available from literature. The qualitative behaviour is established through the sensitive analysis of the main process variables, while the efficacy of the model is proved by the agreement between the simulated pilot plant and the measured values from previous works.

3.1 Pilot plant simulation

In order to prove the validity of the systems of equations proposed for batch and fed-batch configuration (Eqs. 2.22 and 2.25 of the previous chapter), they should be benchmarked with a real case study. In fact, before running the simulation, several data are required to characterize both the feed stream and the filtration unit, in terms of membrane features, modules rearrangement and operation mode. As already discussed, a ceramic membrane in a multi-channel tubular layout is employed in the context of this work, due to the clear advantages that it provides: it is suitable for fermentation broth clarifications, resistant to chemical cleaning, and more durable than plastic membranes. The selection of the feed to be processed, thus the final target of the simulated filtration operation, depends tightly on the availability of data from literature, both to describe the feed stream and to compare the model output with the experimental results. Their comparison provides

important information about the validity of this work and it is the only method to prove model applicability and feasibility. For this purpose, the proposed resistance-in-series model is tested considering the detailed experimental data provided in previous works, dealing with *L. delbrueckii* filtration for lactic acid production [7, 78, 79]. They described the batch downstream process of fermentation broth clarification in a pilot plant for recovery and purification of lactic acid, produced by fermentation. The feed characteristics and the membrane properties are listed in Tab. 3.1.

Table 3.1: Simulated fermentation broth characteristics and membrane properties.

Fermentation broth[a]		Membrane[b]	
Microorganism	*L. delbrueckii*	Shape	Tubular/multichannel
Shape	Rod	Channel diameter	5.75 mm
Size d/L	1/8 μm	Module length	1.178 m
Equivalent diameter	2.28 μm	Channels/module	7
Wet cell density	1100 kg/m^3	Total filtration area	0.1491 m^2
Wet cell concentration	2.6 kg/m^3	Material	Ceramic
Viscosity	0.78E-3 Pa s	Pore diameter	100 nm
Temperature	48 °C	Roughness height	5E-6 m
Permeate volume	11.26E-3 m^3/s	Membrane resistance	3.27E11 m^{-1}
Colloidal content	0.1-0.3 kg/m^3	Unit volume hold-up[c]	120 L
		Cleaning time[d]	20 minutes

a - Data from [7]

b - Commercial membrane Kerasep K01BX

c - Comprehensive of membranes, piping, pumps and retentate tank

d - Value reported in [47]

The main result of previous works was a semi empirical Darcy-based model able to fit the experimental data. However, that model relied on several empirical parameters, many of them determined by the particular configuration of the pilot plant. In particular, cake deposition and concentration polarization were described

using empirical correlations, with adaptive parameters, to determine the back diffusion phenomenon and the values of those resistances. The different descriptions of caking and polarization phenomena are the main novelty introduced by this work, where an accurate model based on material balances, thus with a sound physical interpretation, is used instead of experimental correlations.

The detailed data provided by these works, in terms of both permeate flux and resistances, are used as benchmark to test the predictive ability of the additive resistances model, developed in the context of this work. The simulated system involves a pilot plant with batch configuration. Thus, the developed model is here applied according to the batch material balances, providing the following resolutive system:

$$\begin{cases} J(t) = \dfrac{\Delta P_{TM}}{\mu \cdot \left[R_m + \left(R_{ads}^{SS} + R_{pol}^{SS}\right) \cdot (1 - e^{-\beta t}) + \alpha_K \cdot {\Delta P_{TM}}^{n} \cdot \dfrac{m_{cells}}{A}\right]} \\ \dfrac{d(m_{cells}^{c}/A)}{dt} = J c_{cells}^{bulk} - k_{mat}\left(c_{cells}^{c} - c_{cells}^{bulk}\right) \\ V \dfrac{d c_{cells}^{bulk}}{dt} = -c_{cells}^{bulk} \dfrac{dV}{dt} \\ \dfrac{dV}{dt} = -J(t) \cdot A \end{cases} \tag{2.22}$$

The corresponding initial conditions are:

$$\begin{cases} J(t_0) = J_{water} = \dfrac{\Delta P_{TM}}{\mu \cdot R_m} \\ m_{cells}^{c}(t_0) = 0 \\ c_{cells}^{bulk}(t_0) = c_{cells}^{0} \\ V(t_0) = V^0 \end{cases} \tag{3.1}$$

where J_{water} is the free water flow, measured when only clean water is filtered, and V^0 is the constant hold-up volume. When filtration starts, no particles are present on membrane surface, as it has been cleaned, thus the cake layer has not yet formed. It is important to remark that the system is composed of differential and algebraic equations (DAEs), whose initial conditions must be consistent: it means that the

condition set for the algebraic equation must fulfill the corresponding equation at initial time.

The solution of the DAEs system provides the permeate flux reduction profile, that could be compared with the experimental curves obtained from the above mentioned literature works. In order to achieve an accurate match, the available experimental points have been used to determine the three uncertain parameters required by the model (solidosity ratio, compressibility index and cake porosity). Thus, the uncertainty propagation in presence of experimentally calculated parameters will be studied in the next chapter (where the model is used in a predictive way). In particular, both the solidosity ratio and the cake porosity have been derived from the values of cake resistance and concentration polarization resistance, regressed by Carrère *et al.* [7]. On the other hand, the value of cake compressibility index provided by Carrère's work has been considered as the "most likely" during possibility distribution build-up. This value was determined from dead-end filtration experiments, involving the calculation of the specific cake resistance by comparing the resistance values deduced from the filtration of the clarified broth and the whole broth: the slope of the line correlating specific cake resistance with transmembrane pressure represented the cake compressibility index. It was found to be equal to 0.63, in the range of those reported by Tanaka *et al.* [69], i.e. from 0.5 to 1.

Table 3.2 summarizes the last fouling properties and the operating conditions that have been considered for the simulations. Once all the numerical values have been determined, it is possible to run the simulation of the pilot plant filtration unit, in order to quantitatively prove the validity of the proposed model. Results are then tested considering the experimental profiles obtained by Carrère *et al.* in their work. As reported in Fig. 3.1, the permeate flux reduction provided by the simulation is in good agreement with the experimental values, measured by Carrère *et al.* using the semi-empirical model, and an average error in the order of 6% has been calculated. The (small) deviation is explained looking at the different cake deposition and concentration polarization models: fully empirical equations based on experimental parameters have been replaced, in the context of this work, by a predictive scheme relying on the physical phenomena that occur on the membrane surface, i.e. material balances and back transport mechanisms.

Table 3.2: Fouling parameters and operating conditions for pilot plant simulation.

Reference	Parameter	Value	Notes
[7]	Specific cake resistance constant	1.20E+09 m/kg/Pa^n	Crossflow measurement
[7]	Compressibility index	0.63	Dead-end measurement
[54, 55]	Limit adsorption resistance	9 times R_m	Conservative value
[7]	Transient constant	3.00E-04 s^{-1}	Experimental evidence
	Operating conditions		
[7, 47]	Transmembrane pressure	2 bar	Industrial practice
[7, 47]	Crossflow velocity	4 m/s	Industrial practice

In addition, it is possible to notice that a “second” steep flux decrease is present and occurs for prolonged filtration operation: the model is able to predict the point at which the caking mechanism becomes dominant and rapidly stops the permeation, an aspect that is not so easily represented by the more recent filtration models [28]. The so-called *switch off condition* means that keeping on the filtration is no more convenient, as the membrane requires cleaning procedures, after which membrane surface is restored and filtration cycle could restart.

Reproducing the switch off condition is of prime importance not only to obtain an accurate description of the filtration behaviour, but also to design, and optimize, the alternation of filtration and washing cycles, required when the permeate flux is lower than a critical value. Filtration stopping criteria, due to membrane fouling, will be further discussed in the next chapters.

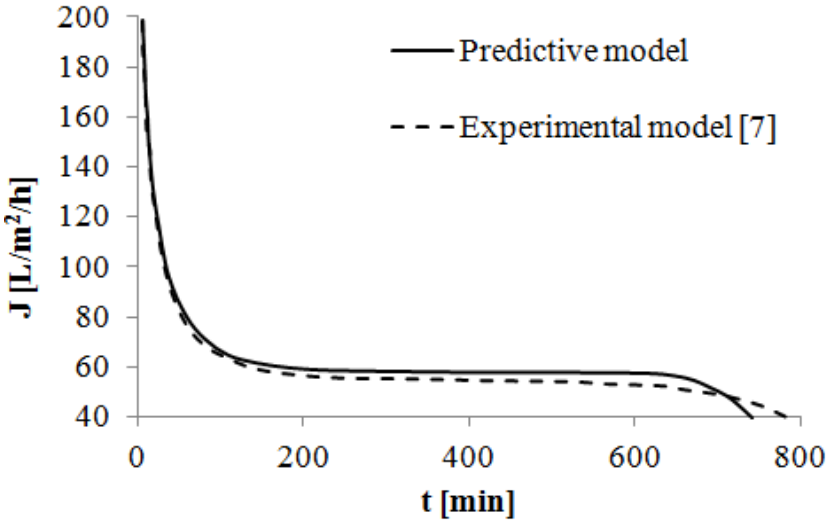

Figure 3.1: Flux reduction profiles for batch L. delbrueckii crossflow filtration.

3.2 Industrial crossflow filtration unit simulation

Once the model has been tested on real pilot plant data, hence its validity has been proved, it is possible to extend its applicability to different industrial filtrations. In particular, exploring a wider range of operating conditions would be of great interest, in order to understand the model flexibility outside the boundaries provided by the pilot plant simulation. For this task, some of the main operating variables have been changed, observing the model response in terms of filtration behaviour, i.e. permeate flux reduction profile. Most of the features listed in Tabs. 3.1 and 3.2 remain unchanged for this second simulation, but two important differences occur: since the technical characteristics of the hypothesized industrial filtration are intended to reproduce typical industrial settings, a bigger membrane unit is considered, characterized by 368 channels per module (instead of the 7-channels unit used for piloting), thus a higher filtration area is involved; in addition, a fed-batch operation mode with constant hold-up volume (as schematized in Fig. 3.2), is simulated, considered as the most common configuration for large-scale commercial processes.

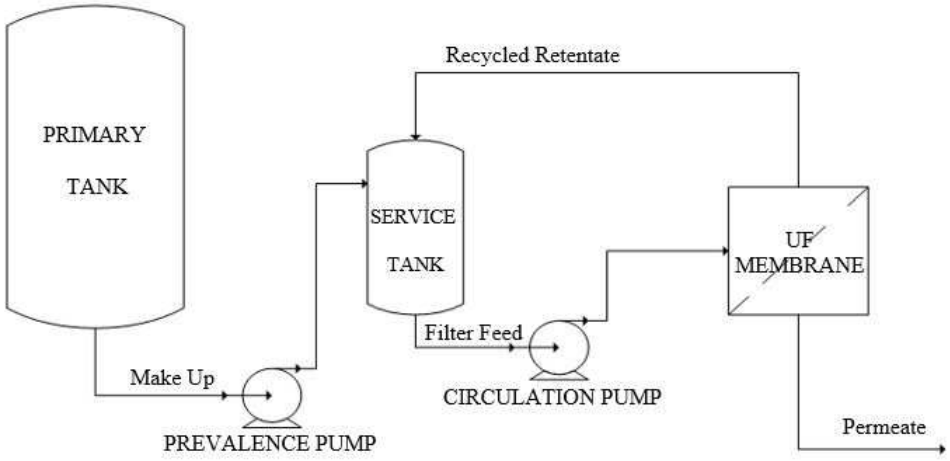

Figure 3.2: Simplified scheme of a fed-batch filtration unit.

Thus, according to fed-batch configuration material balances, the system to be solved is the following:

$$\begin{cases} J(t) = \dfrac{\Delta P_{TM}}{\mu \cdot \left[R_m + \left(R_{ads}^{SS} + R_{pol}^{SS}\right) \cdot (1 - e^{-\beta t}) + \alpha_K \cdot {\Delta P_{TM}}^n \cdot \dfrac{m_{cells}}{A}\right]} \\ \dfrac{d(m_{cells}^c/A)}{dt} = J c_{cells}^{bulk} - k_{mat}\left(c_{cells}^c - c_{cells}^{bulk}\right) \\ \dfrac{dc_{cells}^{bulk}}{dt} = \dfrac{c_{cells}^0}{V} \cdot J(t) \cdot A \\ \dfrac{dV}{dt} = 0 \end{cases} \tag{2.25}$$

having the same initial conditions set for batch configuration (Eq. 3.1).

For the pilot plant simulation, a transmembrane pressure of 2 bar and a crossflow velocity of 4 m/s have been hypothesized as operating conditions. A Montecarlo sampling is implemented in order to study the model sensitivity with respect to both pressure and velocity, investigating their thorough domains of variability: typical industrial values are comprised between 1-4 bar and 2-5 m/s (to ensure turbulence flow) for pressure and velocity, respectively [7, 47]. The main results of the sensitivity analysis are the qualitative behaviour and the response of the model to the change of the main macroscopic variables.

Fig. 3.3 depicts a sharp flux decline at low velocities. This trend is explained considering the role of crossflow velocity with respect to the membrane fouling

mechanism, particularly to cake deposition. As velocity increases, the cells back-transport from membrane surface to bulk becomes faster and it determines a lower cake thickness, that affects the overall cake resistance. In other words, higher tangential flow enhances the shear stress, that swipes away the rejected particles from the membrane surface, decreasing the resistance offered by the cake layer. For the same reason, concentration polarization resistance is lowered, although the effect has less importance. However, increasing crossflow velocity could result in a too short residence time, almost inadequate, besides affecting the overall process economics, increasing the pumping costs.

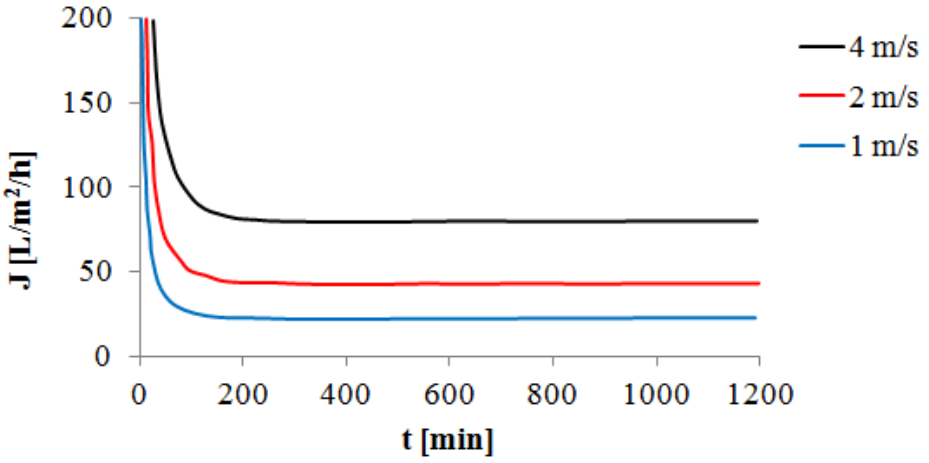

Figure 3.3: Modelled flux decline at different crossflow velocities.

The sensitivity analysis with respect to transmembrane pressure should result in a proportional variation of the permeate flux, as filtration units are pressure-driven systems: filtration performances are expected to increase with higher transmembrane pressure. However, because of the intrinsic complexity of membrane behaviour, a linear correlation between transmembrane pressure and permeate flux is not possible. In fact, higher pressure also acts on the cake compressibility, making the foulant layer on the membrane surface more compact and increasing, as consequence, the specific cake resistance. The model response to the changing pressure, shown in Fig. 3.4, respects this trend.

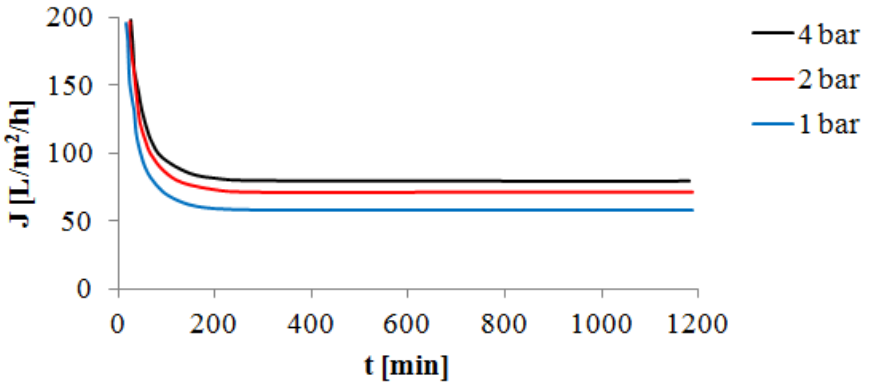

Figure 3.4: Modelled flux decline at different transmembrane pressures.

A further analysis involves the model response for different particle sizes, whose results are shown in Fig. 3.5. It points out that a strong deviation occurs for particles having 500 nm diameter. This anomaly is explained reminding that particles having diameter in the range of 500 nm belong to a transition region between two different mobility mechanisms, Brownian and shear-induced diffusion models. These particles have been considered as the main responsible for the concentration polarization resistance, since their accumulation causes the gel layer build-up, as discussed in Chapter 2.

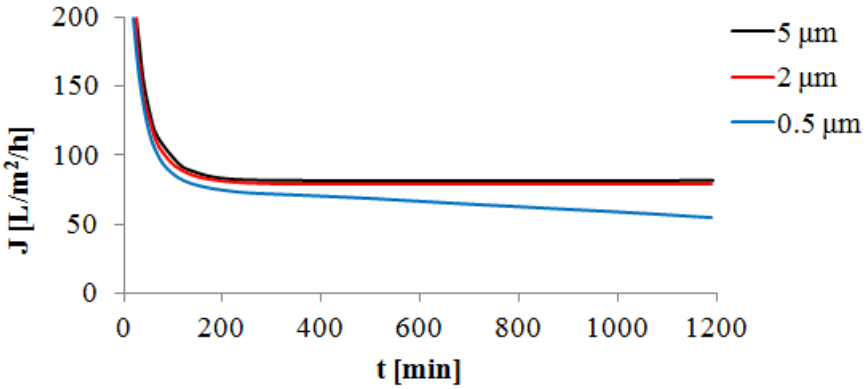

Figure 3.5: Modelled flux decline at different particle sizes.

When a fermentation broth with these characteristics (500 nm diameter bacteria) is simulated, the contributions of concentration polarization and caking resistance are overlapped, generating a different fouling behaviour. However, the size of industrially relevant bacteria is far above from the 500 nm value, thus the deviation

shown in Fig. 3.5 does not involve real situations, but it is important to underline the physical consistency of the developed model.

As in previous cases, the sensitivity analysis with respect to the main process variables provides positive information about the model validity: its behaviour in response to external change of operating conditions not only has physical meaning, but also confirms the expected trends.

When longer filtration time is considered, it is possible to notice that the permeate flux reduction profile assumes a particular shape, as shown in Fig 3.6.

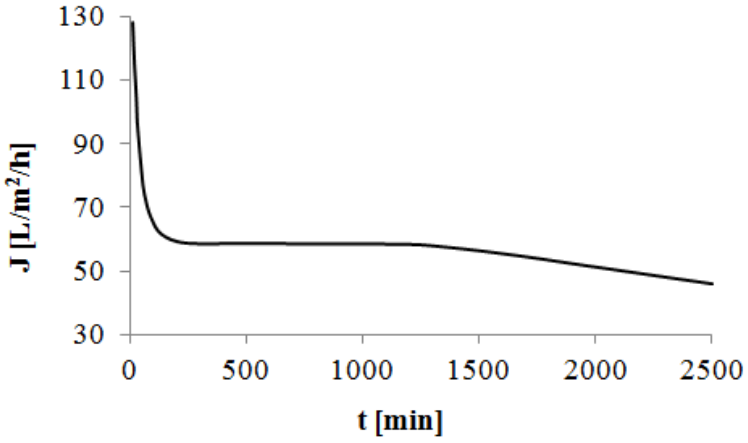

Figure 3.6: Flux profile and switch off condition.

The qualitative behaviour of the model has proven to be in line with the physical phenomena that occur during membrane filtration, and both the sensitivity analysis and the flux profile for longer operating time demonstrate the model predictive ability.

Proven the efficacy of the model in a “known” boundary, the next step involves the evaluation of its predictive ability associating the propagation of uncertainty. Before doing so, as the final purpose of this work requires economic assessments, it is necessary to implement a cost function, in order to correlate the model output, i.e. permeate flux, with filtration expenses.

Chapter 4

Cost estimation in microfiltration and ultrafiltration processes

In this chapter a cost function for microfiltration and ultrafiltration fed-batch processes is developed. It is obtained by coupling the amortized capital cost, due to the initial investment for membrane modules and associated equipments and facilities, with the annual operating costs involved in running the process.

Cost estimation is commonly led to compare the cost of membrane separation processes with alternative treatment technologies, and to evaluate different design options in order to provide better separation per unit cost. In the context of this work, apart from assessing the expenses related to the use of membrane filtration, cost evaluation facilitates the understanding of the uncertainty propagation effect, providing an “economic value” of the limited experimental knowledge: the uncertainty introduced by empirical parameters propagates through the model until reaching the permeate flux, and it is then correlated to economic assessments by means of the cost function, yielding easily legible and understandable results.

Estimating the capital and operating costs associated to membrane systems still remains a challenge: the development of an accurate cost model requires an industrial knowledge based on extensive experimentation and on-field experience, that obviously cannot be found in literature. Furthermore, historical cost data on

microfiltration and ultrafiltration facilities have been limited [80], though the number of published data has growth in recent years, due to the increasing interest on membrane separation processes. However, cost estimation is necessary for decision making and planning efforts, as well as for assessing the economic feasibility of a new process. Previous approaches for modeling the filtration cost typically present an overall cost function, depending on the main macroscopic variables, but this method does not provide any insight on the different economies of scale related to the involved manufactured equipment. In order to overcome this limitation, a model which incorporates individual cost correlations for the several categories of employed components has been implemented, as it is suitable to be used during design studies.

The economics of membrane systems are determined by the sum of the amortized cost of capital equipments, computed with established correlations able to describe the cost behaviour of individual components, and the various operating costs, that include expenses associated with energy requirement, maintenance, labour and chemicals for cleaning procedure. The permeate flux, which is governed by the different fouling mechanisms discussed in Chapter 2, is one of the major factors influencing the capital as well as the operating costs. Hence, membrane fouling translates into high treatment costs, by affecting membrane area and energy requirements. Apart from all the variables that act on the permeate flux reduction, the economics of filtration separations are also affected by membrane materials and characteristics, module geometry, plant layout, frequency of cleaning and other economic factors and operational parameters. Membrane performances are evaluated by the developed model, which provides the permeate flux reduction profile, while engineering design equations are used to determine the size and quantity of the plant components. In addition, parameters are required to define a case-study for which the costs are calculated. The values and ranges of parameters are obtained from vendor quotes and typical industrial practice, thus they are tightly dependent on the type of equipment employed in membrane filtration systems. Detailed descriptions of correlations, equations and operational parameters involved in the economic assessments of filtration units are further discussed in the next sections, dedicated to the estimation of the capital (Section 4.1) and operating (Section 4.2) costs associated with microfiltration and ultrafiltration.

Every membrane process has different characteristics, providing distinct cost compositions, but there are some aspects that are almost universal. All filtration systems have in common the economies of scale of membrane and equipments surrounding and supporting it, as well as the general trend contemplating a greater contribution of capital costs to the total filtration economics with respect to that of the operating costs. Although some cost data of microfiltration and ultrafiltration are now available, which correlate the total costs to plant capacity or installed membrane area [81-83], the economics of these technologies are currently not very well understood. The limited history of cost data [80] and the poor detailed cost estimates available in literature, due to the relative novelty of these processes, the complexity of crossflow operations, the fact that the economics are tightly application dependent, they all are the major obstacles to the development of overall trends, as it is difficult to generalize from available case studies.

In order to evaluate the treatment costs of filtration in this work, correlations and power law relationships have been employed, whose coefficients and exponents have been established by previous works [47, 80, 84] or handbooks [85].

4.1 Capital costs estimate and economies of scale

Capital costs represent the initial investment required to provide a given capacity for the plant production, and they are computed as the sum of the individual purchase costs of all of the equipment employed in running the process. Typically, all capital cost components are observed to scale directly with the plant size, and this economy of scale is represented in the form of a power law:

$$Cost = k \cdot (size)^n \tag{4.1}$$

The value of the exponent n expresses the manner in which the cost of an item increases with the size parameter, determining the behaviour of the associated incremental costs, defined as:

$$IC = \frac{d(cost)}{d(size)} = k \cdot n \cdot (size)^{n-1} \quad (4.2)$$

If $n = 1$, the incremental costs are constant and no economies of scale exist; if $n < 1$, then increasing the size results in a decrease in the incremental cost, and economies of scale are said to be realized with size.

Practically, each plan component presents a distinct value of the exponent n, reflecting the different economies of scale involved. Capital costs due to membrane and membrane-related equipment are thought to have values of n close to unit, demonstrating insignificant economy of scale; conversely, other equipment employed in membrane filtration separations are known to have cost functions with corresponding values of $n < 1$, thus the total capital costs associated with membrane facilities should exhibit economies of scale [84].

The different behaviour with respect to size parameter suggest the division of capital costs into non-membrane and membrane-related costs:

$$C_{CAP} = C_{membrane-related} + C_{non-membrane} \quad (4.3)$$

The distinction into these two main categories facilitates the identification of the several components that contribute to the total plant capital costs. In addition, it allows to group different equipment on the basis of the presence of economies of scale, simplifying the cost analysis and the development of cost correlations. The several individual components affecting both membrane-related and non-membrane capital costs are discussed hereafter.

4.1.1 Membrane-related capital costs

Membrane-related costs account for the membrane itself and the vessels required to hold the membrane, if applicable:

$$C_{membrane-related} = C_{mem} + C_{ves} \quad (4.4)$$

The capital cost attributable to the initial purchase of membrane modules is proportional to the installed membrane area, and it is expressed as follows:

$$C_{mem} = C_m \cdot A_{tot} \tag{4.5}$$

where C_m is the unit cost per square meter of membrane and A_{tot} is the total membrane area required to provide the design capacity.

The vessel cost is assumed to be a one-time cost, because membranes replacement does not require replacing the vessels. Polymeric membranes typically come with plastic housings, whose costs are included in the basic membrane costs, thus the vessels cost contribution is only applicable to the ceramic membranes. It is calculated as the product of the unit cost and the number of required membrane modules:

$$C_{ves} = C_v \cdot N_{units} \tag{4.6}$$

As expressed by Equations 4.5 and 4.6, the capital costs of a membrane plant are correlated to the total membrane area or to the number of membrane modules installed. Equivalently, they could be calculated relying on the design capacity of the plant, though producing limiting correlations unable to provide information on the involved design and operating parameters. For this reason, a cost function based on the design capacity as the independent parameter cannot be used to estimate capital costs for variable operating conditions. Conversely, design and operating variables play a major role in determining the number of membrane modules, hence the use of this size parameter could overcome the limitation related to the design capacity. However, a cost correlation formulated with the number of modules as independent variable is too specific, as it is valid only for a particular module with well-known characteristics (flow pattern, diameter, length, etc.). Since membrane modules have sizes depending on the manufacturer, a different correlation should be specified and used each time one module feature changes. Hence, the membrane area required to provide the desired capacity seems to be the most general and suitable size parameter to estimate the preliminary capital costs of the different components. Like the number of membrane modules, the final value of membrane area is a function of the design and operating variables, but it is versatile and easier to be used not depending on specific module characteristics.

The total area of membrane required to produce a given design flow Q_{target} is calculated from the ratio of the design capacity to the net permeate flux:

$$A_{tot} = \frac{Q_{target}}{J_{net}} \tag{4.7}$$

where J_{net} is the "real" flux of permeate, that accounts for the total time for one complete operating cycle, involving not only the filtration, but also the backwashing procedure. The prolonged time provides a net flux that is lower than the average flux, and defined as:

$$J_{net} = \bar{J} \cdot \frac{t_{fil}}{t_{op}} \tag{4.8}$$

where $\bar{J}$ is the time-averaged permeate flux during filtration, t_{fil} is the filtration time and t_{op} represents the total operational time, calculated as the sum of t_{fil} and the backwashing time, t_{bw}. Periodic backwashing of the membrane removes a portion of the materials accumulated on the membrane surface during filtration operations, and restores the plant performances.

Once the total membrane area is calculated, the number of membrane modules required to generate the desired flow rate can be determined using the following equation:

$$n_{mod} = NEAREST\ INTEGER\left(\frac{A_{tot}}{A_{mod}} + 0.5\right) \tag{4.9}$$

where A_{mod} is the surface area of membranes per module. In order to obtain an integer value, it is necessary to round the number of modules to the next highest integer. In this way, Eq. 4.9 provides the number of modules required to produce a flow at least as large as Q_{target}.

4.1.2 Non-membrane capital costs

The other main contributions, which are referred to as non-membrane capital costs, include all facilities and equipment necessary to support the use of membranes, such as pumps, instrumentation and controls, piping, valves, etc. Typically, non-membrane costs are assumed to scale directly with the plant size, and are estimated by fitting historical data and vendor quotes to power law correlations.

Previous works expressed the economies of scale correlating the non-membrane capital costs to the number of installed membrane modules [80], or using the more popular "six-tenths power rule" with design capacity as size parameter. In summary, the different studies result in economies of scale characterized by exponents n between 0.4 and 0.8, indicating that economies of scale should be realized as plant capacity increases. However, lumping together all non-membrane costs means losing insight on the distinct economies of scale of the individual components. For this reason, different cost correlations for major types of capital cost equipment are employed, whose factors have been established by previous works [84]. Non-membrane equipment and facilities are separated into different categories, including pipes and valves, instruments and controls, tanks and frames, miscellaneous, chemical cleaning devices, feed pumps and recirculating pumps:

$$C_{non-membrane} = C_{PV} + C_{IC} + C_{TF} + C_{MI} + C_{CC} + C_{FP} + C_{RP} \qquad (4.10)$$

Apart from pumps, which require a particular design parameter as discussed below, and chemicals used in cleaning procedure, the other cost components are expressed according to the power law relationship of Eq. 4.1. Thus, the costs associated with these categories are described by the following equations:

1. Pipes and valves

$$C_{PV} = k_{PV} \cdot (A_{tot})^{n_{PV}} \qquad (4.11)$$

2. Instruments and controls

$$C_{IC} = k_{IC} \cdot (A_{tot})^{n_{IC}} \qquad (4.12)$$

3. Tanks and frames

$$C_{TF} = k_{TF} \cdot (A_{tot})^{n_{TF}} \qquad (4.13)$$

4. Miscellaneous

$$C_{MI} = k_{MI} \cdot (A_{tot})^{n_{MI}} \qquad (4.14)$$

The miscellaneous category is defined to include all the other items that contribute to the plant costs, such as process equipment building, electrical supply and distribution, disinfection facilities, storage and recovery systems.

Leading coefficients and exponents representing the economies of scale of the different components are established by Sethi *et al.* [84], who collected membrane system cost data from different sources providing calibrated correlations. It is important to notice that the values of the exponent vary significantly for different cost categories, proving that each equipment has a distinct economy of scale. The values of exponents and constants for the categories of non-membrane equipment considered are summarized in Tab. 4.1.

Table 4.1: Exponents and constants associated with Eqs. 4.11 through 4.14.

Category	Exponent	Constant
Pipes and valves	$n_{PV} = 0.42$	$k_{PV} = 5926.13$
Instrumentation and controls	$n_{IC} = 0.66$	$k_{IC} = 1445.50$
Tanks and frames	$n_{TF} = 0.53$	$k_{TF} = 3047.21$
Miscellaneous	$n_{MI} = 0.57$	$k_{MI} = 7865.02$

Instead of the total area of membrane, pumps capital costs estimate requires a different design parameter, involving the product of pump flow and pressure. Hence, the power law relationship is the following:

$$C_{pump} = k_{pump}(flow\ rate \cdot pressure)^{n_{pump}} \tag{4.15}$$

In order to determine both the exponent and the leading coefficient of the cost correlation, the pump cost curve for general-purpose-single and two-stage-single-suction centrifugal pumps presented by Sethi *et al.* [84] is employed. It is expressed as:

$$C_{pump} = I \cdot f_1 \cdot f_2 \cdot C_{lab} \cdot 81.27 \cdot (Q \cdot P)^{0.39} \tag{4.16}$$

where I is the cost index ratio, necessary to update the cost to recent year; f_1 and f_2 are factors depending on the construction material and the suction pressure, respectively; C_{lab} is a factor used to incorporate labour cost; Q is the pump flow rate (expressed in m^3/h) and P is the pressure (in kPa).

Fig 4.1 shows the behaviour of the base pump cost (excluding the multipliers) with the size factor: the curve is based on Sethi's work, the base cost (C') is evaluated for the first quarter of 1979 and includes pump, drive, base plate and coupling.

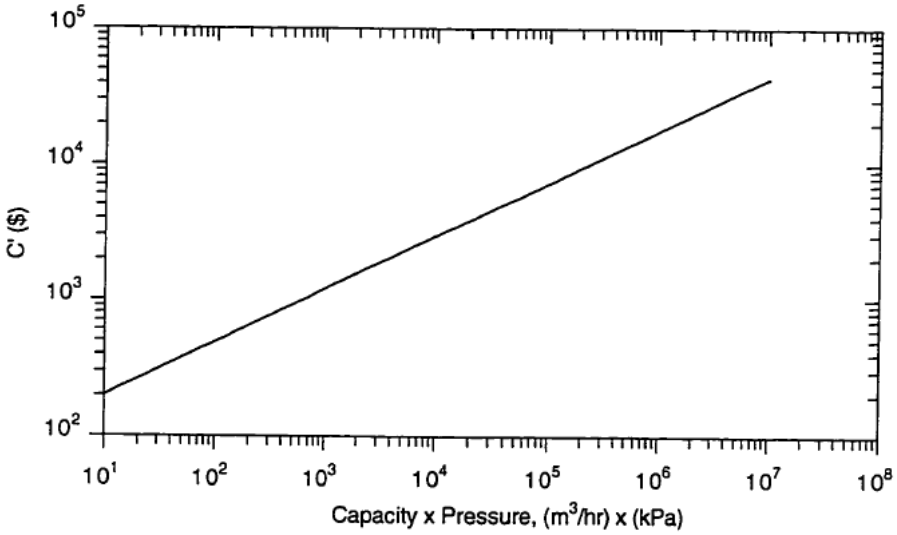

Figure 4.1: Behaviour of pump costs with size.

The cost index ratio I updates the base cost from January 1979 to recent years, in the case in analysis November 2014, found as the latest available index and thus selected as the base year for this work. It can be obtained from technical journals and periodicals such as "Chemical Engineering", which publishes pumps index on a regular basis. A value of $I = 3.53$ is applied to update the pump costs to November 2014.

The factors f_1 and f_2 are used to adjust for construction material and suction pressure range. Their values are reported in Tab. 4.2 and are discussed in detail in chemical engineers' handbooks. The simulations performed in this work involve stainless steel (316) surfaces and pressure below 150 psi (1034.5 kPa), since microfiltration and ultrafiltration are defined as low-pressure membrane separations, implying that $f_1 = 1.5$ and $f_2 = 1.0$ are assumed throughout this work.

Table 4.2: Material and suction pressure factors.

Factor	Value
Material factors f_1	
Ductile iron	1.0
304 stainless steel	1.4
316 stainless steel	1.5
Cd-4	1.6
Durimet 20	1.7
Titanium	3.0
Hastelloy C	3.7
Hastelloy B	4.1
Suction pressure factors f_2	
Up to 150 psi	1.0
150 - 500 psi	1.6
500 - 1000 psi	2.1

The factor C_{lab} accounts for labour costs, that are typically in the order of 40%, as reported for installation of manufactured equipment [47]. For this reason, a value of $C_{lab} = 1.4$ is employed.

The correlation expressed in Eq. 4.16, whose factors assume the values above mentioned, is used to evaluate the individual capital costs for both feed pump and recirculating pump. However, they refer to different values of the design parameter, since they operate in different conditions, in terms of flow rate and pressure. Engineering design equations are necessary to evaluate these quantities, as well as it is required to define properly the layout of the system. In order to avoid excessive complications, a simplified scheme is first considered in this chapter, as the actual purpose is the development of the cost function. For this task, a single-module configuration is employed, while a more suitable commercial layout is considered for the simulation of Chapter 5. This simplification facilitates the evaluation of pump flow rate, since the single-module layout involves only one feed pump and one recirculating pump.

The feed pump is sized so that it delivers the feed (make-up) solution to the retentate tank at the pressure required inside the membrane unit. For this reason, the transmembrane pressure is considered as the pump pressure, while the pump capacity equals the permeate flow rate leaving the system, calculated as:

$$Q_{feed} = Q_{perm} = J_{net} \cdot A_{mod} \tag{4.17}$$

Hence, the capital costs associated to the feed pumps are expressed as:

$$C_{fp} = I \cdot f_1 \cdot f_2 \cdot C_{lab} \cdot 81.27 \cdot \left(Q_{feed} \cdot \Delta P_{TM}\right)^{0.39} \tag{4.18}$$

The recirculating pump operates with the solution that is still present in the filtration cycle, and pumps it at a pressure equal to the pressure drops across the module. Thus, the recirculating pump capacity is given by a balance on the overall solution:

$$Q_{rec} = Q_{tot} - Q_{feed} \tag{4.19}$$

where the total volumetric flow rate Q_{tot} is necessary to maintain a high crossflow velocity through the channels. It is expressed as the product of the cross sectional area of the single channel, the number of channel and the crossflow velocity:

$$Q_{tot} = \pi \frac{d^2}{4} \cdot n_{\mathrm{ch}} \cdot v \tag{4.20}$$

The pressure drops across the membrane module are determined from classical theory describing a fluid flows in a pipe [84] :

$$P_{drops} = \frac{2f \cdot L \cdot \rho \cdot v^2}{d} \tag{4.21}$$

where f is the friction factor, L and d are the length and the diameter of the membrane module, ρ the density of the solution and v the crossflow velocity. The friction factor is calculated using the Blasius correlation for turbulent flow [85]:

$$f = 0.046 \cdot Re^{-0.2} \tag{4.22}$$

Hence, the estimation of capital costs for recirculating pumps is based on the following equation:

$$C_{rp} = I \cdot f_1 \cdot f_2 \cdot C_{lab} \cdot 81.27 \cdot \left(Q_{rec} \cdot P_{drop}\right)^{0.39} \quad (4.23)$$

The cost of the chemical cleaning devices is assumed to be constant and equal to $ 25000, based on typical industrial practice [47].

4.1.3 Annual capital costs

Once the cost correlations have been specified for each individual cost component, it is possible to calculate the total membrane-related and non-membrane cost contributions using Eqs. 4.4 and 4.10, whose sum represents the initial investment associated to membrane filtration unit (Eq. 4.3).

Capital costs are often reported as amortized values over the design life of the plant, in order to obtain an annual capital cost: it represents the yearly payment on the total capital costs over the plant lifespan at the annual interest rate. Annual capital costs are calculated as:

$$C_{CAP,ann} = C_{CAP} \cdot f_a \quad (4.24)$$

where f_a is the amortization factor. It is a function of both the interest rate, i, and the total number of yearly payments, n_y, according to the duration of the loan.
Hence, the amortization factor is defined as:

$$f_a = \frac{i}{1 - (1 + i)^{-n_y}} \quad (4.25)$$

The number of total payments n_y, expressed in years, represents the time over which the capital costs are amortized.

Eq. 4.24 results in a more useful indication of the total capital costs of a filtration unit, as the annual value can be directly compared with the amount of operating costs, providing a thorough assessment of plant economics.

4.2 Operating costs

Typically, for low-pressure processes like microfiltration and ultrafiltration, the operating cost contributions are dominated by the capital costs, particularly for small plant capacities. As size increases, the capital costs usually decrease due to the economies of scale involved, as discussed above, while the operating costs do not change, as they are not significantly affected by size plant. For this reason, operating costs can be expected to be comparable to capital costs at very high plant capacities.

The annual operating costs include expenses associated with energy requirements, labour and personnel, chemicals used for membrane cleaning and maintenance operations. As capital costs, they are computed as the sum of the different individual contributions, according to the following equation:

$$C_{OP} = C_{energy} + C_{sal} + C_{maint} + C_{clean} \tag{4.26}$$

Performing generic assessment of operating costs is a difficult task, as costs associated with energy as well as labour are highly dependent on factors such as geography, application, scale and type of membrane filtration process. In particular, the contribution of labour to the total operating costs may vary from negligible to dominant, based on plant location and scale. Although some cost contributions are highly application-specific, the typical percentages of each of these components to the total operating costs are listed in Tab 4.3 [22].

Table 4.3: Typical percent contributions to operating costs.

Operating cost item	% of total operating costs
Energy	45 - 60
Labour	25 - 35
Cleaning costs	5 - 30

This study does not include the membrane replacement cost, usually considered as an operating or variable cost rather than a periodic investment in capital: the contribution of replacing membrane to the total expenses is assumed to be negligible, as a ceramic membrane is employed, whose warranty offered by ceramic membrane manufacturers is currently 20 years. The most common reason leading to membrane module replacement is the loss of productivity due to irreversible fouling, but an accurate cleaning strategy as well as the use of proper chemicals can reduce this occurrence. In addition, the manufacturer estimates for membrane life are usually able to cover the filtration plant lifespan, thus avoiding the module replacement. According to these "practical" assumption, the equation that evaluates the operating costs does not take into consideration the contribution associated with the membrane module replacement, as expressed by Eq. 4.26.

A different situation emerges from employing polymeric membranes, whose life cycle is lower than ceramic ones, hence membrane replacement costs are in this case far from negligible, but even dominant in assessing the operating costs. Since the comparison of the performances of different membrane materials is not the purpose of this work, ceramic membranes only are considered in developing the cost function.

The different contributions to the total operating costs appearing in Eq. 4.26 are individually discussed in the following sections.

4.2.1 Energy cost

The total energy cost for a membrane unit depends mainly on the energy requirements for pumping the feed solution and recycling the retentate flow rate, i.e. the energy consumed by feed pumps and recirculating pumps:

$$C_{energy} = C_{OP,pump} = C_{fpw} + C_{rpw} \tag{4.27}$$

Each contribution is calculated as the product of the unit energy cost (UEC), considered as a constant value based on the average industrial electricity rates, and the pump work, as generically expressed by the following equation:

$$C_{OP,pump} = UEC \cdot W_{pump} \tag{4.28}$$

Pump work is proportional to the pressure and the flow rate of the fluid, according to Eq. 4.29:

$$W_{pump} = \frac{Q \cdot P}{\eta_{pump}} \tag{4.29}$$

where η_{pump} is the efficiency of the pump, expressed as a decimal fraction. The value of the pump efficiency is assumed to be equal to 0.8, a suitable value for industrial applications. As for pump capital costs, it is necessary to separate the contribution of feed and recirculating pumps, since they work in different conditions, involving different fluid velocities and pressures. The single-module configuration still holds, since it simplifies the evaluation of flow rates. In practical applications, more complex layout solutions are adopted, as further discussed in the next chapter, where a real plant will be simulated.

The energy consumed for pumping the feed solution depends on feed flow rate and pressure:

$$W_{fp} = \frac{Q_{feed} \cdot \Delta P_{TM}}{\eta_{pump}} \tag{4.30}$$

The energy requirements for the retentate recycle are calculated from the work done to compensate the pressure drops across the module and thereby maintain a proper crossflow velocity, thus involving the recycle flow rate:

$$W_{rp} = \frac{Q_{rec} \cdot P_{drop}}{\eta_{pump}} \tag{4.31}$$

According to Eq. 4.28, the energy costs for feed and recirculating pumps are hence calculated by multiplying the corresponding work with the unit energy cost, whose value is assumed to be equal to 0.1 $/kWh. It is based on a conservative approach that provides a higher value with respect to the average industrial electricity rates. It should be reminded that the electricity cost is strongly dependent on the plant location.

4.2.2 Labour cost

Typically, labour cost amounts to approximately 30% of operating costs [81], as summarized in Tab. 4.3. Labour contribution is simply calculated as the product of the number of personnel, n_{lab}, and the personnel salary per year, sal,:

$$C_{sal} = n_{lab} \cdot sal \tag{4.32}$$

The cost of labour associated with operating the filtration unit is highly application-specific. The trivial relationship expressed by the previous equation is, on the contrary, very insidious, as both the parameters depend on plant location and scale. Site-specific estimates are required to determine the number of employees, depending on plant size, and the personnel salary, which may vary significantly on geographical basis.

4.2.3 Cleaning and maintenance costs

Cleaning procedures are necessary to restore the membrane permeability and to control the membrane fouling, particularly foulant agents that are not removed by backwashing. The frequency of chemical cleaning is dependent on the operation of the plant, as well as on the average feed solution characteristics. Each cleaning cycle usually requires around 6 hours to complete, and the frequency ranges from once every 5 years to 50 times per year, with a median of 4 cleanings per year; recently, more frequent less extensive cleanings are becoming more common: their median frequency is once per day, and they typically last for 30 minutes to 1 hour [49].

Costs associated with cleanings include the costs of chemicals, as well as the expenses related to the aqueous waste disposal. It is common to recycle a large percentage of cleaning chemicals, in order to reduce the volume of waste, thus the associated costs. Quite often, most of washing liquors can be neutralized and discharged to the sewage system, with negligible costs. However, disposal must be carefully considered and applicable discharge regulations must be respected. Therefore, also the evaluation of chemical cleaning costs is affected by the plant location, as regulations differ depending on local laws.

In addition, there are a wide variety of chemicals that can be employed in cleaning operations, and they are usually combined in order to address multiple types of fouling. Hence, it is clear that no correlations are available to the estimate of cost associated with chemical cleaning. For this reason, a fixed cost is employed in the context of this work, whose value is calculated as an average cost for industrial chemical cleanings.

A similar approach is adopted in the evaluation of the maintenance cost contribution to the total operating expenses, as this estimate requires several historical data, as well as an intimate knowledge of the plant. From industrial practice, annual maintenance costs are calculated as a small percentage (usually around 1.5%) of the non-membrane capital costs.

4.3 Cost model limitations

The sum of annual capital costs and operating expenses yields the yearly total costs associated with microfiltration and ultrafiltration processes, according to the following equation:

$$C_{tot} = C_{CAP,ann} + C_{OP} \tag{4.33}$$

The model for both capital and operating costs presented hitherto can be used to produce preliminary estimates of filtration unit economics as a function of operating variables that are unique for low-pressure membrane systems.
In this task, it is subjected to some limitations:

- a cost model results in an approximate estimation of the real economics of industrial units, since power law relationships and average values have been considered in developing the cost correlations. Thus, the proposed cost function can be seen as a tool for preliminary cost estimates. To conduct more accurate cost assessments application-specific vendor quotes and parameters are required;

- the capital costs of pumps, tanks, piping and other equipment are modelled as continuous function in this application, while normally they are produced and sold in discrete sizes;

- the model presented here is specific for a particular combination of membrane material, type and industrial layout, i.e. ceramic membrane in a multi-channel tubular arrangement employed in a single-module fed-batch configuration. Every change in one of these features requires a model modification and a new analysis, since the range of configurations encompassed by this module is far from exhaustive;

- the cost estimates presented in this work have been generally developed following a conservative approach, usually adopted during early design stages.

Despite the several assumptions, simplifications and limitations associated to the cost model development, the calculated values are in line with industrial filtration costs, as will be seen in the next chapter.

It is important to notice that in studying the different cost correlations presented in this chapter, the year of the reference should be kept in mind in order to account for inflation, update quotes from manufacturers and other market parameters.

Chapter 5

Results

Results and discussion pertaining to all aspects investigated in this work are presented in this chapter. The different tools, analysed and discussed in the previous chapters, are combined here in simulating full scale filtration operations, in order to evaluate the model predictive ability. The fouling model developed in Chapter 2 is used to examine the flux reduction profile, which is then correlated to economic assessments using the cost function discussed in Chapter 4. Possibility theory is applied to study the uncertainty propagation to the model output, providing the range of variability of the upper costs of filtration processes. First, a full scale plant for lactic acid production is simulated, involving a *L. delbrueckii* broth clarification; then, the model applicability is extended to other systems, in order to prove the model flexibility in representing other microorganisms.

5.1 Full scale analysis of lactic acid filtration process

The resolutive algorithm including the fouling model, the cost function and the uncertainty propagation assessment is tested for a real industrial application, involving the simulation of a full scale plant. For this task, a lactic acid production process is chosen, since the whole set of data necessary to run the simulation is available from previous works [7,77,78]: it includes the membrane features, the

typical operating conditions and the bacterial strain characteristics, whose values have been determined from independent experiments and small-scale applications.

5.1.1 Uses and applications for lactic acid

Lactic acid is produced industrially by fermentation of carbohydrates or synthetic methods, and, due to the presence of a chiral carbon, it occurs as a racemate (DL) and in two optically active forms, as shown in Fig. 5.1. It is used in three main applications: foods (as salt), polymers (as poly ester) and in compounding in other specialty chemicals.

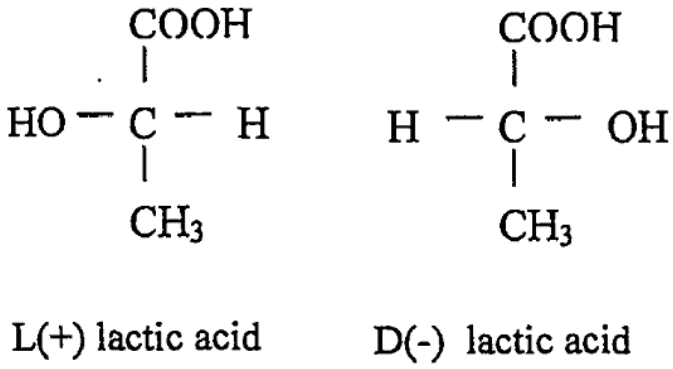

Figure 5.1: Structures and optical isomers of lactic acid.

Historically, food industry has been the largest consumer of lactic acid and lactate esters, as they are mainly used as acidulants and food preservatives. Lactic acid is a natural additive and has mild taste that does not overpower weaker flavours: it is encountered in variety of foods and beverages, as well as candies, meat and sauces. Another important application in food and drug industries includes the formation of calcium lactate to make calcium-enhanced products.

Lactic acid can be used as monomer for the production of polymers, such as polylactic acid or polylactide (PLA), and this route represents its faster growing use. PLA production starts from the condensation of two molecules of lactic acid, that produces a lactide, which is then employed via ring-opening polymerization in the formation of PLA, as schematized in Fig 5.2. The main applications of this polymer

are films for packaging as well as rigid containers for the food and the beverage industries.

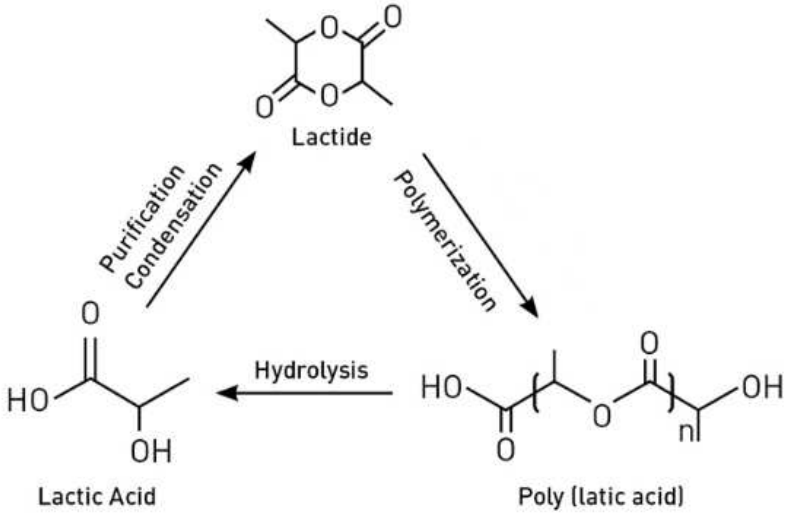

Figure 5.2: Polylactic acid (PLA) synthesis pathway.

Industrial uses of lactic acid and its derivatives include the manufacture of cosmetics, paints and inks, electronics and metal cleaning. They are also used in textile and leather industries and as animal feed in agriculture.

Since high chiral purity is required for the food and polymer markets, production by fermentation has increased over the last decade, because the highly enantiopure *L*-lactic acid is obtained following this approach. However, more efficient and economic downstream operations are necessary for the recovery of lactic acid in the case of production from fermentation, as the fermentation broth has a wide composition, characterized by the presence of various impurities, such as the by-products from the microorganism metabolism. Together with proteins, amino acids, sugars and organic acids, they have to be removed by suitable unit operations. Purification requirements may be minimal, as for certain food applications, or considerable, as for monomers for polylactide production. In all cases, fermentation broth clarification is the first step of the separation process, since the microorganisms must be removed from the product stream.

For this purpose, a wide availability of separation technologies exists. For example, traditional industrial bioprocesses perform the lactic acid extraction using precipitation stages, but high quantities of low-value by-product salt (calcium

sulphate, or gypsum) are produced, that must be treated as waste. In order to reduce the environmental impact, thus the overall economics of separation processes, alternative downstream configurations have been investigated. In this context, crossflow membrane filtration seems to be a suitable solution to perform the separation of the biomass from the fermentation broth, as it does not involve any adjuvant and avoids the formation of by-product salts.

5.1.2 Case study: *L. delbrueckii* filtration

A full scale plant for lactic acid production is simulated, starting from the experimental data reported for a pilot plant, involving the clarification of a *L. delbrueckii* fermentation broth. Since the purpose of this work concerns the development of a micro- and ultrafiltration predictive model able to estimate the process economics of this unit operation solely, the simulation neglects the further downstream processing. It means that the clarified stream is characterized by a minimal purity grade, as it still contains small solutes that are not eliminated in the first separation step.

Lactic acid production is briefly discussed, for the sake of completeness. The fermentation process requires carbohydrates, nutrients and microorganisms in order to produce lactic acid. Molasses are used as carbohydrates sources, while vitamins, peptides, amino acids, phosphate and ammonium salts are the nutrient required by microorganisms. A strain of *Lactobacillus delbrueckii* is employed for fermentation: these bacteria are rod-shaped with average size of 1 μm diameter and 8 μm length, as previously discussed. During fermentation, the pH of the system must be controlled, in order to avoid microorganisms inhibition. For this purpose, ammonium hydroxide is used to neutralized the lactic acid produced in the broth to adjust the pH in the range of 6.2 - 6.5. At these conditions, it is possible to obtain high lactic acid yields with respect to fermentable sugars, while the concentrations of by-products (mainly acetic and formic acid) are usually very low. The fermentation broth thus obtained contains the lactic acid together with a wide variety of compounds, having different characteristics.

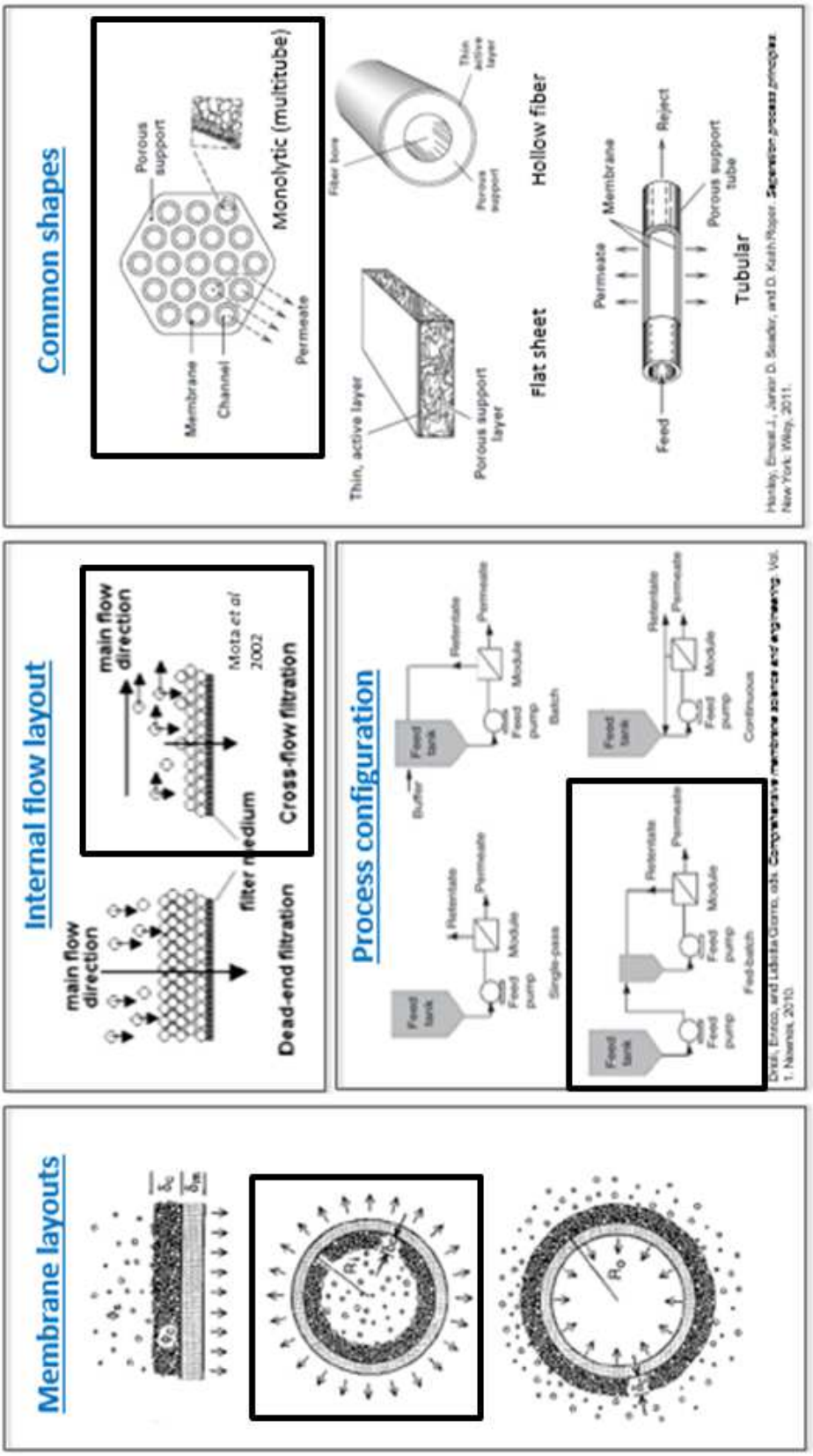

Figure 5.3: Summary of the possible plant specifications. The features adopted in the simulation are contained in the black boxes.

Separation and purification stages are carried out in the following plant section. The stream leaving the fermenter is fed to a crossflow filtration unit, where microorganisms are separated from the fermentation broth. The simulated membrane system is sized so that it ensures a productivity of 350000 m^3/year of permeate, corresponding to ca. 30000 ton/year of lactic acid. According to Carrère *et al.* [7, 79], the fermentation broth is characterized by a cell concentration of 2.6 kg/m3, as wet cell concentration. The fed-batch configuration is adopted to perform the separation, as it represents the typical industrial layout for commercial units. Fig. 5.3 highlights the filtration unit features that have been adopted in running the simulation: the plant involves the fed-batch crossflow filtration, using multi-channel tubular modules of ceramic membranes.

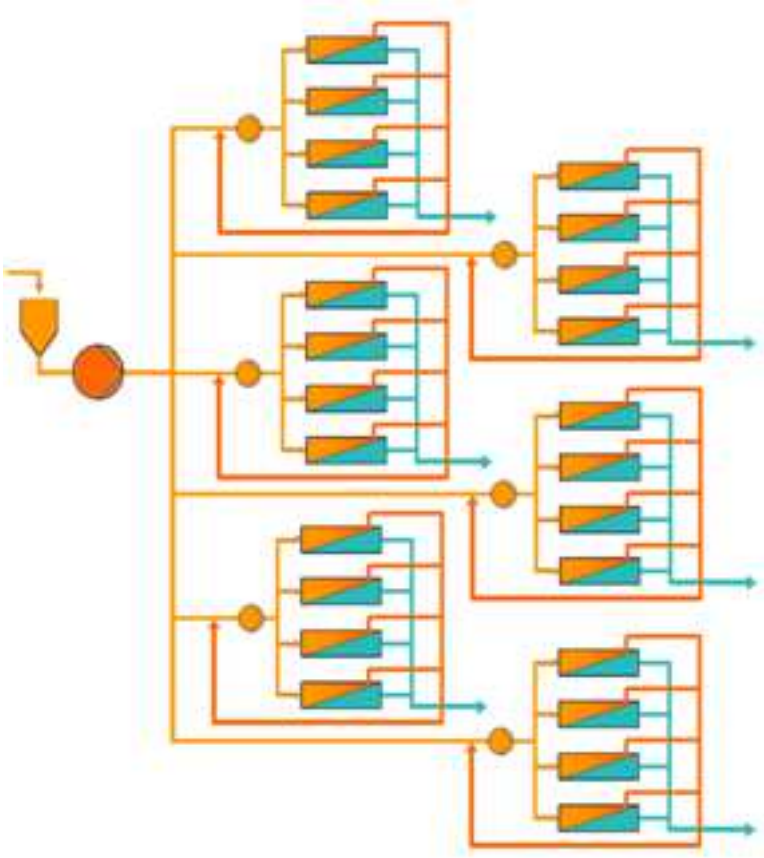

Figure 5.4: Schematization of the simulated plant disposition.

In the previous chapter a single-module configuration has been hypothesized, involving two pumps (feed and recirculating pump, respectively) for each membrane

module; however, this configuration is far from applicable in real filtration, where more complex dispositions have been developed, in order to optimize the pumping expenses, e.g. multiple array with booster pumps, Christmas-tree network, etc. Since this level of detail is not advisable during conceptual design, a simplified layout is adopted in the context of this work, where each feed pump is assumed to serve 24 parallel membrane modules, while each recirculating pump 4 modules, as schematized in Fig. 5.4. Using a different disposition with respect to that adopted in developing the cost function requires the correction of the pumps cost correlations, thus considering the effective flow rate and the number of feed and recirculating pumps involved: it is a trivial multiplication between the flow rate of a single module and the number of modules served by the corresponding pump. The configuration of the plant, shown in Fig. 5.4, seems to be in line with the typical commercial unit layouts, where the number of recirculating and feed pumps is below the number of modules, as can be seen in Fig. 5.5, where commercial filtration units are showed.

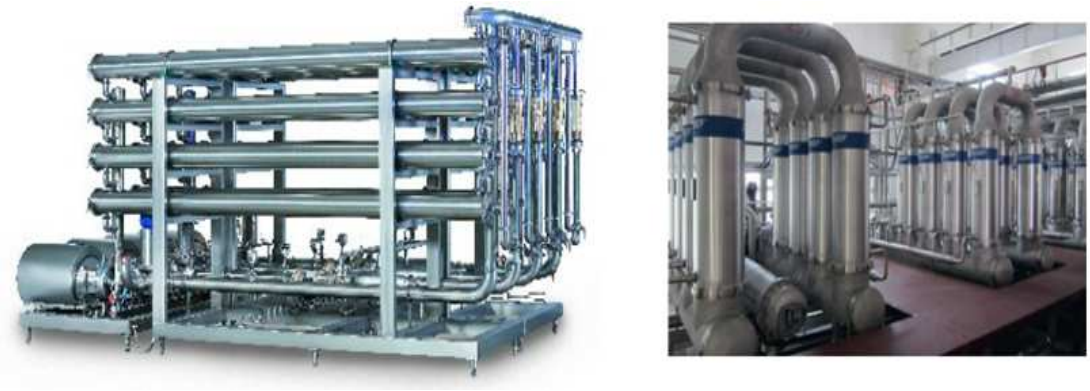

Figure 5.5: Industrial crossflow filtration units.

According to the selected plant configuration, the additive resistance Darcy-based model, developed in Chapter 2, is applied in order to determine the flux reduction profile associated with the proposed filtration unit. The simulation solves the system of differential and algebraic equations (DAEs) for fed-batch operating mode with constant hold-up volume, summarized as follows:

$$\begin{cases} J(t) = \dfrac{\Delta P_{TM}}{\mu \cdot \left[R_m + \left(R_{ads}^{SS} + R_{pol}^{SS}\right) \cdot (1 - e^{-\beta t}) + \alpha_K \cdot {\Delta P_{TM}}^n \cdot \dfrac{m_{cells}}{A}\right]} \\ \dfrac{d(m_{cells}^c/A)}{dt} = J c_{cells}^{bulk} - k_{mat}\left(c_{cells}^c - c_{cells}^{bulk}\right) \\ \dfrac{dc_{cells}^{bulk}}{dt} = \dfrac{c_{cells}^0}{V} \cdot J(t) \cdot A \\ \dfrac{dV}{dt} = 0 \end{cases} \tag{5.1}$$

The solution of the simulation depends on the set of initial conditions associated with the system, which is the following:

$$\begin{cases} J(t_0) = J_{water} = \dfrac{\Delta P_{TM}}{\mu \cdot R_m} \\ m_{cells}^c(t_0) = 0 \\ c_{cells}^{bulk}(t_0) = c_{cells}^0 \\ V(t_0) = V^0 \end{cases} \tag{5.2}$$

whose meaning has been already discussed in Chapter 3.

Based on industrial practice, the integration time is stopped, i.e. membrane cleaning is considered, when one of the following stopping criteria is reached:

- the permeate flux is 10% the initial value (free water flow);
- the final bulk cell concentration is eight time the initial value (87.5% permeate recovery);
- the time limit of 20 hours is reached.

Operation stops when carrying out the filtration is no more convenient, due to either the low permeate flux, which can be restored via membrane cleaning procedures, or the high viscosity of the recirculating solution inside the filtration cycle. If none of them occurs, then filtration lasts for 20 hours. These stopping criteria have been considered in running the simulation and implemented in the resolutive algorithm.

A transmembrane pressure of 2 bar and a crossflow velocity of 4 m/s are hypothesized as operating variables, as these values are intended to reproduce typical industrial settings. The membrane features and the fermentation broth

characteristics adopted in the full scale plant simulation are the same summarized in Tab. 3.1, previously considered to perform the sensitivity analysis (Section 3.1). All the numeric values of the quantities used in the simulation are listed in Appendix A.

It is important to remind that the system of equations describing the permeate flux reduction profile has been developed with the aid of three empirical parameters, affected by epistemic uncertainty. In order to overcome the tricky estimates of their values, statistical concepts from the field of Possibility theory have been adopted, as already discussed. The uncertainties associated with solidosity ratio $\Phi_x^{gel}/\Phi_x^{bulk}$, cake compressibility index n and cake porosity ε are represented according to possibility distributions, whose shapes are summarized in Fig. 5.6.

The way in which uncertainty propagates from empirical parameters to the model output is analyzed according to the α–cuts method, directly derived from the extension principle of fuzzy set theory, as discussed in Section 1.4. In broad terms, the range of variability of the three uncertain parameters is built for each value of α–cut, providing the corresponding interval for the model output; following this iterative mechanism, the uncertainty of the input variables is used to obtain the possibility distributions of the final results.

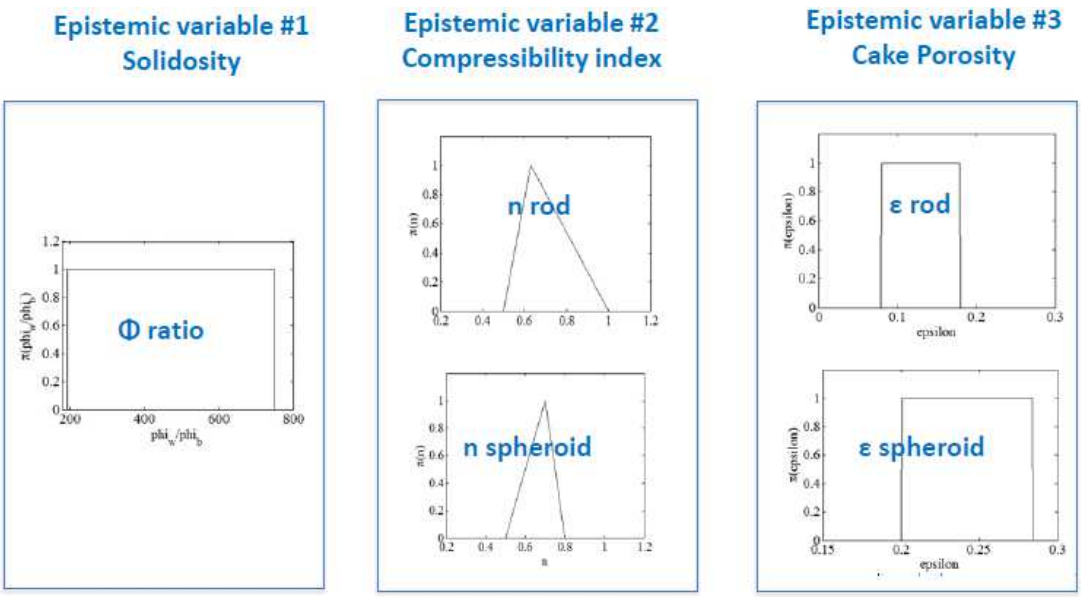

Figure 5.6: Summary of possibility distributions of the empirical parameters for spheroid and rod-shaped bacteria.

Given a value for the α–cut, the simulation can solve the DAEs system providing the associated permeate flux reduction profile, from which it is possible to calculate the "real" average flux J_{net}, considering the total time for a complete operation cycle (the corresponding equations have been already discussed in Section 4.1.1). In reality, the DAEs system is solved twice for each single value of α–cut, since the simulation requires the estimate of both the limit values, according to the MinMax problem. Iterating for all the set of α–cuts provides the uncertainty profile of the real average flux, in terms of its possibility distribution.

A MATLAB® built-in genetic algorithm has been applied to solve the MinMax problem, using *ode15s* with mass matrix as solver for the stiff DAEs system. Simulation characteristics are listed in Appendix A, together with numerical data. As the implemented algorithm was time-demanding and computationally intensive, a more efficient approach has been considered, based on the *BzzMath* library involving C++ programming. The use of a robust optimization algorithm as *BzzMinimizationRobust* for the minimization problem provides the same shape of possibility distributions, despite requiring less computing time.

The uncertainty propagation results in a more conservative value of the permeate flux, as the possibility distribution of Fig. 5.7 shows. The "reasonable" flux spans between 26 and 53 L/m^2/h, with the most likely value around 36 L/m^2/h.

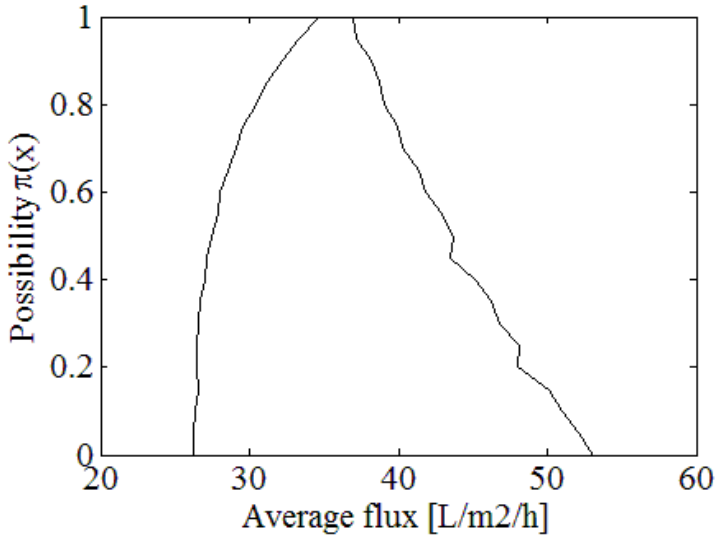

Figure 5.7: Average permeate flux possibility distribution for the full-scale fed-batch filtration of L. delbrueckii fermentation broth.

Once the model has provided the permeate flux reduction profile, thus the real average flux is known, it is possible to correlate the filtration unit performance to economic assessments, using Eqs. 4.7 and 4.9 in order to determine, respectively, the total area of membrane and the number of modules required to produce the given design flow rate. These quantities are the size parameters used as input variables for the cost function. Since the concept of possibility distribution still holds for the average flux J_{net}, then the cost estimates are affected by the same uncertainty. The whole set of numerical data employed to estimate the filtration expenses is listed in Appendix B. Fig. 5.8 shows the estimated annualized costs as a possibility distribution.

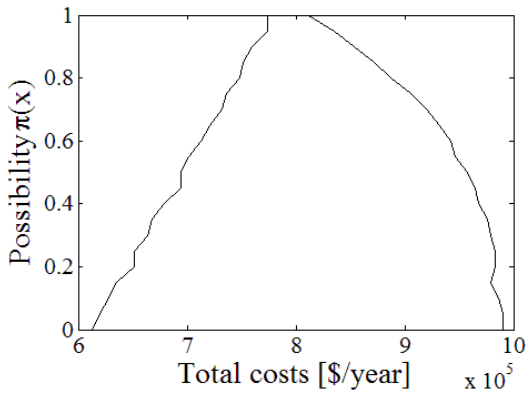

Figure 5.8: Cost possibility distribution associated to the fed-batch full-scale filtration plant.

Results can also be represented through the corresponding limit cumulative density functions (CDF), whose main advantage is providing an easier interpretation of the data: in terms of cumulative probability, it is possible to say that, given a certain level of confidence, the higher cost limits of the proposed fed-batch filtration plant will be comprised between two fixed values. The CDF representation (Fig. 5.9) sets the range of variability of the upper costs of filtration between 774000 $/year and 986000 $/year, with a 95% of confidence, while possibility distribution provides a total cost around 800000 $/year as most likely value. A purely conservative approach would take the value of 986000 $/year as the final estimate to be included in the feasibility study considerations; the application of Possibility theory, instead, includes the extra information that an amount of 212000 $/year is

the contribution of the lack of knowledge on the system, thus the economic risk due to the limited experimental knowledge.

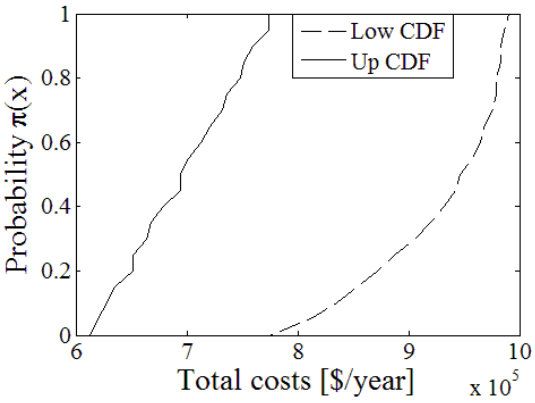

Figure 5.9: Limit cumulative probability functions (CDF) associated with cost assessments of the proposed full-scale filtration plant.

Since a conservative approach has been followed for both the model development and the correlation to cost assessments, the simulation yields conservative cost estimates, as desirable in conceptual design evaluations, that are however in line with typical cost values of similar industrial applications. The resulting costs composition respects the general trend contemplating a contribution of capital cost higher than that of operating expenses, showing an average composition based on capital costs for the 63% and operating costs for the 37%. A detailed partition of cost contributions is shown in Fig. 5.10.

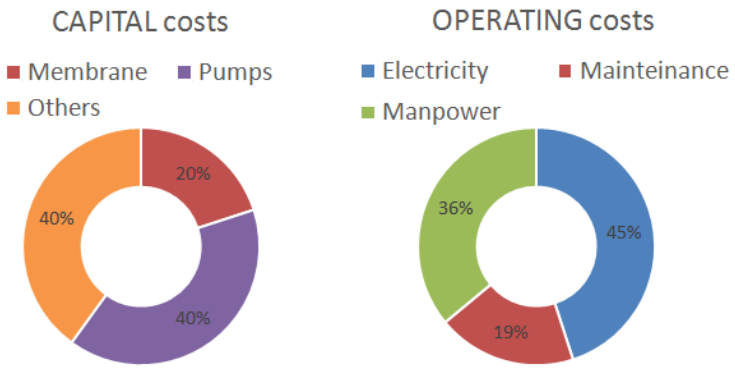

Figure 5.10: Average composition for both capital (left) and operating (right) costs.

Membrane system costs are most commonly described in terms of total production cost per volume of permeate produced, thus this quantity is used as main variable to compare the proposed plant to other similar filtration applications. The total cost per unit volume of permeate is defined as the sum of the amortized capital cost and the annual operating cost per volume of permeate produced and is obtained by simply dividing the limit cost values resulting from the simulation with the target productivity of the plant: hence the filtration costs of permeate spans between 2.21 $\$/m^3$ and 2.82 $\$/m^3$. Despite the poor availability of filtration plants economics, the model predictive ability has been first tested by comparing the obtained range of filtration cost with the generalized cost curves used to evaluate membrane filtration facilities expenses in water treatment applications [86]. Fig. 5.11 includes curves for high, medium and low fluxes, as both capital and operating costs vary with the flux at which system is operated. Using the given design capacity of the plant, a total cost of 1.45 $\$/m^3$ is obtained for high flux, corresponding to 2.10 $\$/m^3$ considering the above mentioned cost composition.

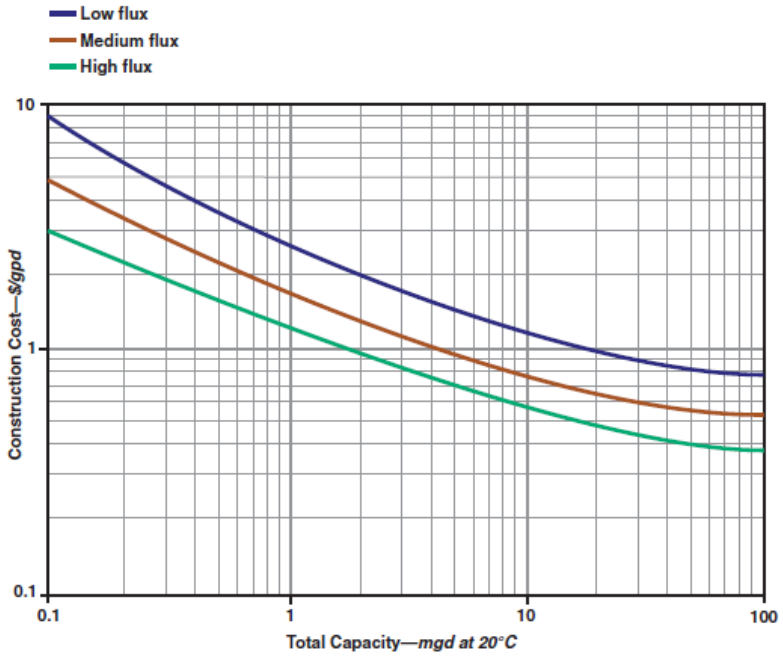

Figure 5.11: Generalized cost curves for membrane filtration facilities, correlating the plant capacity (in mgd, millions of gallons per day) to the unit volume cost (in dollars per gallons per day).

Model validity has been further proved by the comparison with wine filtration costs, assessed around 1.80 $/m^3 [1].

5.2 Extension to other applications

In order to better assess the potential of the model, the same full-scale fed-batch plant configuration has been simulated for different bacterial strains, to check the model applicability to other industrial filtrations. For this task, clarifications of *Saccharomyces cerevisiae* and *Escherichia coli* fermentation broths have been considered for simulation, as these microorganisms are industrially relevant. In these cases no pilot plant benchmark is possible for a lack of data. For this reason the only purpose is to show the effects on the output uncertainty by changing the uncertainty of the input parameters.

The microorganisms characteristics adopted to run the simulations and other parameters are listed in Appendix C.

5.2.1 Clarification of *S. cerevisiae* fermentation broth

Baker's yeast is widely used in industrial biotech and its filtration behaviour has been well investigated [67-70]. Typically, cells are compressible, spherically shaped with an average cell size of 5 μm [67] and a density of 1.10 g/mL [76]. The values of cake compressibility index and cake porosity are represented also in this case by different possibility distributions, shown in Fig. 5.12. According to literature data, compressibility index is represented using a triangular distribution, while a rectangular shape is adopted to describe the cake porosity, as already discussed in Chapter 2.

[1] http://www.bared.it/prodotti/filtrazione-tangenziale-a-membrana/

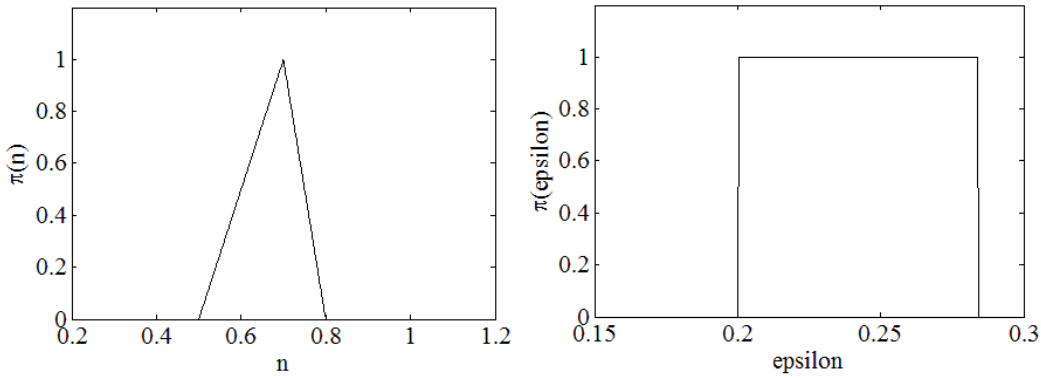

Figure 5.12: Cake compressibility index (left) and cake porosity (right) possibility distributions of S. cerevisiae.

The full-scale fed-batch clarification of the *S. cerevisiae* fermentation broth has been simulated keeping constant the membrane features, the plant configuration and the operating conditions adopted for the lactic acid production plant; the only variables that differ rely on microorganisms characteristics and possibility distributions of the input parameters. The less broad cake compressibility index distribution denotes a higher agreement between literature data. This is reflected by the simulation results, represented in terms of limit cumulative density functions in Fig. 5.13.

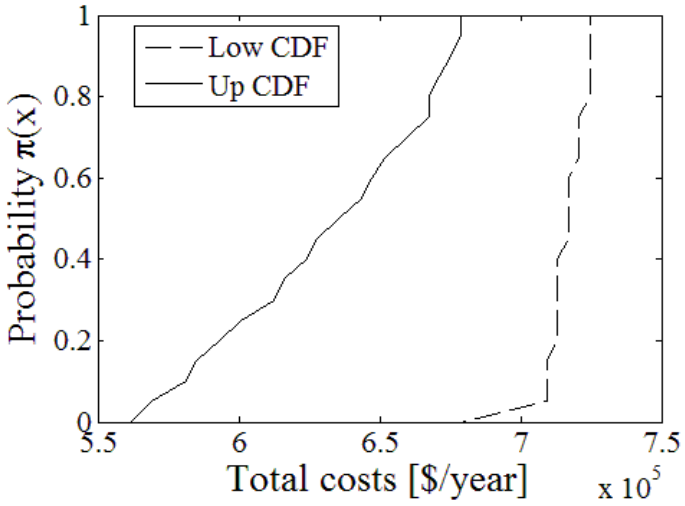

Figure 5.13: Limit cumulative probability functions for a full-scale fed-batch clarification of S. cerevisiae fermentation broth.

It is evident how the span between the limit upper filtration costs is reduced if compared to the previous simulation, where a larger possibility distribution of the input parameter (cake compressibility index) gave a wider range of costs variability. For *S. cerevisiae* filtration, the better knowledge of the system, thus the narrower shape of the possibility distribution (Fig. 5.12 left), reduces the "impact of uncertainty" to only 47000 $/year (with the 95% of confidence), as shown in Fig. 5.13.

5.2.2 Clarification of *E. coli* fermentation broth

E. coli is a rod shaped bacterium, which complicates the packing properties: its filtration behaviour should be studied on a case-by-case basis, also because different filtration conditions, and the inner variability of the strain (depending on the type of strain, growth conditions, etc.), add great variability to the downstream performances. These difficulties are reflected by the possibility distributions associated with the empirical parameters of *E. coli*, i.e. cake compressibility index and porosity. The first one is described using a rectangular shape, bounded by the lowest and highest values available in literature (Fig. 5.14), in absence of the more detailed data of *S. cerevisiae*. Cake porosity for rod-like particles has been already discussed for lactic acid production, thus the same possibility distribution is considered.

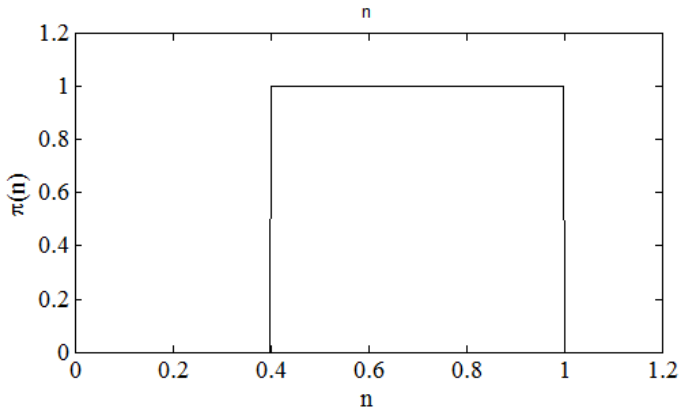

Figure 5.14: Cake compressibility index possibility distribution for E. coli.

Once the different uncertainties of the input parameters have been represented, it is possible to run the simulation using the available data for *E. coli*. Results are represented through the limit cumulative density functions, shown in Fig. 5.15.

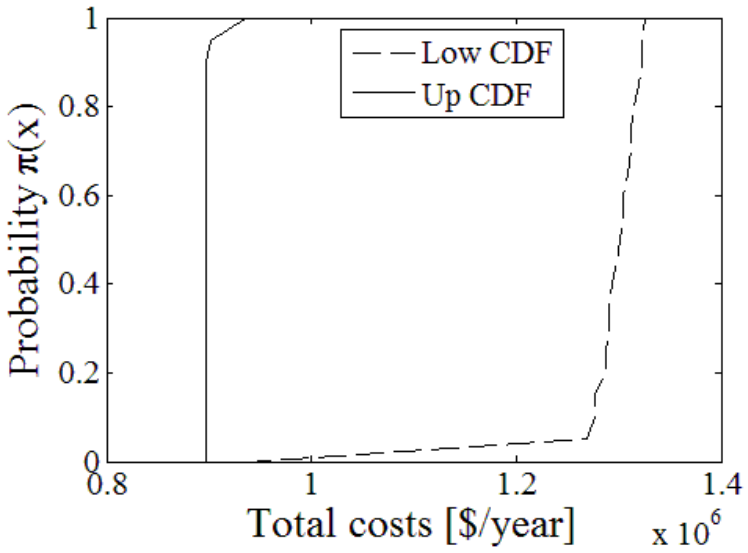

Figure 5.15: Limit cumulative probability functions for a full-scale fed-batch clarification of E. coli fermentation broth.

The shape of uncertain profile of input parameters directly affects the possibility distribution and the CDF representation of model output. As expected, a wider span for the limit cumulate cost is obtained, due to the poorness of available data. For *E. coli* filtration, the lack of experimental knowledge provides a wider range of upper cost variability, which amounts to 422000 $/year.

Chapter 6

Conclusions

This thesis work has the main purpose to evaluate a new conceptual design and cost estimation approach for crossflow filtration units, relying on the combination of a predictive permeate flux reduction model and an uncertainty propagation analysis based on fuzzy logic theory. A simple and general formulation of the Darcy's law with additive resistance contributions has been preferred for its validity in many applications in order to describe the permeate flux reduction profile of a filtration unit. The empirical parameters required by the model, characterized by an uncertainty deriving from model and measurement approximations, have been treated with statistical methods from the field of Possibility theory, which applies the extension principle of fuzzy set theory to estimate the uncertainty propagation from input parameters to the final overall economics. In this way the model can be applied for predictive filtration simulations, further providing an indication of the contribution of uncertainty to the final result.

The clarification of a *L. delbrueckii* fermentation broth for lactic acid production has been selected as benchmark to test the validity of the model, since the data for a pilot plant were available from literature. A conservative approach has been adopted during modelling (of both the physical phenomena and the cost function), and the results have proven to be in line with experimental data. The model, though simplified, is able to reproduce properly the data provided by the pilot plant experimentation, whilst being more flexible and general than other models presented in literature. Once a good agreement with experimental points has

been achieved, the model has been used to analyse a biorefinery case study, involving the simulation of a full-scale filtration plant, having a target productivity of 30000 ton/year of lactic acid. Membrane unit performance, described through the permeate flux reduction profile, is the main model output, then has been correlated to economic estimates via a cost function, developed relying on empirical cost correlations. The proposed algorithm solves the system of equations, describing the filtration unit, with the associated uncertainty propagation. The simulation yields conservative results: the average permeate flux spans between 26 and 53 $L/m^2/h$, with the most "reasonable" value around 36 $L/m^2/h$. In terms of economic assessment, it means that the higher cost limits of the proposed filtration plant are comprised between 774000 and 986000 $/year, providing the extra information that an amount of 212000 $/year is the contribution of the lack of knowledge on the system. In the framework of a process feasibility study carried out when R&D is still ongoing, this information can help to set the priority of the aspects to be investigated, given the risk of extra expenses high as the variation range.

To better assess the potential of the model, the same full-scale plant configuration has been simulated for *S. cerevisiae* and *E. coli*, with the only purpose to show the effects on the output uncertainty changing the uncertainty in the input parameters. The different grade of knowledge about those bacterial strains is reflected by the results given by the simulations. The span between the limit upper costs is reduced to 47000 $/year for the clarification of *S. cerevisiae* broth, for which a higher agreement between literature data exists. On the contrary, the poorness of available experimental data results in a wider span of 422000 $/year for the limit cumulate costs for *E.coli* filtration.

The fouling model, as well as the cost function, have been developed for a definite filtration system, thus several aspects require further investigations before extending the applicability of the model to other systems, with different layouts and/or types of membrane. More extensive benchmarking on industrial applications of membrane filtration is necessary, in order to characterize the flexibility of the model in representing other microorganisms and filtration operating conditions. Cost function refining has to be considered too, since the approximate correlations used to estimate the plant economics can be improved through comparisons with real industrial cost quotes, providing more accurate evaluations.

In the context of this work, fouling has been evaluated considering standard operating conditions (crossflow velocity and transmembrane pressure) during the simulations, due to the poorness of experimental data about limit or critical conditions. If further information were available, it would be possible to implement an optimization system for plant layout, for example combining membrane filtration units with centrifuge stages via multivariable optimizations (as recently performed by Alfa Laval), in order to minimize the overall plant costs.

Future works could be aimed at the analysis and simulation of different combined systems involving microfiltration and ultrafiltration together with traditional downstream processing techniques, as conventional filter or centrifugal separation, adopting the proposed model to describe membrane filtration units

As far as uncertainty propagation is concerned, the use of experimental data that could be incomplete, partial or extended from “similar” systems affects the final cost estimates. Epistemic uncertainty is common in all R&D problems, thus the developed algorithm to describe the uncertainty propagation from input parameters to model output could be applied to other systems involving empirical variables.

Biorefining separations are more complex to standardize than in oil-industry, hence predictive models become more desirable, but at the same time more risky, if uncertainty is not properly treated. The developed method is an attempt to give a design tool able to treat in advance some separation issues, providing, together with the cost estimations necessary for feasibility assessment, an indication of the importance of more detailed research. This could help to set the priority of applied research and to allocate the R&D resources.

Appendix A

Input data for *L. delbrueckii* simulation

All the numerical values used to simulate the full-scale fed-batch filtration plant for lactic acid production are listed in Tab. A.1.

Table A.1: Input data for the simulation of L. delbrueckii broth clarification.

Data	Unit of measure	Value
Transmembrane pressure	bar	2
Crossflow velocity	m/s	4
Target productivity	m^3/h	40
Fluid dynamic viscosity	Pa·s	7.80E-04
Fluid density	kg/m^3	1000
Reference pressure	bar	1
Wet cell density	kg/m^3	1100
Solidosity ratio (range)	-	193 - 750
Cake porosity (range)	-	0.08 - 0.18
Compressibility index (range)	-	0.5 - 1
Cake resistance coefficient	$m/kg/Pa^n$	1.20E+09
Cell size (equivalent diameter)	μm	2

Table A.1 (continued): Input data for the simulation of L. delbrueckii broth clarification.

Data	Unit of measure	Value
Membrane diameter	mm	5.75
Membrane length	m	1.178
Channels/module	-	368
Roughness height	m	5.00E-06
Membrane resistance	m^{-1}	3.27E+11
Unit volume hold-up	L	120
Time parameter	s^{-1}	3.00E-04
Colloids diffusivity	m^2/s	3.64E-12
Inlet wet cell concentration	kg/m^3	2.6
Integration time-step	s	10
Integration time	h	20
Cleaning time	min	20
Number of α-cuts	-	21

Appendix B

Input data for cost correlations

Table B.1: Cost function input values.

Data	Unit of measure	Value
Ceramic membrane cost	$/m^2	500
Vessel cost	$/unit	2000
Chemical cleaning capital cost	$	25000
Modules per feed pump	-	24
Modules per recirculating pump	-	4
Pump cost index ratio	-	3.53
Pump efficiency	-	0.8
Interest rate	-	15%
Number of yearly payments	-	7
Personnel salary	$/person/year	40000
Number of personnel	-	3
Chemical cleaning operating cost	$/year	25000

Appendix C

Microorganisms features

The values used to simulate the clarifications of *S. cerevisiae* and *E. coli* are summarized in Tab. C.1 and C.2, respectively. Since membrane and plant features are the same adopted for the lactic acid production plant, the only different values rely on the microorganism characterization.

Table C.1: S. cerevisiae fermentation broth clarification data.

Data	Unit of measure	Value
Cake porosity (range)	-	0.20 - 0.28
Compressibility index (range)	-	0.5 - 0.8
Wet cell density	kg/m^3	1100
Cell size (equivalent diameter)	μm	5
Cake resistance coefficient	$m/kg/Pa^n$	1.01E+09

The possibility distribution of the cake compressibility index has a triangular shape, with a most likely value of 0.7, while the cake porosity possibility distribution is rectangular.

Table C.2: E. coli fermentation broth clarification data.

Data	Unit of measure	Value
Cake porosity (range)	-	0.08 - 0.18
Compressibility index (range)	-	0.4 - 1
Wet cell density	kg/m^3	1160
Cell size (equivalent diameter)	μm	0.98
Cake resistance coefficient	$m/kg/Pa^n$	3.16E+10

For *E. coli*, also the possibility distribution of the cake compressibility index is rectangular, and it spans from 0.4 to 1.

List of Figures

List of Tables

Bibliography

1. Lutz, H., *Ultrafiltration for bioprocessing*2015: Elsevier.
2. Juang, R.-S., H.-L. Chen, and Y.-S. Chen, *Resistance-in-series analysis in cross-flow ultrafiltration of fermentation broths of Bacillus subtilis culture.* Journal of Membrane Science, 2008. **323**(1): p. 193-200.
3. van der Sman, R.G.M., et al., *Review of hypotheses for fouling during beer clarification using membranes.* Journal of Membrane Science, 2012. **396**: p. 22-31.
4. Mohammad, A.W., et al., *Ultrafiltration in Food Processing Industry: Review on Application, Membrane Fouling, and Fouling Control.* Food and Bioprocess Technology, 2012. **5**(4): p. 1143-1156.
5. van Reis, R. and A. Zydney, *Bioprocess membrane technology.* Journal of Membrane Science, 2007. **297**(1): p. 16-50.
6. Abels, C., F. Carstensen, and M. Wessling, *Membrane processes in biorefinery applications.* Journal of Membrane Science, 2013. **444**: p. 285-317.
7. Carrère, H., F. Blaszkow, and H.R.D. Balmann, *Modelling the clarification of lactic acid fermentation broths by cross-flow microfiltration.* Journal of Membrane Science, 2001. **186**(2): p. 219-230.
8. Wang, C., et al., *Clarification of succinic acid fermentation broth by ultrafiltration in succinic acid bio–refinery.* Journal of Chemical Technology and Biotechnology, 2013. **88**(3): p. 444-448.
9. Van De Graaf, M.J., et al., *Process for the crystallization of succinic acid,* 2014, Google Patents.
10. Coulson, J., *Coulson and Richardson's Chemical Engineering: Particle Technology and Separation Processes v. 2. Coulson and Richardson's Chemical Engineering*, 1996, Butterworth-Heinemann Ltd.

11. Hsieh, H., *Inorganic membranes for separation and reaction*. Vol. 3. 1996: Elsevier.
12. Strathmann, H., *Membrane Separation Processes, 1. Principles,* in *Ullmann's Encyclopedia of Industrial Chemistry*2000, Wiley-VCH Verlag GmbH & Co. KGaA.
13. Tarleton, E.S. and R.J. Wakeman, *Understanding flux decline in crossflow microfiltration: Part I - Effects of particle and pore size.* Chemical Engineering Research and Design, 1993. **71**(A4): p. 399-410.
14. Tarleton, E.S. and R.J. Wakeman, *Understanding flux decline in crossflow microfiltration: Part II - Effects of process parameters.* Chemical Engineering Research and Design, 1994. **72**(A3): p. 431-440.
15. Tarleton, E.S. and R.J. Wakeman, *Understanding flux decline in crossflow microfiltration: part III - effects of membrane morphology.* Chemical Engineering Research and Design, 1994. **72**(A4): p. 521-529.
16. Belfort, G., R.H. Davis, and A.L. Zydney, *The behavior of suspensions and macromolecular solutions in crossflow microfiltration.* Journal of Membrane Science, 1994. **96**(1-2): p. 1-58.
17. Nakanishi, K., T. Tadokoro, and R. Matsuno, *On the specific resistance of cakes of microorganisms.* Chemical Engineering Communications, 1987. **62**(1-6): p. 187-201.
18. Nagata, N., et al., *Cross-flow membrane microfiltration of a bacterial fermentation broth.* Biotechnology and bioengineering, 1989. **34**(4): p. 447-466.
19. Gatenholm, P., et al., *Performance of synthetic membranes during cell harvesting of E. coli.* Process biochemistry, 1988. **23**(3): p. 79-81.
20. Foley, G., P.F. MacLoughlin, and D.M. Malone, *Membrane Fouling during Constant Flux Crossflow Microfiltration of Dilute Suspensions of Active Dry Yeast.* Separation Science and Technology, 1995. **30**(3): p. 383-398.
21. McCarthy, A.A., P.K. Walsh, and G. Foley, *Experimental techniques for quantifying the cake mass, the cake and membrane resistances and the specific cake resistance during crossflow filtration of microbial suspensions.* Journal of Membrane Science, 2002. **201**(1-2): p. 31-45.
22. Noble, R.D. and S.A. Stern, *Membrane separations technology: principles and applications*. Vol. 2. 1995: Elsevier.

23. Guo, W., H.-H. Ngo, and J. Li, *A mini-review on membrane fouling.* Bioresource Technology, 2012. **122**: p. 27-34.
24. Hermans, P. and H. Bredee, *Zur kenntnis der filtrationsgesetze.* Recueil des Travaux Chimiques des Pays-Bas, 1935. **54**(9): p. 680-700.
25. Grace, H., *Structure and performance of filter media. II. Performance of filter media in liquid service.* AIChE Journal, 1956. **2**(3): p. 316-336.
26. Bolton, G., D. LaCasse, and R. Kuriyel, *Combined models of membrane fouling: development and application to microfiltration and ultrafiltration of biological fluids.* Journal of Membrane Science, 2006. **277**(1): p. 75-84.
27. Sabia, G., M. Ferraris, and A. Spagni, *Model-based analysis of the effect of different operating conditions on fouling mechanisms in a membrane bioreactor.* Environmental Science and Pollution Research, 2016. **23**(2): p. 1598-1609.
28. Iritani, E., *A Review on Modeling of Pore-Blocking Behaviors of Membranes During Pressurized Membrane Filtration.* Drying Technology, 2013. **31**(2): p. 146-162.
29. Liu, Q.-F. and S.-H. Kim, *Evaluation of membrane fouling models based on bench-scale experiments: a comparison between constant flowrate blocking laws and artificial neural network (ANNs) model.* Journal of Membrane Science, 2008. **310**(1): p. 393-401.
30. Paipuri, M., et al., *Numerical modelling of concentration polarisation and cake formation in membrane filtration processes.* Desalination, 2015. **365**: p. 151-159.
31. Bowen, W.R., M.G. Jones, and H.N.S. Yousef, *Dynamic ultrafiltration of proteins – A neural network approach.* Journal of Membrane Science, 1998. **146**(2): p. 225-235.
32. Delgrange, N., et al., *Modelling of ultrafiltration fouling by neural network.* Desalination, 1998. **118**(1): p. 213-227.
33. Mhurchú, J.N. and G. Foley, *Dead-end filtration of yeast suspensions: correlating specific resistance and flux data using artificial neural networks.* Journal of Membrane Science, 2006. **281**(1): p. 325-333.
34. Douglas, J.M., *Conceptual design of chemical processes*. Vol. 1110. 1988: McGraw-Hill New York.
35. Kolmogorov, A.N., *Foundations of the Theory of Probability.* 1950.

36. De Finetti, B., *Fondamenti logici del ragionamento probabilistico*1930: Azzoguidi.
37. Ramsey, F.P., *Truth and probability (1926).* The foundations of mathematics and other logical essays, 1931: p. 156-198.
38. Zadeh, L.A., *Fuzzy sets as a basis for a theory of possibility.* Fuzzy Sets and Systems, 1978. **1**(1): p. 3-28.
39. Walley, P., *Statistical reasoning with imprecise probabilities.* 1991.
40. Aven, T., et al., *Uncertainty in Risk Assessment: The Representation and Treatment of Uncertainties by Probabilistic and Non-Probabilistic Methods*. Uncertainty in Risk Assessment: The Representation and Treatment of Uncertainties by Probabilistic and Non-Probabilistic Methods2014. 1-186.
41. Ross, T.J., *Fuzzy logic with engineering applications*2009: John Wiley & Sons.
42. Pedroni, N. and E. Zio, *Empirical comparison of methods for the hierarchical propagation of hybrid uncertainty in risk assessment, in presence of dependences.* International Journal of Uncertainty, Fuzziness and Knowledge-Based Systems, 2012. **20**(04): p. 509-557.
43. Baudrit, C., D. Dubois, and D. Guyonnet, *Joint propagation and exploitation of probabilistic and possibilistic information in risk assessment.* IEEE transactions on fuzzy systems, 2006. **14**(5): p. 593-608.
44. Buzzi-Ferraris, G. and F. Manenti, *Nonlinear systems and optimization for the chemical engineer: solving numerical problems*2013: John Wiley & Sons.
45. Charcosset, C., *Membrane processes in biotechnology: an overview.* Biotechnology advances, 2006. **24**(5): p. 482-492.
46. El Rayess, Y., et al., *Analysis of membrane fouling during cross-flow microfiltration of wine.* Innovative Food Science & Emerging Technologies, 2012. **16**: p. 398-408.
47. Guerra, K. and J. Pellegrino, *Investigation of low-pressure membrane performance, cleaning, and economics using a techno-economic modeling approach*, in *Science and Technology Program Report*2012.
48. Meireles, M., P. Aimar, and V. Sanchez, *Effects of protein fouling on the apparent pore size distribution of sieving membranes.* Journal of Membrane Science, 1991. **56**(1): p. 13-28.

49. Li, S.L., et al., *Study on the microfiltration of Escherichia coli-containing fermentation broth by a ceramic membrane filter.* Journal of Membrane Science, 1996. **110**(2): p. 203-210.
50. Jiraratananon, R. and A. Chanachai, *A study of fouling in the ultrafiltration of passion fruit juice.* Journal of Membrane Science, 1996. **111**(1): p. 39-48.
51. Marshall, A.D., P.A. Munro, and G. Trägårdh, *Influence of permeate flux on fouling during the microfiltration of β-lactoglobulin solutions under cross-flow conditions.* Journal of Membrane Science, 1997. **130**(1): p. 23-30.
52. Mockel, D., E. Staude, and M. Guiver, *Static protein adsorption, ultrafiltration behavior and cleanability of hydrophilized polysulfone membranes.* Journal of Membrane Science, 1999. **158**.
53. Lapointe, J.-F., et al., *Fouling of a nanofiltration membrane by a β-lactoglobulin tryptic hydrolysate: impact on the membrane sieving and electrostatic properties.* Journal of Membrane Science, 2005. **253**(1–2): p. 89-102.
54. Siitonen, J. and T. Sainio, *Unified design of chromatographic separation processes.* Chemical Engineering Science, 2015. **122**: p. 436-451.
55. Ma, L., et al., *Influence of the filtration modes on colloid adsorption on the membrane in submerged membrane bioreactor.* Colloids and Surfaces A: Physicochemical and Engineering Aspects, 2005. **264**(1–3): p. 120-125.
56. Bowen, W.R. and F. Jenner, *Theoretical descriptions of membrane filtration of colloids and fine particles: An assessment and review.* Advances in Colloid and Interface Science, 1995. **56**: p. 141-200.
57. Porter, M.C., *Concentration polarization with membrane ultrafiltration.* Industrial & Engineering Chemistry Product Research and Development, 1972. **11**(3): p. 234-248.
58. Bacchin, P., et al., *A unifying model for concentration polarization, gel-layer formation and particle deposition in cross-flow membrane filtration of colloidal suspensions.* Chemical Engineering Science, 2002. **57**(1): p. 77-91.
59. Tiwari, P., S.P. Antal, and M.Z. Podowski, *Modeling shear-induced diffusion force in particulate flows.* Computers & Fluids, 2009. **38**(4): p. 727-737.
60. Chellam, S. and M.R. Wiesner, *Evaluation of crossflow filtration models based on shear-induced diffusion and particle adhesion: Complications*

induced by feed suspension polydispersivity. Journal of Membrane Science, 1998. **138**(1): p. 83-97.

61. Cho, J., et al., *Measurements of effective sizes and diffusivities of nano-colloids and micro-particles.* Colloids and Surfaces A: Physicochemical and Engineering Aspects, 2006. **274**(1-3): p. 43-47.
62. Mondor, M. and C. Moresoli, *Shear-induced hydrodynamic diffusion model for cross-flow microfiltration: role of the particle volume fraction.* Desalination, 2002. **145**(1): p. 123-128.
63. Song, L. and M. Elimelech, *Theory of concentration polarization in crossflow filtration.* Journal of the Chemical Society, Faraday Transactions, 1995. **91**(19): p. 3389-3398.
64. Gekas, V. and B. Hallström, *Mass transfer in the membrane concentration polarization layer under turbulent cross flow.* Journal of Membrane Science, 1987. **30**(2): p. 153-170.
65. Elimelech, M. and S. Bhattacharjee, *A novel approach for modeling concentration polarization in crossflow membrane filtration based on the equivalence of osmotic pressure model and filtration theory.* Journal of Membrane Science, 1998. **145**(2): p. 223-241.
66. Fillaudeau, L. and H. Carrère, *Yeast cells, beer composition and mean pore diameter impacts on fouling and retention during cross-flow filtration of beer with ceramic membranes.* Journal of Membrane Science, 2002. **196**(1): p. 39-57.
67. Mota, M., J.A. Teixeira, and A. Yelshin, *Influence of cell-shape on the cake resistance in dead-end and cross-flow filtrations.* Separation and Purification Technology, 2002. **27**(2): p. 137-144.
68. Tanaka, T., et al., *Characteristics in Crossflow Filtration Using Different Yeast Suspensions.* Separation Science and Technology, 1997. **32**(11): p. 1885-1898.
69. Tanaka, T., et al., *Filtration behaviors of rod-shaped bacterial broths in unsteady-state phase of cross-flow filtration.* Journal of Chemical Engineering of Japan, 1996. **29**(6): p. 973-981.
70. Tanaka, T., et al., *Filtration characteristics and structure of cake in crossflow filtration of bacterial suspension.* Journal of Fermentation and Bioengineering, 1994. **78**(6): p. 455-461.

71. Fane, A., et al., *Microfiltration of biomass and biofluids: effects of membrane morphology and operating conditions.* Filtration & separation, 1991. **28**(5): p. 332-331.
72. Kromkamp, J., et al., *Effects of particle size segregation on crossflow microfiltration performance: Control mechanism for concentration polarisation and particle fractionation.* Journal of Membrane Science, 2006. **268**(2): p. 189-197.
73. Okamoto, Y., K. Ohmori, and C.E. Glatz, *Harvest time effects on membrane cake resistance of Escherichia coli broth.* Journal of Membrane Science, 2001. **190**(1): p. 93-106.
74. Hodgson, P.H., et al., *Cake resistance and solute rejection in bacterial microfiltration: The role of the extracellular matrix.* Journal of Membrane Science, 1993. **79**(1): p. 35-53.
75. Mota, M. and M.C. Flickinger, *Modeling the influence of slurry concentration on Saccharomyces cerevisiae cake porosity and resistance during microfiltration.* Biotechnology Progress, 2012. **28**(6): p. 1534-1541.
76. Bryan, A.K., et al., *Measurement of mass, density, and volume during the cell cycle of yeast.* Proceedings of the National Academy of Sciences of the United States of America, 2010. **107**(3): p. 999-1004.
77. Godin, M., et al., *Measuring the mass, density, and size of particles and cells using a suspended microchannel resonator.* Applied Physics Letters, 2007. **91**(12).
78. Milcent, S. and H. Carrère, *Clarification of lactic acid fermentation broths.* Separation and Purification Technology, 2001. **22–23**: p. 393-401.
79. Carrère, H., F. Blaszkowa, and H. Roux de Balmann, *Modelling the microfiltration of lactic acid fermentation broths and comparison of operating modes.* Desalination, 2002. **145**(1-3): p. 201-206.
80. Pickering, K.D. and M.R. Wiesner, *Cost model for low-pressure membrane filtration.* Journal of Environmental Engineering, 1993. **119**(5): p. 772-797.
81. Adham, S.S., J.G. Jacangelo, and J.-M. Laine, *Characteristics and costs of MF and UF plants.* American Water Works Association. Journal, 1996. **88**(5): p. 22.
82. Cheryan, M., *Ultrafiltration and microfiltration handbook*1998: CRC press.

83. Kulkarni, S.S., E.W. Funk, and N.N. Li, *Applications and economics*, in *Membrane Handbook*1992, Springer. p. 446-453.
84. Sethi, S. and M.R. Wiesner, *Cost modeling and estimation of crossflow membrane filtration processes.* Environmental engineering science, 2000. **17**(2): p. 61-79.
85. Perry, R.H. and D.W. Green, *Perry's chemical engineers' handbook*1999: McGraw-Hill Professional.
86. Association, A.W.W., *Microfiltration and Ultrafiltration Membranes for Drinking Water (PDF).* Journal-American Water Works Association, 2008. **100**(12): p. 84-97.